AN EXPERIMENTAL STUDY OF NOISE PRODUCED BY OPEN TURBULENT FLAMES

A THESIS

Presented to

The Faculty of the Division of Graduate

Studies and Research

By

Belur Narayana Shivashankara

In Partial Fulfillment

of the Requirements for the Degree

Doctor of Philosophy in the School of Aerospace Engineering

Georgia Institute of Technology

August, 1973

AN EXPERIMENTAL STUDY OF NOISE PRODUCED

BY OPEN TURBULENT FLAMES

Approved:

Warren C. Strahle, Chairman

Robin B. Gray

Ben T. Zinn

Date approved by Chairman: 8/13/73

ACKNOWLEDGMENTS

I would like to express my appreciation to Professor Warren C. Strahle for his suggestion of the thesis topic. Many discussions with my thesis advisor, Professor Warren C. Strahle, concerning various aspects of the investigation were both stimulating and enlightening; his guidance and encouragement are sincerely appreciated. The careful examination of the manuscript by Professor Warren C. Strahle and other members of my reading committee, Professors Robin B. Gray and Ben T. Zinn, is appreciated.

I am grateful to Mr. John C. Handley for his assistance during the experimental phase of this work. The many hours we spent discussing the experimental aspects of the problem were invaluable. I wish to thank Mr. Raymond J. Strickland for his assistance during the initial phase of the direct photography experiments.

I am grateful for the financial assistance provided by the School of Aerospace Engineering, the Air Force Office of Scientific Research under Grant No. AFOSR-72-2365 and the National Science Foundation under Grant No. GK 32544.

I wish to thank Ms. Candy Avery for her excellent typing of the manuscript.

TABLE OF CONTENTS

LIST OF ILLUSTRATIONS

LIST OF TABLES

NOMENCLATURE

a_o	speed of sound in quiescent surroundings
C	an autocorrelation function of reaction rate time derivative
d	a correlation distance
D	burner diameter
E	ethylene
f	frequency
f_c	peak frequency -- frequency on the spectrum corresponding to maximum amplitude
F	fuel mass fraction in the reactants
G	a cross-correlation function
H	heating value per unit mass of fuel
I	emission intensity
$\dot{I}$	dI/dt
J	intensity of turbulence
K	a constant
ℓ_t	scale of turbulence
L_{ac}	distance between the burner port and the acoustic center
L_{flame}	length of flame
$\dot{m}$	mass flow rate of reactants
$\dot{m}_f$	mass flow rate of fuel
p	acoustic pressure
P	acoustic power or propane
Py	propylene

r	radius
S_L	laminar flame speed
S_t	turbulent flame speed
t	time
T	total time or absolute temperature
U	mean flow velocity of reactants
V	volume of reaction zone
V_d	a correlation volume
x_i	space coordinate
γ	ratio of specific heats
η_{ta}	thermo-acoustic efficiency
θ	azimuth (measured from flow direction)
ρ	acoustic component of density
ρ_o	density of reactant mixture or density of ambient air
ρ_1	density of combustion products
ρ_T	turbulence component of density in the turbulence zone
τ^*	time delay between $p(t)$ and $\dot{I}(t)$
ϕ	equivalence ratio $= \dfrac{(\text{fuel/air})_{\text{actual}}}{(\text{fuel/air})_{\text{stoichiometric}}}$
ω	reaction rate

Superscripts

$-$	time average
$\cdot$	time derivative

Subscripts

subscripts x and t denote partial differentiation

SUMMARY

Experiments which were conducted to study noise generation from turbulent combustion zones are described. The measurements are done in an anechoic chamber. Pilot flame stabilized turbulent flames at the end of burner tubes of diameters 0.402" to 0.96" are employed. Propane, propylene and ethylene fuels are used with air as the oxidizer. The mean flow velocity of reactants is varied between 50 and 600 fps.

The noise generation process is studied through three separate sets of experiments. They are:

1. Acoustic Experiments in which sound pressures are measured around the flame in the far field. Directionality patterns, scaling laws for the acoustic power radiated, the thermo-acoustic efficiency and the spectral content are deduced. Both fuel-lean and fuel-rich mixtures are used.

2. Direct Flame Photography in which scaling laws for the volume of the reaction zone are deduced for fuel-lean to stoichiometric flames.

3. Optical Emission Studies in which the optical and acoustical emissions from the flame are correlated.

Combustion noise is shown to be weakly directional for both fuel-lean and fuel-rich flames. Comparison with Strahle's theory for fuel-lean flames shows that the refraction of sound at temperature discontinuities and the convection of sources by the flow are capable of

qualitatively explaining the experimental directionality patterns. The spectra of the noise radiation indicate that combustion noise is broad-band noise with a single peak. Over the entire range of parameters the noise from hydrocarbon-air flames is shown to peak in the 250-700 Hz range. An expression in the form $f_c \propto U^{0.18} D^{-0.08} S_L^{0.53} F^{-0.69}$ is obtained for the peak frequency of fuel-lean to stoichiometric flames.

Acoustic power radiated by fuel-lean flames is shown to scale as $P \propto U^{2.7} D^{2.8} S_L^{1.4} F^{0.4}$. Errors involved in obtaining the scaling law are discussed. A thermo-acoustic efficiency as high as 10^{-6} is observed for the 600 fps flame, indicating that noise generation from high speed flames could be substantial. For fuel-rich flames an acoustic power law $P \propto U^3 D^2$ is obtained. The thermo-acoustic efficiency of fuel-rich flames is shown to be independent of the burner diameter.

Detailed scaling laws on flame volume of fuel-lean to stoichiometric flames, obtained by a direct flame photography technique, are shown to be quite useful in the study of combustion noise scaling laws. The flame volume study indicates that the turbulence structure in the flame is primarily decided by the pipe flow process and not by the flame.

Optical emission studies employing a cross-correlation technique and spectral analysis show that over a wide range of experimental conditions a one-to-one correspondence exists between the optical and the acoustical emissions from the flame. Based on these experiments, combustion noise sources are shown to be primarily located in the visible flame zone.

The results of the overall program are compared with existing

theories and other experimental results. The comparison with Strahle's theory shows that the analytical solution for the far field radiation is reasonable. The scaling laws for the acoustic power, however, are not completely in line with the experimental results. It is shown that the disagreement between the theoretical and experimental results arises from possible errors in the order of magnitude estimates of the autocorrelation function of the reaction rate.

CHAPTER I

INTRODUCTION

General

"Noise is unwanted sound." Noise produces annoyance, decreases efficiency and can impair hearing. With increasing population density around airports and military airfields, aircraft noise has become a problem of primary concern.

It is a well known fact that turbulent combustion generates noise and that most of the combustion processes in practice are turbulent. A substantial portion of the noise, in aircraft using turbo-propulsion systems, could be due to combustion in primary combustors and afterburners. In the case of afterburning turbojets and turbofans a substantial portion of the basic engine noise could originate from the afterburner combustion process, and for "quiet" lifting fans a large contributor to the noise could be the primary gas turbine combustors. In industrial furnaces combustion roar is a primary source of noise.

Noise suppression could be achieved either at the source or by some treatment of the medium separating the source and the environment. The merits of decreasing the noise at the source are easily recognized. In order to attempt reduction of combustion noise at its source a detailed study of the mechanism of noise generation is essential. Also, radiation characteristics from the source would be essential for devising methods to control the noise by the use of acoustic baffles and sound absorbent

liners.

Literature Review

The subject of combustion noise has received very little attention in the literature. The mechanisms of generation and radiation have not been understood to any appreciable extent. Although combustion generated noise itself is nothing new, the study of it is of a recent nature.

At the outset, it can be seen that all the theoretical studies were restricted by the lack of a clear understanding of the mechanism of turbulent combustion. On the experimental side, a serious limitation has been noticed as far as acoustic power calculations. Except in a very few cases, the scaling laws for acoustic power radiated were obtained from a single-microphone sound pressure measurement and the assumption of spherical symmetry. This could lead to incorrect power scaling laws since the combustion noise, in almost all the experiments, was found to be directional, although weakly so. Also, a substantial amount of experimental data available in the literature is for particular burner configurations, thus tending to make the task of deriving general scaling rules almost impossible.

In a theoretical study of the interaction of a free flame with a turbulence field, Tucker[1] showed that appreciable noise generation could result in the region of interaction. He also showed that the intensity of noise generated would be a strong function of the laminar flame speed. No expression for acoustic power radiated was derived in this work.

Bragg[2] developed a theory based on the wrinkled flame concept of turbulent flames. The theory predicted the mechanism of turbulent com-

bustion noise generation to be due to a distribution of monopole-like sources in the reaction zone. Thermo-acoustic efficiency, a measure of the total energy of the flame converted into acoustic radiation, was shown to vary as the square of the flow velocity.

At about the same time, Smith and Kilham[3] presented experimental data on noise produced by open premixed turbulent flames. The burner sizes varied from $\frac{1}{4}$" to $\frac{1}{2}$" in diameter with flow velocities up to 350 ft/sec. Gaseous fuels ethylene, methane, propane, and propylene were used with air as the oxidizer. It was observed that the acoustic power radiated was proportional to $(UDS_L)^2$ where U is the flow velocity, D the burner diameter and S_L the laminar flame speed. A more detailed work[4] showed that the scaling with S_L could vary between 0.6 and 3.4 while the scaling with respect to D and U was quite precise. However, except for scaling with respect to U, the scaling laws were inferred from sound pressures measured at the 90° microphone. The results of the experiments for directionality showed that the noise generated was weakly directional (~ 3 db) and that the directionality pattern systematically changed with the flow velocity. The maximum sound pressure was found to occur at angles of 50° to 80° to the flow direction.

Smith and Kilham observed the combustion noise to be a broad band noise with a single peak in the range of 250-500 Hz. The peak frequency, in general, was found to increase with the flow velocity. The rate of increase with velocity, however, was different for different fuels. The thermo-acoustic efficiency, the ratio of acoustic power radiated to the total energy per unit time released by combustion, varied between 10^{-8} and 10^{-7} (thermal inputs of 1-7 kw) and was found to increase linearly

with flow velocity. Since ethylene flames showed higher efficiencies almost twice those for propylene, it was concluded that fuels with higher S_L were more efficient sound generators.

A study of the noise of diffusion flames was reported by Kotake and Hatta[5]. Based on an analysis using the conservation equations and upon examination of diffusion flames structure, an acoustic model containing a distribution of monopole and dipole sources in the reaction zone was postulated. The theoretical analysis would allow an acoustic power scaling of U^2D^3 in low velocity flames and a scaling of U^4D^3 in high velocity flames. Experiments conducted with equivalence ratios of 1, 2, and 3, over a rather narrow velocity range of 9 m/sec to 23 m/sec, were shown to substantiate both the scaling laws. The frequency spectra were flat at lower frequencies and dropped off at higher frequencies. These frequency spectra were quite unlike the spectra reported by other investigators which always exhibited a recognizable peak and amplitude fall off on both sides of the peak frequency. Once again, the scaling rules depended on the measurements at a single microphone location. No details are available as to the acoustic environment for these experiments. The burner sizes were 6.8 mm to 21.8 mm. The flames were stabilized at the end of convergent nozzles in contrast with those of Reference 3 where fully developed pipe flow existed at the burner exit.

Bollinger et al[6] could recognize the presence of combustion noise in rocket motor exhaust noise when operating fuel rich. They experimented upon a 500 lb-thrust RP1-LOX motor and noticed a predominant component of noise in the low frequency range ($\sim$ 500 Hz) when the rocket motor was

fired with excess fuel. The authors concluded that the combustion of the unburned fuel in the atmosphere outside the nozzle is the most likely source of this noise.

An entirely new line of approach to the study of combustion noise resulted due to the experiments of Thomas et al[7]. They found a one-to-one correspondence between the instantaneous rate of change of the radius of the flame front and the pressure for spark ignited combustible gases contained in spherical soap bubbles. Hurle et al[8] showed that the rate of change of emission intensity of CH and C_2 radicals in the reaction zone can be used to derive the instantaneous sound pressure generated by the flame for the spherically expanding flame fronts as well as for open turbulent flames. Such a correlation implies a direct relation between the sound pressure and the volume integral of the first time derivative of the global reaction rate. A good correlation was obtained in Reference 8 when the bandwidth of the signals was limited to 50 Hz-1kHz. Due to increased noise in the optical system, correlation was poor when higher frequencies were included. In the computation of the frequency spectrum from the optical measurements the signal to noise ratio was very low and hence the comparison between the optically and acoustically obtained spectra should be viewed with reservations. Hurle et al concluded that the mechanism of combustion noise conforms to the monopole behavior.

The work of Hurle et al was extended by Price et al[9] to include diffusion flames and liquid spray combustion. A good correlation between the first time derivative of the emission intensity of the C_2 radical and the instantaneous sound pressure was demonstrated in all these cases of turbulent combustion. The only limitation to this technique was that

there should be no continuum radiation in the flame. The acoustic radiation from premixed, diffusion and liquid spray combustion was shown by this study to conform to a monopole source distribution. Experiments using turbulence grids showed that both r.m.s. sound pressures and r.m.s. values of the time derivative of the emission intensity increase with turbulence intensity.

Smithson and Foster[10], in a short paper, reported a thermo-acoustic efficiency variation with U^2 for a Meker burner using town's gas. Flow rates of town's gas varied from 0.092 to 0.12 litres/sec with air/gas ratios from 1 to 6. The microphone distance quoted would be in the near field for laboratory Meker burners (1 to 2 cm in diameter) and hence the scaling rules may be in error. The lowest value of acoustic efficiency ($\sim 3 \times 10^{-9}$) was reported by Powell[11] for a gasoline vapor primus stove flame. The burner size was about 0.2" in diameter. The frequency peaked in the 300-600 Hz range.

Giammar and Putnam[12] have studied the noise generated by pure diffusion flames. Two burner configurations, axially impinging jets and an "octopus" burner, were used. Flow rates were as high as 12 SCFM in the case of the octopus burner. The only drawback of this extensive body of data on pure diffusion flames is the complicated burner configuration. Sound power scaled with firing rate to an exponent of 1 to 2; a thermo-acoustic efficiency as high as 6×10^{-7} was obtained for the impinging jets. In all the experiments the peak frequency was found to be in the range 300-500 Hz. In a recent paper[13], Giammar and Putnam have presented the results of some experiments on premixed fuel rich flames on commercial burners of sizes $1\frac{1}{4}$", $1\frac{1}{2}$" and 2". Heat inputs were of the order of 0.25

to 0.69 million BTU/hr (75-200 kw). Both single burners and burners in pairs showed that sound power varies, in general, as the square of the firing rate. The experimental data showed a tendency to follow an exponent slightly lower than 2.

Further experiments on diffusion flames were reported by Knott[14]. Hydrogen and ethylene were burned with air and oxygen. Co-flowing jets and impinging jets configurations were studied. A volume of experimental data has been presented but in a manner very difficult to interpret. Flow velocities were 250 fps to 1000 fps. The thermo-acoustic efficiency was found to be in the range 10^{-8} to 10^{-5} and it varied as $\dot{m}_f$ for co-flowing jets, $1/\dot{m}_f$ for impinging jets and as $\dot{m}_f^3$ for the premixed case. Here, $\dot{m}_f$ is the mass flux of fuel. The highest value of thermo-acoustic efficiency of 2×10^{-5} was reported for the ethylene-oxygen flame. The hydrogen-oxygen system had a cold flow peak frequency of 6000 Hz and the corresponding combustion noise peaked around 2000-4000 Hz. For the ethylene-air system (Re. No. 50,000) the combustion noise had a peak in the 600-900 Hz frequency range. The burner sizes for co-flowing jets were 1.835 cm diameter for the outer tube and 0.813 cm and 0.391 cm for the inner tube. For the impinging jet burner both the tubes had the same diameter, 1.303 cm, 0.8079 cm or 0.4981 cm.

Seebold[15] has reported noise data obtained from a full scale test furnace as well as from process plant furnaces. The heat release varied from 1-10 million BTU/hr. The corresponding fuel flow rates would be roughly 10-100 SCFM. Power output was found to scale with the square of the heat release. The frequency spectra were found to peak in the 125-500 Hz range.

The three papers by Strahle[16,17,18] perhaps form the most extensive theoretical analysis on combustion noise. A rather detailed description of this work is given here because of the particular significance of the prediction from Strahle's theory of combustion noise to the experimental program described in this report.

Following the classical method of Lighthill[19,20] in his work on aerodynamic noise, Strahle's theory starts with (Reference 16)

$$\rho_{tt} - a_o^2 \rho_{x_i x_i} = F_s \tag{1}$$

as the wave equation describing the noise generated from a region undergoing turbulent fluctuations. Physical arguments were presented to show that the appropriate source term F_s for the case of combustion noise is given by $-a_o^2 \rho_{T_{x_i x_i}}$. With this source term the solution to the wave equation was shown to be

$$\rho = \frac{1}{4\pi a_o^2 r} \frac{\partial^2}{\partial t^2} \int_V \rho_T \left(\underset{\sim}{r}_o, t - \frac{r}{a_o}\right) dV \left(\underset{\sim}{r}_o\right) \tag{2}$$

where V corresponds to the volume undergoing turbulent combustion where ρ is dominated by turbulent fluctuations and not by the acoustics. Further developments of the solution gave the important result (Reference 17)

$$\rho = \frac{\gamma - 1}{\gamma} \frac{H\bar{\rho}_1}{4\pi \bar{a}_o^2 r \bar{p}} \int_V \omega_t \left(\underset{\sim}{r}_o, t - \frac{r}{a_o}\right) dV \left(\underset{\sim}{r}_o\right) \tag{3}$$

where ω_t is the time derivative of the global reaction rate. This showed that regardless of the turbulence structure and whether or not the flame is of premixed or of diffusion type, the far field acoustic density (or pressure) is proportional to the volume integral over the reacting volume V of the time derivative of the global reaction rate. With this result Strahle's theory could explain the one-to-one correspondence established between the optical and acoustic emissions by the experiments of References 8 and 9.

In Reference 17, considering the particular case of premixed, fuel lean flames, an expression was developed for the acoustic power P radiated from a region undergoing turbulent combustion in the form

$$P = \frac{(\Delta\rho/\rho_o)^2}{\bar{\rho}_o \bar{a}_o 4\pi F^2} \int_V dV\,(\underset{\sim}{r}_o) \int_{V_d} C(\underset{\sim}{r}_o, \underset{\sim}{d})\, dV\,(\underset{\sim}{d}) \qquad (4)$$

where $\Delta\rho$ represented the density change across the flame, F the fuel mass fraction, C an autocorrelation of the time derivative of the reaction rate, V the reacting volume and V_d a correlation volume.

Strahle has shown that scaling laws for acoustic power can be obtained from the above equation by making order of magnitude estimates for the quantities involved. Since the order of magnitude estimates would very heavily depend on the model of turbulent combustion used in Reference 17 the scaling laws were deduced for three possible phenomenological models of turbulent combustion, namely, a) wrinkled flame, b) slow distributed reaction and c) fast distributed reaction. A similar analysis

was made in Reference 18 for the scaling laws for diffusion flames. Strahle's theory recognized flow velocity U, laminar flame speed S_L, burner dimension D, fuel mass fraction F, scale of turbulence ℓ_t, and intensity of turbulence ϑ as the important parameters in the study of combustion noise. Further, it was predicted that acoustic power radiated could be expressed by a law of the type

$$P = K\, U^{a_1}\, S_L^{a_2}\, F^{a_3}\, D^{a_4}\, \ell_t^{a_5}\, \vartheta^{a_6} \tag{5}$$

where the prefactor K and the exponents $a_1, \ldots, a_6$ are constants. Reference 18 studied the effects of convection and refraction on the directionality of combustion noise and showed that the observed directionality of combustion noise could be explained qualitatively by these effects but the quantitative agreement with existing experiments is poor.

Kushida and Rupe[21], in an investigation of the effect on supersonic jet noise of nozzle plenum pressure fluctuations, observed that pressure fluctuations in the plenum chamber of a supersonic nozzle can strongly increase the noise radiated from the jet plume. Since some appreciable pressure fluctuations do exist in turbojet engines, the authors conclude that the reduction or elimination of plenum chamber pressure fluctuations may be an important method of reducing the total noise from jet engines.

A similar result was obtained by Abdelhamid *et al*[22]. They found a good cross correlation between the pressure oscillations in the combustor and the far field sound pressure. A 3-inch combustor with a 2-inch nozzle was used in this study. The major conclusion reached was that a large

portion of the far field noise due to jet aircraft could be from the combustors.

The literature survey leads to the following conclusions:

1. Combustion noise exists as an identifiable phonomenon in many practical systems.

2. In almost all the configurations, combustion noise occupies the lower range of the frequency spectrum; a typical range is between 150-500 Hz.

3. The acoustic power radiated is found to scale with U to an exponent between 1 and 4, with D to an exponent between 2 and 3 and with S_L to an exponent between 0.6 and 3.4. This represents a very wide variation in the scaling rules, thus making them virtually useless. Furthermore, many of the power scalings in the literature were based on single-microphone measurement and the assumption of spherical symmetry. This could give misleading results because of the weak directionality of the combustion noise. Also, only a few of the reported experiments were conducted in an anechoic enclosure. Finally, the choice of independent variables with which to derive scaling laws has been insufficient.

4. Very little work has been done on the directionality of the acoustic radiation. A systematic correlation of the spectral content with the flow variables and the chemistry has not been attempted in any of the existing experimental results.

5. The theories of References 16, 17 and 18 can, with experimental support and verification at various stages of the theoretical

solution, yield useful scaling rules for the acoustic power, spectral content and directionality of the combustion generated noise.

6. Without firm scaling laws it is impossible at this point to quantitatively estimate the true importance of combustion noise to the total turbo-propulsion noise problem.

Objectives of Research

The literature survey points out a need for further experimentation in the area of combustion noise. The experimental results, in order to be applicable to turbopropulsion systems of aircraft, should be obtained at velocities comparable to those found in afterburners ($\approx$ 600 ft/sec). Also, in order to get a true indication of the acoustic radiation from flames, all the experiments should be conducted in an anechoic chamber so that free field conditions can be closely approximated. The sound pressure should be measured at various azimuthal positions around the flame and then integrated for power radiated. A detailed directionality study should be made. The scaling laws for spectral content should be generated.

The objectives of the experimental program were decided by the needs expressed above. However, only the case of open turbulent flames would be considered because of the simplicity of the burner configuration. The objectives can be listed as follows:

1. To conduct noise experiments on three burners in an anechoic chamber to flow velocities of 600 ft/sec using both fuel-lean and fuel-rich mixtures. These experiments will be called "Acoustic Experiments" and are designed to yield scaling laws for acoustic power, thermo-acoustic

efficiency, and spectral content. Detailed directionality information will also be obtained.

2. To analyze the scaling rules for the volume of the reaction zone. These experiments will be entitled "Direct Flame Photography" since direct flame photography techniques will be employed in reducing the scaling laws. The analysis of the reacting volume will provide an independent diagnostic check for Strahle's theory of combustion noise.

3. To compare the optical and acoustic emission from the flames in order to isolate the origin of combustion noise.

4. To compare the experimental findings with the theories of References 16, 17 and 18.

5. To present the results of the investigation in a form useful to practicing engineers.

Thus, it is believed that this study would lead to a better understanding of the mechanism of generation of combustion noise and provide useful scaling rules for the noise generated by open turbulent flames.

CHAPTER II

ACOUSTIC EXPERIMENTS

The experiments conducted, to determine the scaling rules for acoustic power, thermo-acoustic efficiency, spectral content and directionality of combustion noise generated by open turbulent flames established at the end of burner tubes, are described in this chapter. The measurements are made in the far field since near field information would be too complicated by the phase relationships to be of any real value. Also, theories exist, e.g., References 16, 17 and 18, which enable a study of the mechanism of noise generation based on experimental far field information to be made. The analytical development used in the theories mentioned above shows that there is a unique relationship between the far field radiation and the source behavior. In addition, the far field measurements are of practical significance in evaluating the noise radiation from sources.

Based on an analysis of the literature, the parameters that affect the noise generation from turbulent flames can be recognized as: U, the flow velocity, D, the burner size, S_L, the laminar flame speed, F, the fuel mass fraction, ℓ_t, the scale of turbulence, and $\mathcal{I}$, the intensity of turbulence. In this chapter only U, D, S_L and F are considered since no effort is made to devise methods to vary the turbulence intensity independently. The experiments are designed so that only one parameter is varied at a time, However, S_L and F can not be varied independently of

each other using the same fuel, but combinations of mixture ratios and fuel can be worked out so as to vary either S_L or F independent of the other. Since the scaling rules sought for can be obtained by regression analysis even when both the parameters vary at the same time, equivalence ratio ϕ was used as one of the parameters. In order to identify the various tests conducted the following notation is used.

P —— 100 —— 0.8 —— 1

Fuel			Burner Diameter
P = Propane	Flow Velocity In Ft/Sec	Equivalence Ratio	1 = 0.402"
E = Ethylene			2 = 0.652"
Py = Propylene			3 = 0.96"

Anechoic Chamber

A 13' x 10' x 6' - 6" (working space) anechoic chamber was built in the Aerospace Propulsion Laboratory in order that acoustic measurements be made in conditions close to free field. The chamber would also serve the secondary purpose of preventing drafts around the flame. Figures 1(a) and (b) show the basic construction details of the anechoic chamber. The two walls of the room formed two outer walls of the chamber. The other two walls were constructed with 8" dry gypsum wall stuffed with fiberglas. The basic acoustic insulation was provided by 18" thick fiberglas and a 3" air space between the walls and the fiberglas insulation. The density of fiberglas used was roughly 0.6 lb/cft. The floor and the ceiling were also covered with 18" thick fiberglas although no air gap was provided. A grating floor, provided in the chamber, was

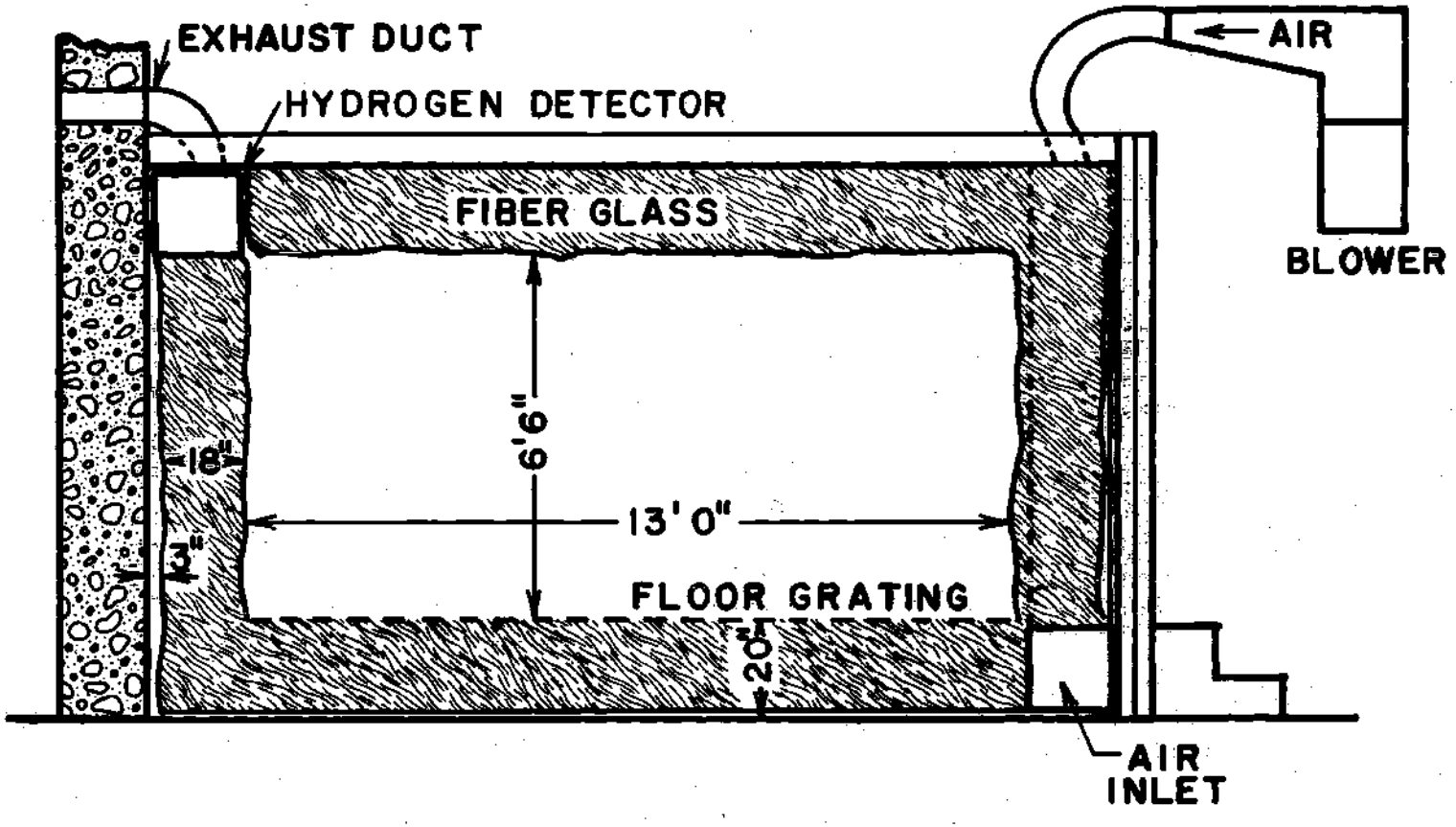

CROSS-SECTIONAL ELEVATION

Figure 1(a). Cross-Sectional Elevation of Anechoic Chamber.

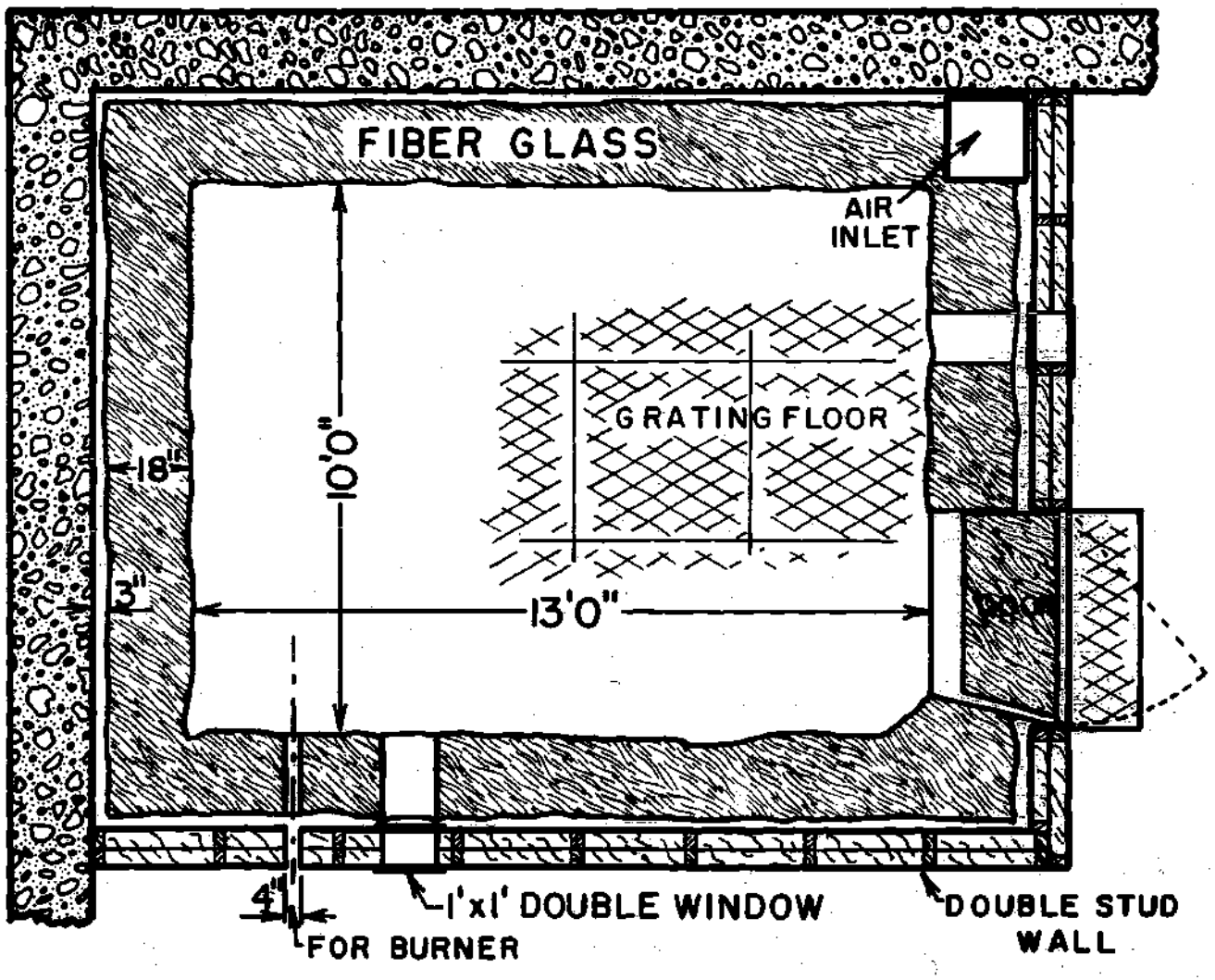

CROSS-SECTIONAL PLAN

Figure 1(b). Cross-Sectional Plan of Anechoic Chamber.

supported on a metal structure. The supporting structure was mounted on $\frac{1}{2}$" rubber pads to isolate structurally carried vibrations to some extent.

The chamber has two windows (1' x 1') so as to keep a close watch on the flame. A hinged door, also with the same thickness of insulation as the walls, provides an entry into the working area. A hydrogen detector has been installed in the ceiling.

The ventilation to the chamber is provided by a blower. The air from the blower passes through a long acoustic duct work and enters the chamber at one of the lower edges. Exhaust ducting with a long and tortuous passage is provided at the opposite edge of the chamber.

The anechoic chamber was tested with an acoustic driver as the source at various discrete frequencies and was found to be reasonably anechoic, in the frequency range of 125 Hz to 5000 Hz, for source to microphone distances of up to 5 ft (Figure 2). However, the ventilation blower was observed to produce low frequency oscillations in the sound meter readings, especially when the sound pressure levels being measured were of the order of 60 db re.0.0002 μ bar (20-20,000 Hz linear). Also, at this level, it was noticed that the external disturbances, such as the laboratory compressors, the air conditioning system, and the noise due to the flourescent tube ballast could add up to 0.5 to 2 db to the measured sound levels inside the anechoic chamber. This suggests that the experiments should be done when all these external disturbances are not operating. The reasons for the appreciable influence of the external disturbances in the anechoic chamber are 1) the chamber is not structurally isolated from other parts of the building, and 2) the walls are made of

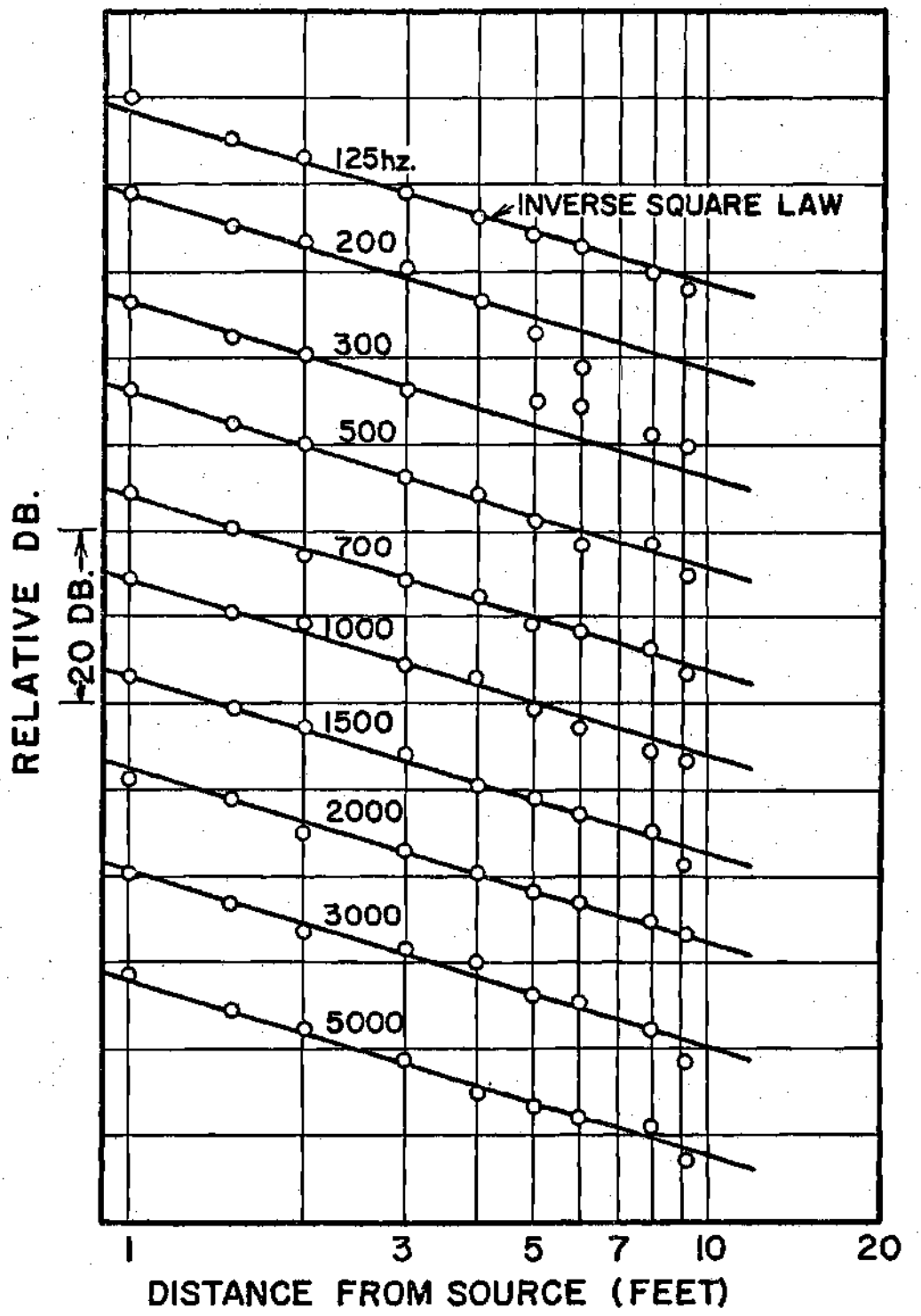

Figure 2. Anechoic Chamber Characteristics .

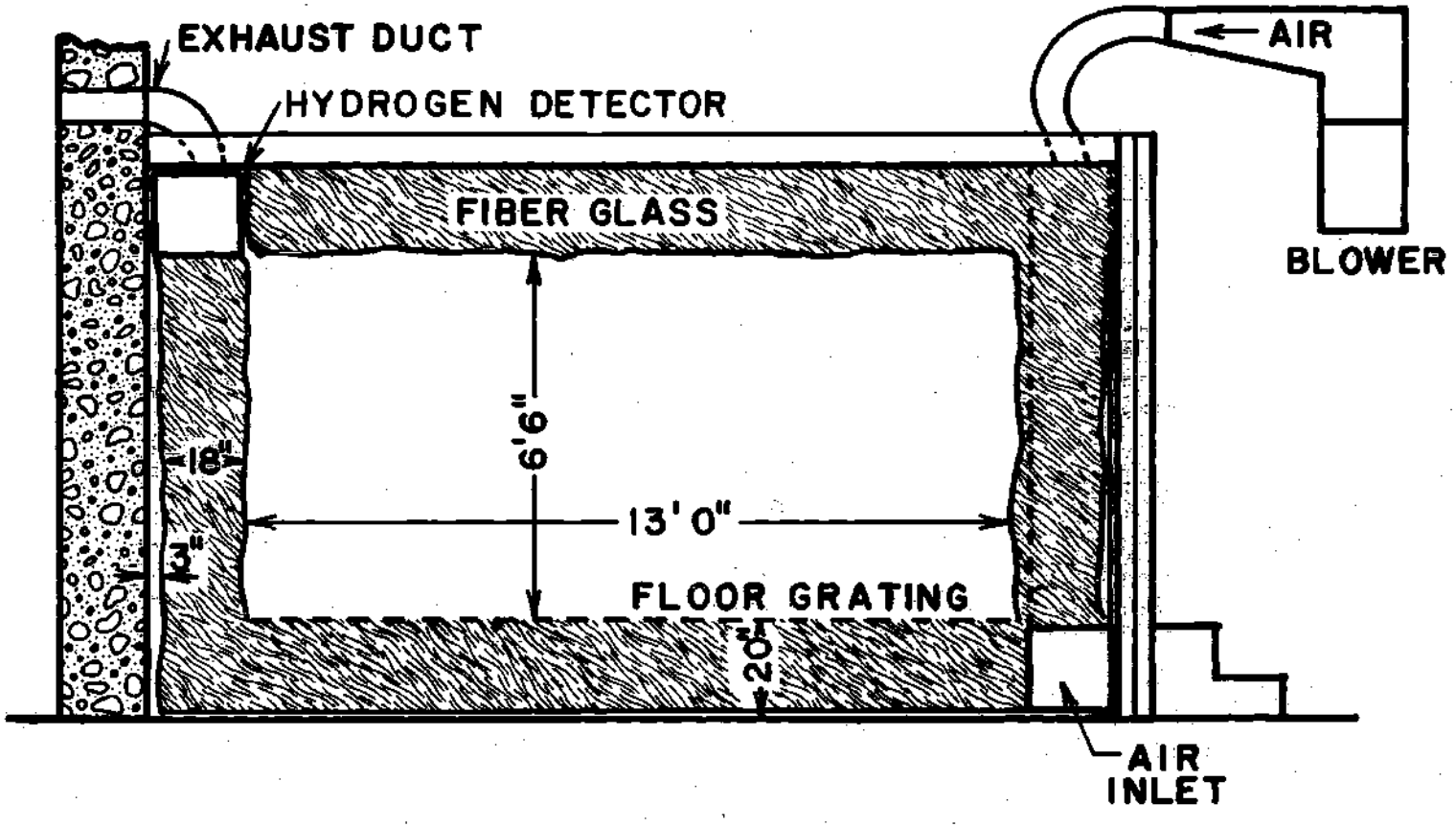

CROSS-SECTIONAL ELEVATION

Figure 1(a). Cross-Sectional Elevation of Anechoic Chamber.

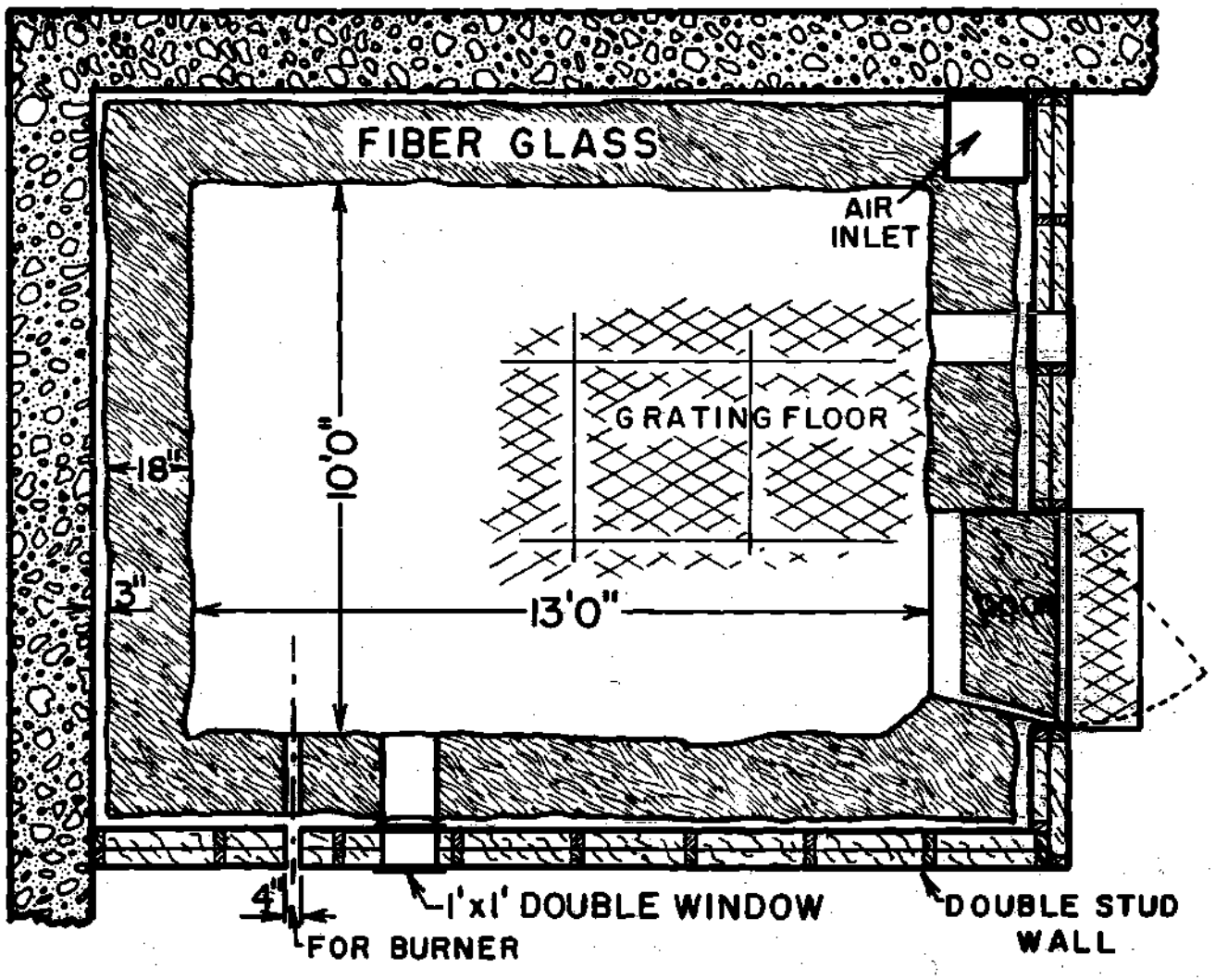

CROSS-SECTIONAL PLAN

Figure 1(b). Cross-Sectional Plan of Anechoic Chamber.

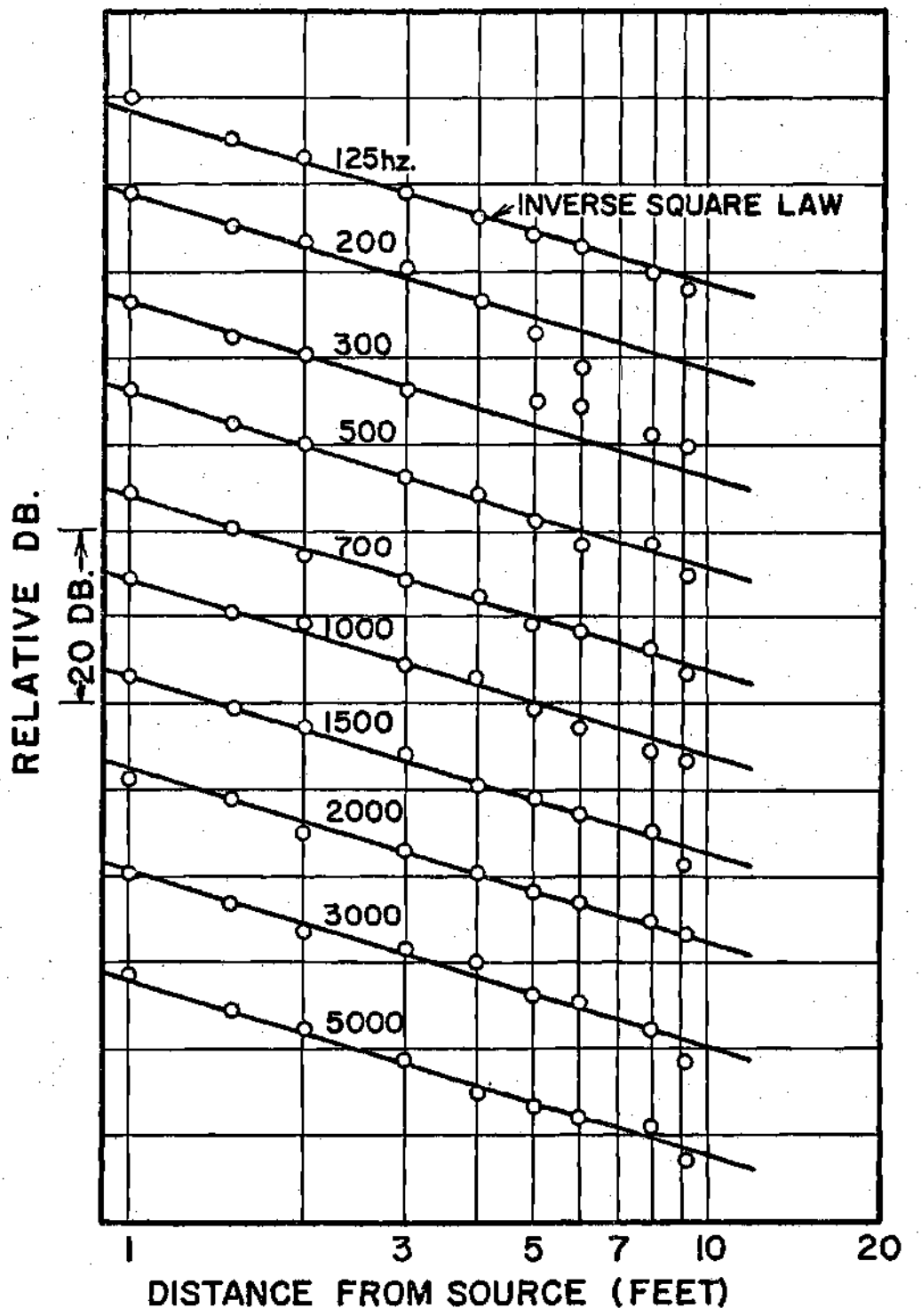

Figure 2. Anechoic Chamber Characteristics .

light-weight construction and are thus fairly inefficient in the prevention of sound transmission through them. In any case, the chamber was designed to have inner walls which are efficient in absorbing the incident sound waves and tests have shown that the purpose has been achieved.

The anechoic chamber has a typical background noise of 52 db re. 0.0002 μ bar (20-20,000 Hz linear). The spectrum of the background noise was nearly flat from 100-10,000 Hz.

Burners and Flow Systems

The burners used in this study have been constructed from coaxial tubing of circular cross section held together by 'Swagelok' heat exchanger T-joints as shown in Figure 3. The mixture of reactants flows through the inner tube and hydrogen for the stabilizing diffusion flames flows through the annular space between the tubes. The burner sizes are 0.402", 0.652" and 0.96" in diameter. The sizes quoted here are the inner diameters of the central tube which determines the size of the flame. The size of the annular gap is less than 1/32 inch in all the three cases. The two smaller burners are built out of copper tubing while the largest burner has a stainless steel inner tube and a copper outer tube. A straight length of 50 diameters is provided for the flow of reactants preceding the burner port. This ensures fully developed turbulent pipe flow conditions at the burner exit. A mixing chamber filled with 4 mm glass balls is introduced in the main burner tube just before the 50 D straight length to aid proper mixing of fuel and air. This mixing chamber, in addition, serves as a flash-back suppressor. The burners are mounted in the anechoic chamber with their axes horizontal at

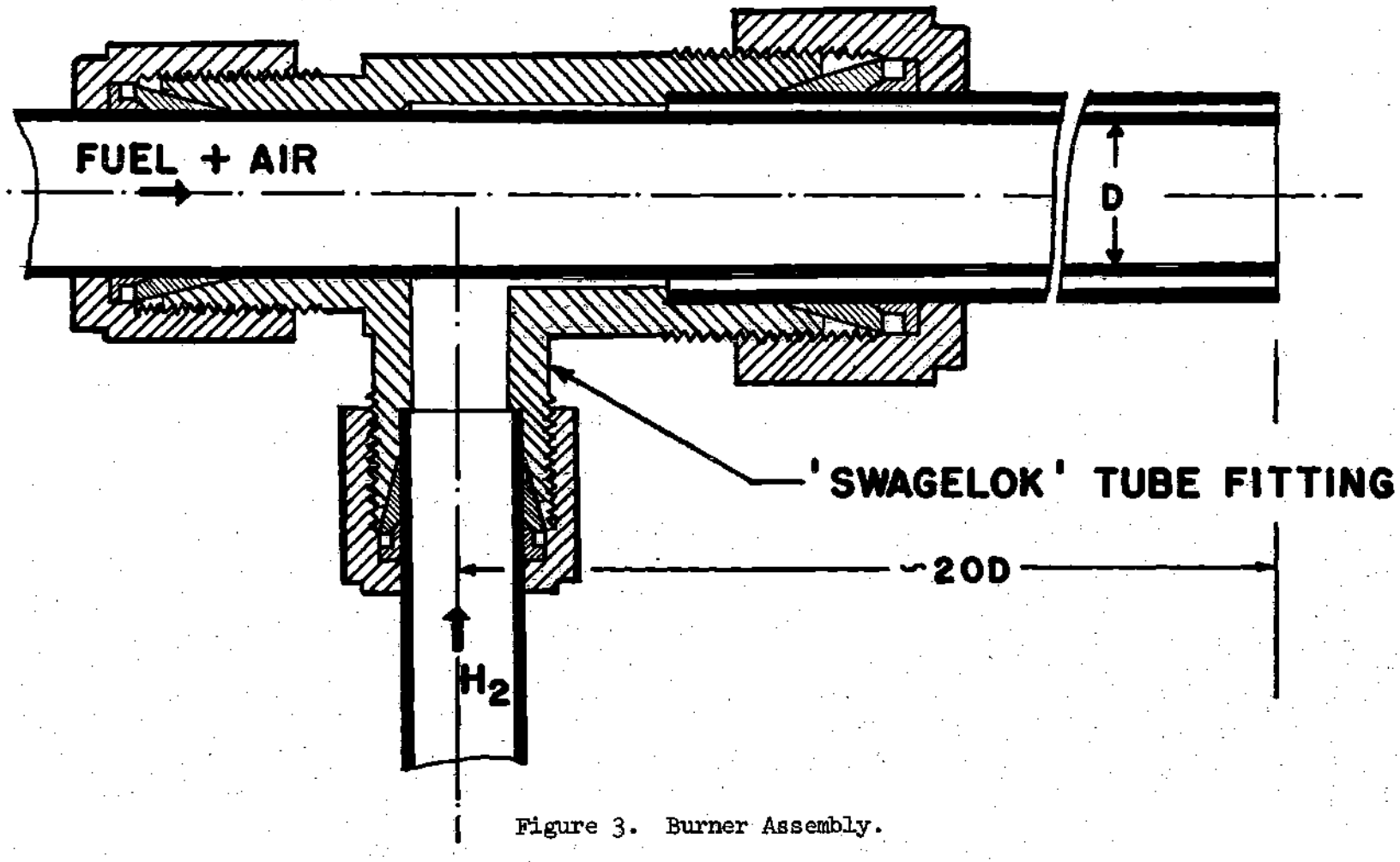

Figure 3. Burner Assembly.

3 ft above the floor grating and at least 2 ft from the walls.

Figure 4 shows the flow system. Air for the experiments is supplied by the 1000 ft^3 125 PSI Air resorvoir. The flow of air is measured by two rotameters with overlapping flow ranges. Fuels and hydrogen are metered by orifice meters; two orifice plates with different orifice dimensions are used on the fuel metering system to cover the entire flow range. The control valve downstream of each flow meter is used to introduce the pressure drop required to maintain a desired upstream pressure at the meter, thus vastly increasing the metering range of each flow meter. Fuels, hydrogen and nitrogen are supplied from gas bottles which are stored outside the room in a separate gas storage area. A muffler is provided in the air line to reduce the flow noises. Also, air leaving the muffler flows through flexible rubber hoses thereby preventing abrupt flow turns which generate flow noises.

The fuel and air are mixed at a T-joint. The hydrogen line entering the anechoic chamber is shrouded by nitrogen. Also, both fuel and hydrogen lines are provided with nitrogen purge.

Instrumentation

Sound pressures are measured by Brüel and Kjaer type 4134 half-inch condensor microphones. Five such microphones mounted on stands in the same horizontal plane as the burner are used. The microphones are placed at constant radius with respect to burner port and at angular locations between 15 and 120° to the flow direction; closer than 15° to the flow direction would be likely to introduce flow noises at the microphone. The outputs of the microphones are directly read out as sound

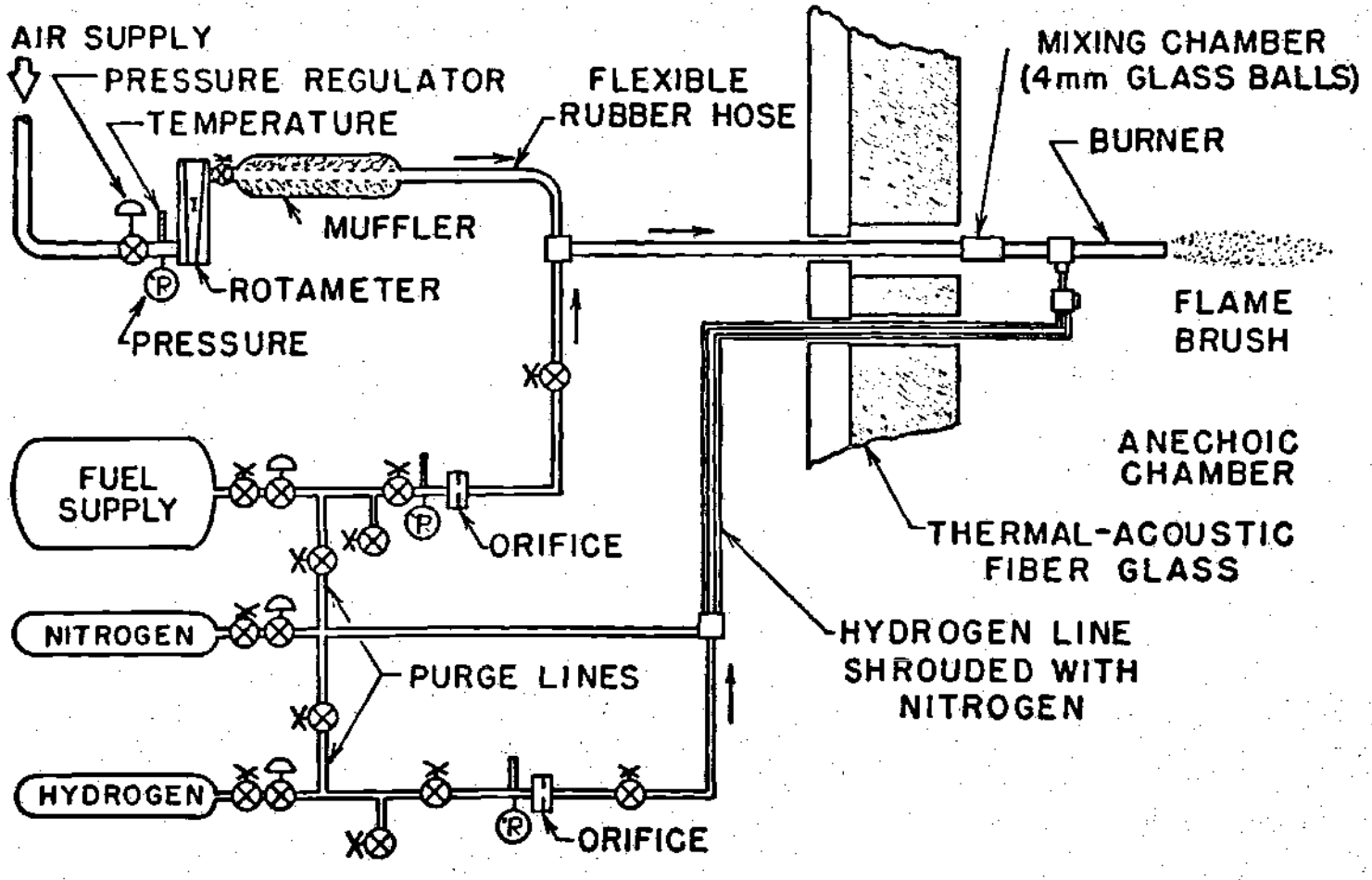

Figure 4. Flow System Schematic.

pressure levels (db re. 0.0002 μbar) on a Brüel and Kjaer type 2604 microphone amplifier, one at a time. They are also amplified by an array of five NEFF type 122 amplifiers and recorded on five channels of an AMPEX FR 1300, 14 channel magnetic tape recorder, usually at 30 ips tape speed. The direct calibration of microphones is done by a Whittaker type PC-125 acoustic calibrator. In order to provide a calibration reference for data analysis the sound output from an acoustic driver, producing a 1000 Hz sound and placed under the burner port, is also recorded on the tape. The sound pressure level at each microphone due to the acoustic driver is read on the microphone amplifier and noted. This procedure enables the calibration of the entire system directly.

The data acquisition and reduction schematic is shown in Figure 5. It can be noticed that only microphones are placed inside the anechoic chamber. The microphone signal carrying cables are brought out of the anechoic chamber through a conduit and connected to the appropriate instruments. The spectral analysis of the noise is performed on a Hewlett Packard type 5645 Fourier analyzer and associated hardware. The spectra are computed digitally using a fast Fourier transform by the machine. A multi-sample averaging technique is used to obtain stable results and eliminate spurious noise from the signal. The output from the Fourier analyzer could be observed on the oscilloscope, plotted on an x-y plotter or printed out on a teletype. In this study x-y plots were preferred over the other modes of output.

Flame Stabilization

The flames were stabilized at the end of burner tubes by an annular

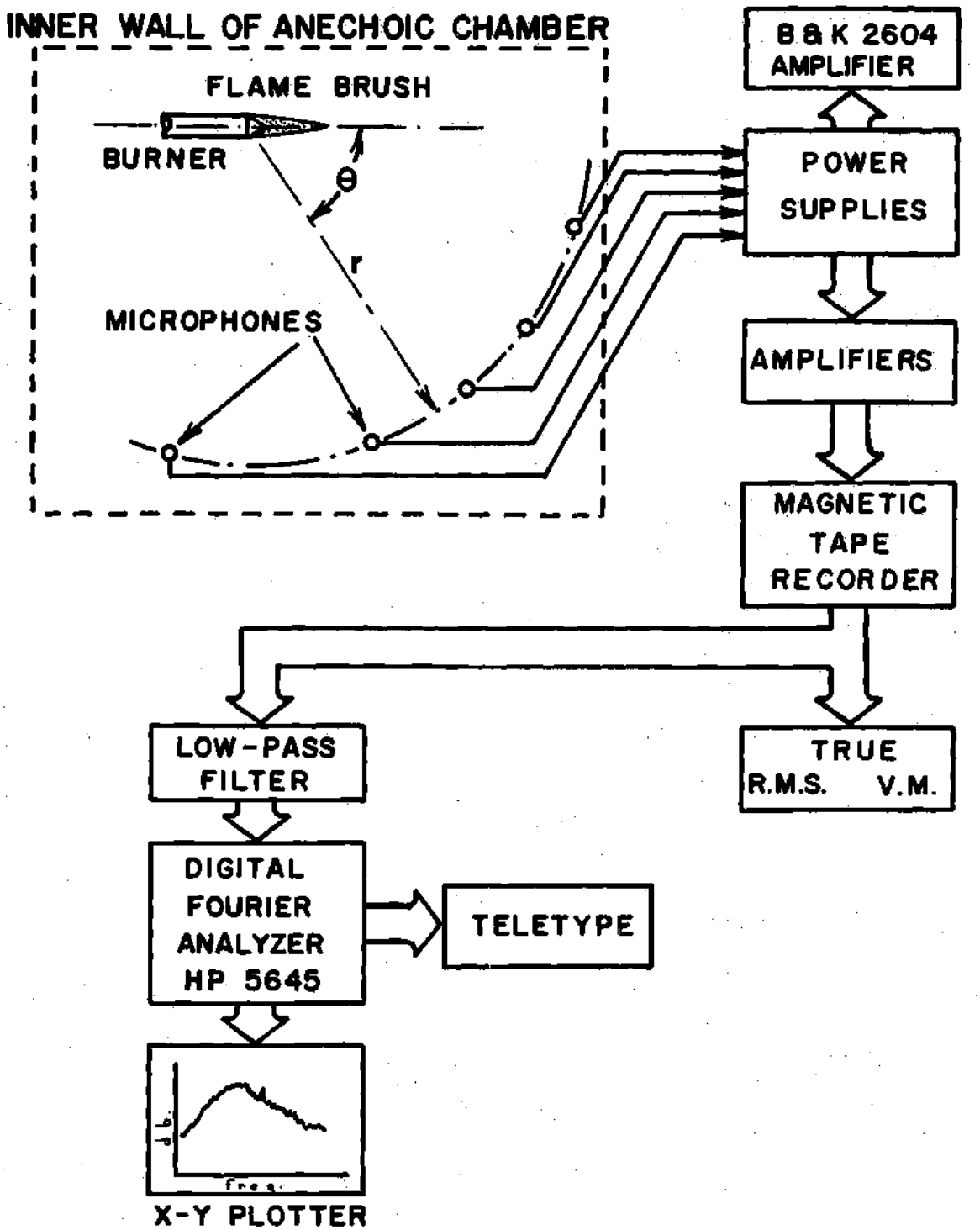

Figure 5. Data Acquisition and Reduction Schematic for Acoustic Experiments.

diffusion flame of hydrogen. Smith and Kilham[3] have studied the effect of various amounts of hydrogen flow on the noise generated. According to their study the optimum amount of hydrogen was found to be between about $2\frac{1}{2}$ to $3\frac{1}{2}$ percent by volume of the main flow. Before using the values for the H_2 required for stabilization from Reference 3, a test measurement was made on one of the typical cases. The result of this experiment is shown in Figure 6. This result is in essential agreement with the results of Reference 3 and, therefore, in all the experiments $2\frac{1}{2}$ percent hydrogen has been used since this would contribute the least to the overall noise output. Although this quantity of hydrogen was found satisfactory in most of the experiments, the flames of velocity greater than 300 ft/sec on a 0.402" burner required 5 percent for satisfactory stabilization of the flame.

Combustion Noise and Jet Noise

The relative importance of combustion noise in comparison with the noise from a pure jet of the same velocity, and also the air jet plus pilot flame combination, is presented in Figure 7. The microphone azimuth of 55° to the flow direction was chosen so as to be somewhat close to the direction of predominant radiation for all three cases. Combustion noise dominates over the entire velocity range from 50 ft/sec to 600 ft/sec. An interesting observation made during these experiments was that the hydrogen diffusion flame was by itself very quiet. However, when the main stream of air was turned on the flame would interact with the outer boundaries of the turbulent jet close to the burner exit and enhance the noise output from the air jet.

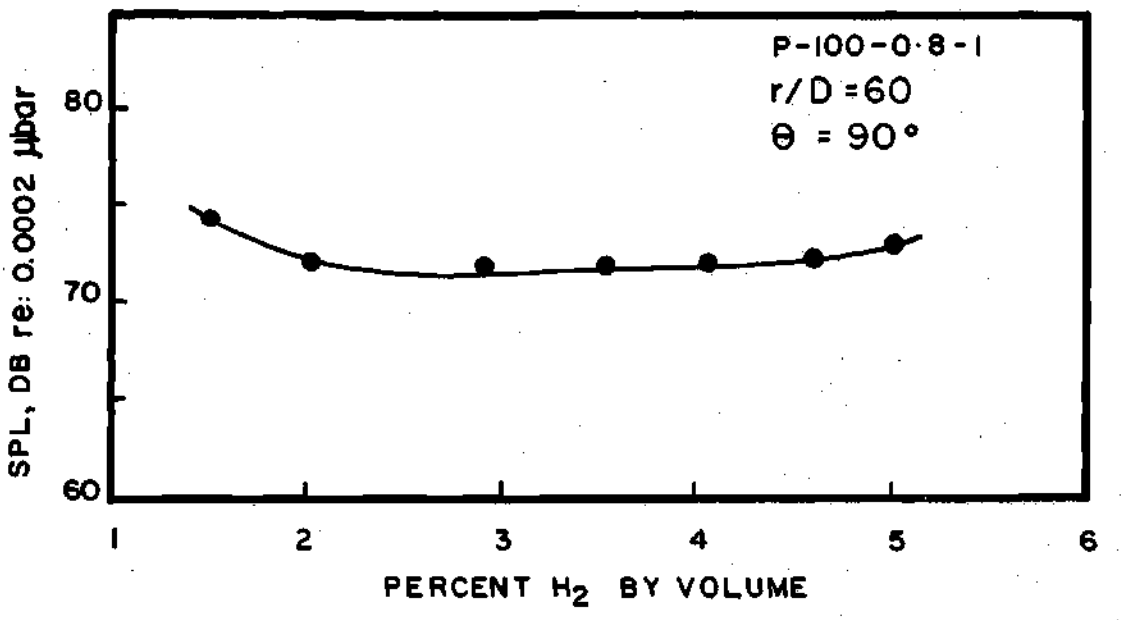

Figure 6. Effect of the Quantity of Hydrogen Used for Flame Stabilization on Overall Noise Level.

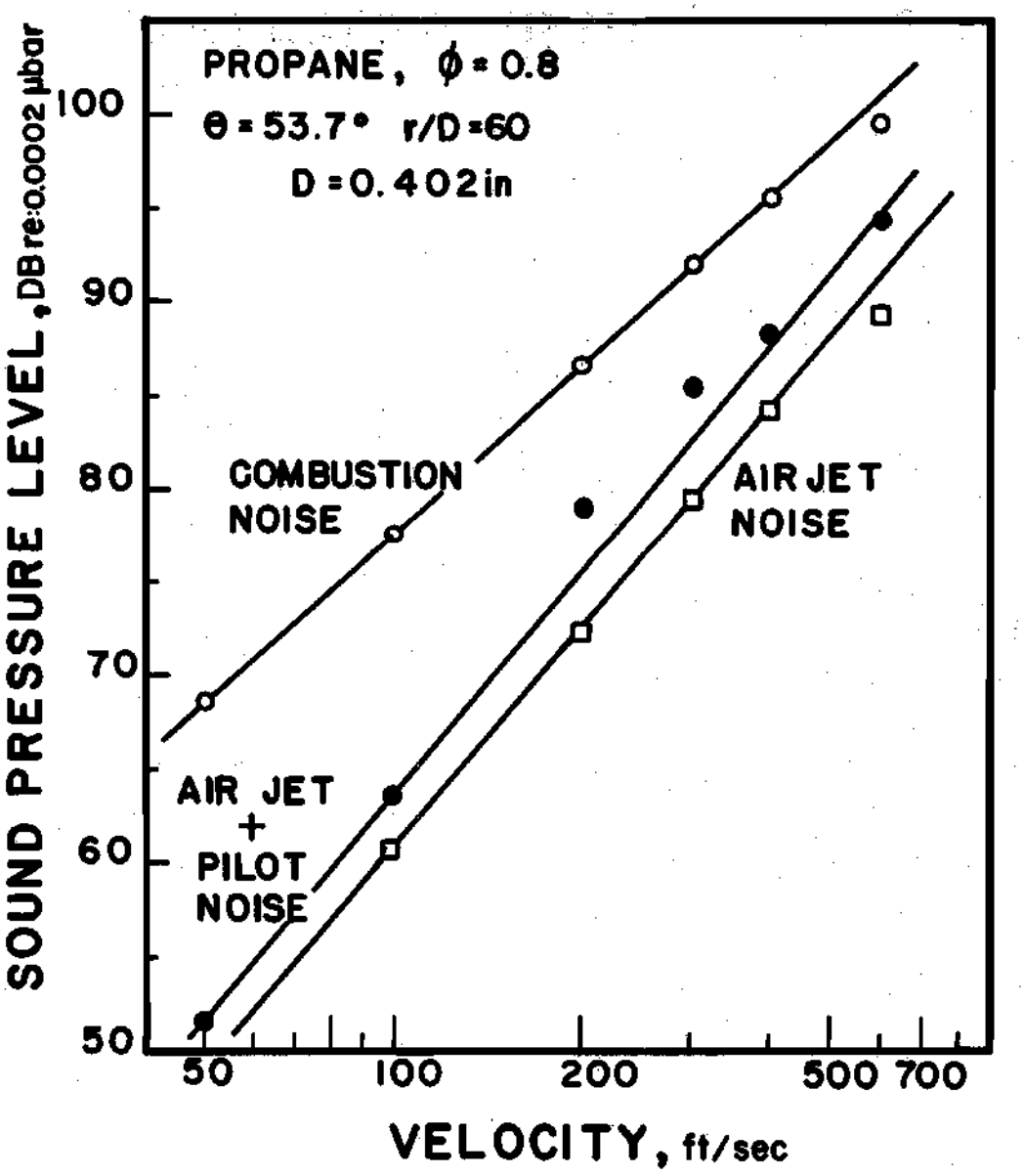

Figure 7. Jet Noise, Combustion Noise and Air Jet plus Pilot Flame Noise at Various Flow Velocities.

The results shown in Figure 7 can be used to determine the approximate scaling laws for power radiated if, for the present, directionality is neglected. The jet noise appears to follow a U^4 law for acoustic power while combustion noise favors an exponent of 2.8. Because of the higher exponent on U the difference between the combustion noise and the jet noise decreases with velocity. Nevertheless, even at 600 ft/sec combustion noise is predominant.

Sound Pressure Measurement

The sound pressures were measured by a B & K type 2604 microphone amplifier using 20-20,000 Hz linear response with the meter set to slow response. In most cases, the meter excursions were less than a db and, in accordance with standard practice[23], the arithmetic mean between the maximum and minimum readings was taken as the sound pressure level. In doing this any occasional highs and lows of the meter readings should be neglected.

As explained earlier, the locations of the microphones are determined with respect to the burner port and the flow direction. For computation of the acoustic power radiated and the directionality it is necessary to reference the sound pressures measured to the acoustic center in the flame. Acoustic center is a point within the noise generating region from which the noise would appear to originate to a far field observer. There is both experimental[8,9] and theoretical[17] evidence to show that the noise emitters in the case of combustion noise are confined to the visible region of the flame. Thus, it can be considered reasonable to state that the acoustic center in the flame would be located at the

point of maximum volume per unit length as determined by direct photographic flame volume measurements. These measurements are explained in detail in the next chapter.

Figure 8 shows sound pressure level distributions along a line parallel to the flow direction, i.e., parallel to the length of the flame. The distance between the microphone and the axis of the burner was kept constant at 9-7/8". If the noise radiation from the flame were spherically symmetric the location of maximum sound pressure level would correspond to the acoustic center. However, since the acoustic radiation from the flame is weakly directional in the forward 90°, the observed maximum will get shifted towards the flame tip. This shift will depend upon the distance between the burner axis and the microphone as well. In the light of these facts the location of the acoustic center cannot be obtained from Figure 8. The acoustic center locations as decided by direct flame photography have been indicated on the sound pressure level traces. It can be noticed that the acoustic center locations do consistently fall below the maximum sound pressure level location.

In order to determine whether the calculation of acoustic power radiated from the flame is very sensitive to the inaccuracies in locating the acoustic center, certain calculations have been made for three typical cases. The acoustic power radiated* was evaluated assuming that the acoustic center lay at a) the location of maximum flame volume per unit length and b) the tip of the flame. Table 1 presents the results of these calculations. Even with a rather drastic shift of the acoustic center to the flame tip the error introduced is less than 0.4 db.

* See page 33 for details.

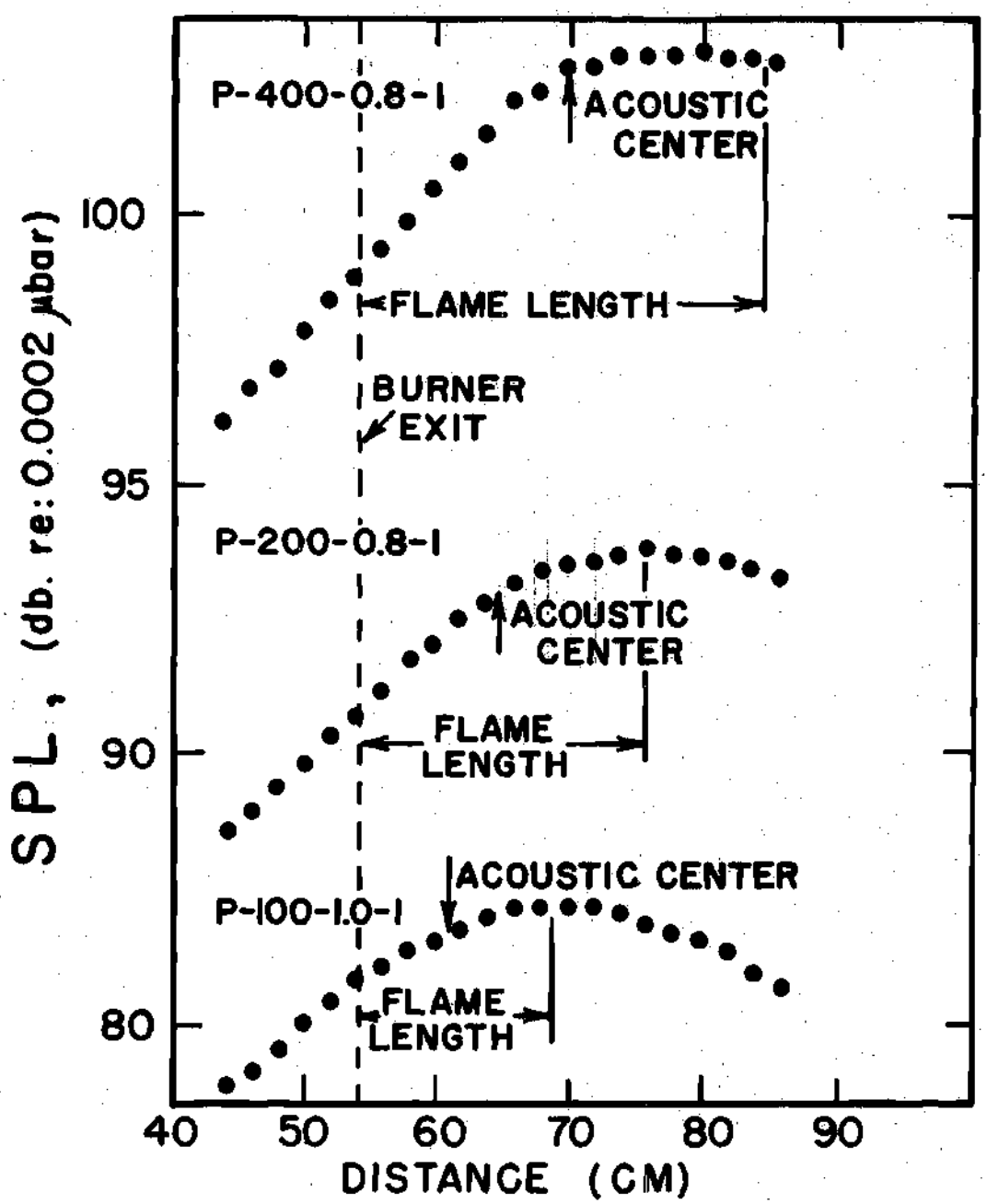

Figure 8. Sound Pressure Levels Along a Line Parallel to the Flame Length 9.875" Below the Burner Axis.

Table 1. Errors in Acoustic Power Due to Inaccuracy in Locating Acoustic Center

Test	Acoustic Power, Watts W_1 Acoustic Center at Max Flame Volume Per Unit Length Location	Acoustic Power, Watts W_2 Acoustic Center at Flame Tip	Difference DB $(= 10 \log_{10} \frac{W_2}{W_1})$
P-100-1.0-1	0.3650×10^{-3}	0.3564×10^{-3}	-0.1
P-200-0.8-1	0.1700×10^{-2}	0.1624×10^{-2}	-0.2
P-400-0.8-1	0.1121×10^{-1}	0.1030×10^{-1}	-0.38

After having established the location of the acoustic center from flame photography experiments, the measured sound pressures were corrected for both geometry and magnitude to account for the change in origin. In the process of calculating the altered values of sound pressures, spherical divergence was assumed since the measurements are in the far field. To the corrected sound pressures a polynomial relation,

$$p^2 = \frac{1}{r^2} \sum_{n=0}^{3} a_n \cos^n \theta \qquad (6)$$

suggested by the theory in Reference 18, was fitted by the method of least squares using all the five sound pressure readings. This polynomial in cos θ was found to fit the data very closely. The maximum error was ± 1 db which is of the same order of magnitude as the accuracy of the instrumentation itself.

Calculation of Acoustic Power Radiated

The acoustic power radiated from the flame is calculated, from the polynomial relation for sound pressure with θ, by integration over a sphere of some radius r assuming axial symmetry. For values of sound pressures beyond the last microphone angular location, the value obtained for the last location was used. To determine the order of magnitudes of the errors involved due to such an extrapolation, three representative experiments were conducted in which a single microphone was traversed around the flame up to 170° with the flow direction. Figure 9(a) shows the microphone traverse used. The sound pressures measured were corrected for the acoustic center and a polynomial in cos θ was fitted to these readings. Figure 9(b) shows a comparison between the single microphone directionality pattern and the one from five fixed microphones. The comparison is quite favorable and is within the accuracy of ± 2 db. More important, however, is the error involved in calculating acoustic power based on 5 microphone data. The power calculated from one microphone covering up to 170° does not involve any appreciable extrapolation and hence is considered to be the true estimate. Table 2 presents a comparison of the acoustic power values due to both cases. It can be seen that the error due to the extrapolation is not excessive. The use of five fixed microphones is preferred from a practical standpoint since the time required for sound pressure measurement is drastically reduced compared to the time it would take to traverse one microphone around the flame. On quite a few tests, the heat input was so high (~ 100 kw) that the duration of the tests had to be restricted to a fraction of a minute to keep the anechoic chamber from getting over-

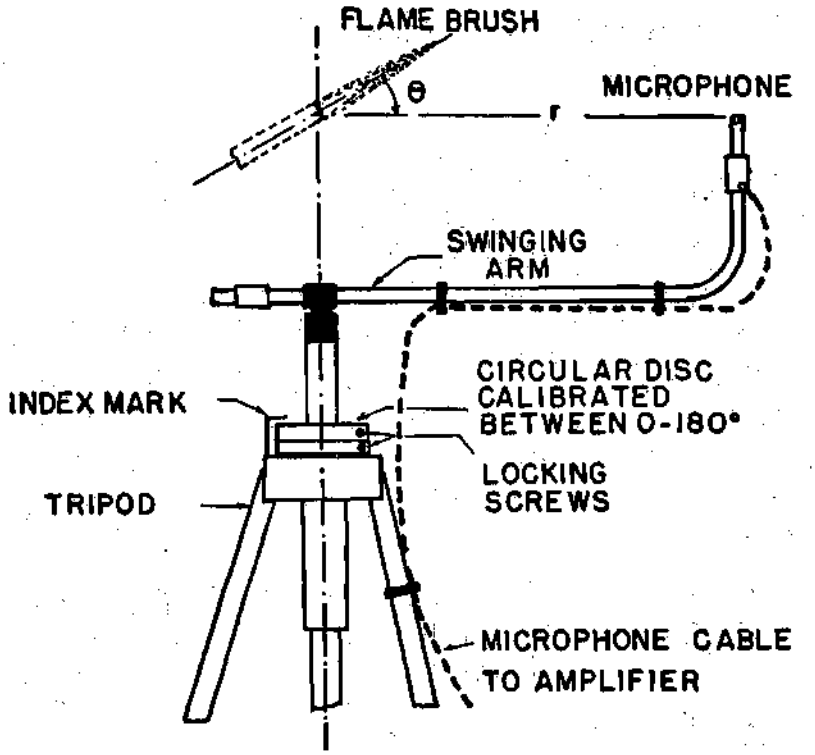

Figure 9(a). Microphone Traverse (Schematic).

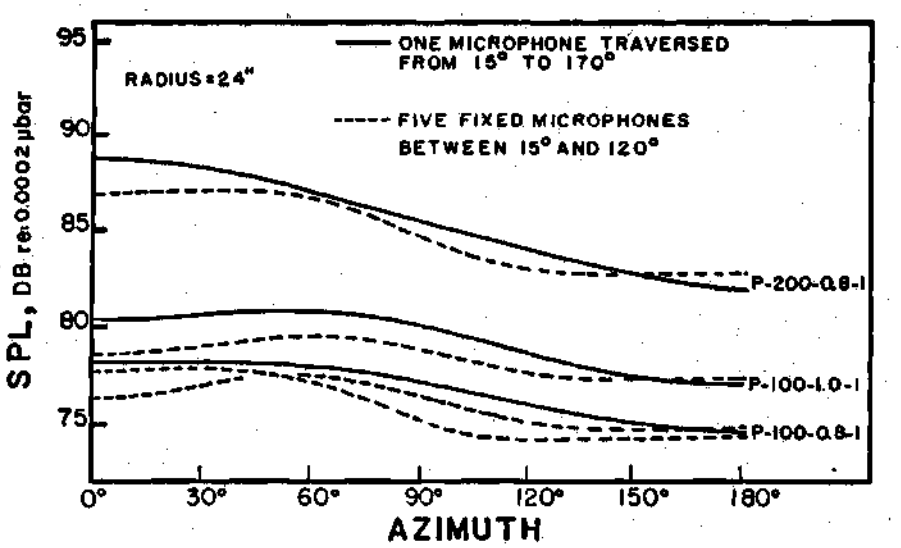

Figure 9(b). Comparison Between Directionality Patterns Obtained by Using Five Fixed Microphones and by Traversing a Single Microphone.

Table 2. Error in Acoustic Power Due to Using Only Five Microphones to Measure the Sound Field Around the Flame

Test	Acoustic Power, Watts W_1 One Microphone Covering 15° - 170°	Acoustic Power, Watts W_2 Five Fixed Microphones Covering 15° - 120°	Difference DB $(= 10 \log_{10} \frac{W_1}{W_2})$
P-100-0.8-1	0.2266×10^{-3}	0.1826×10^{-3}	0.94
P-100-1.0-1	0.4286×10^{-3}	0.3199×10^{-3}	1.28
P-200-0.8-1	0.1790×10^{-2}	0.1536×10^{-2}	0.66

heated.

Another source of error in the calculation of the acoustic power is the temperature variation in the anechoic chamber. This affects the characteristic impedance ($\rho_o a_o$) of the medium (air) through which noise is transmitted from the flame to the microphone. However, $\rho_o \propto 1/T$ and $a_o \propto \sqrt{T}$, so that $\rho_o a_o \propto 1/\sqrt{T}$. The temperature in the anechoic chamber, during the various experiments of this study, was found to lie in the range of 70° - 95°. Thus, without committing much error the temperature variation in the chamber could be neglected. Therefore, for all experiments, it was assumed that the temperature inside the anechoic chamber was 70°F.

Referring back to Figure 9(b), two traces (corresponding to 5 fixed microphone data) are presented for the P-100-0.8-1 case. These are from the same experiment repeated on two different days. The difference in the power calculated between the two traces is about 0.3 db which shows good repeatability of data. However, the tests of equivalence ratio of 0.6 had a tendency to be rather unstable and, consequently, the repeatability in such instances was not as good. Some experiments of $\phi = 0.6$ case could reproduce only within a $\pm$ 2 db limit.

Experimental Results for Fuel-Lean Flames

Directionality of Noise Radiation

The directionality of the far field radiation from a source can give some indications regarding the nature of the source. At the same time, the directional information is required for deciding the most effective locations for acoustic liners. The directionality patterns

presented here are the polynomials in cos θ (i.e., see Equation (6)) fitted to experimental sound pressure measurements as explained earlier in this chapter. The origin of reference is the acoustic center in the flame and the azimuthal positions are measured from the flow direction. The difference between the maximum sound pressure level observed (any θ) and the value at the axis (θ = 0) for a constant radius traverse in the plane of the flame can be considered as a quantitative measure of the directionality of the source.

Figure 10 shows the directionality patterns at various flow velocities for propane-air flames of equivalence ratio 0.8. It can be seen that the effect of velocity on the directionality is to shift the maximum sound pressure location closer to the axis of the flame. The convection of sources by the flow causes this shift towards the axis with an increase in flow velocity.

The effect of burner diameter on the direction of maximum sound radiation can be seen in Figure 11. Results are obtained for all the three fuels, propane, propylene and ethylene. The sound pressure levels have been converted to refer to a radius of 57" and are plotted on the graph instead of quoting all the results at a certain r/D distance. This was done so as to be able to observe the amplitudes of noise from the three burners at the same distance from the source. Figure 11 shows that there is a distinct effect of diameter on the directionality pattern. With an increase in diameter the peak in the directionality curve shifts away from the burner axis, an effect opposite to the velocity influence. Another effect due to an increase in burner diameter appears to be increased directionality. Furthermore, comparing traces from various

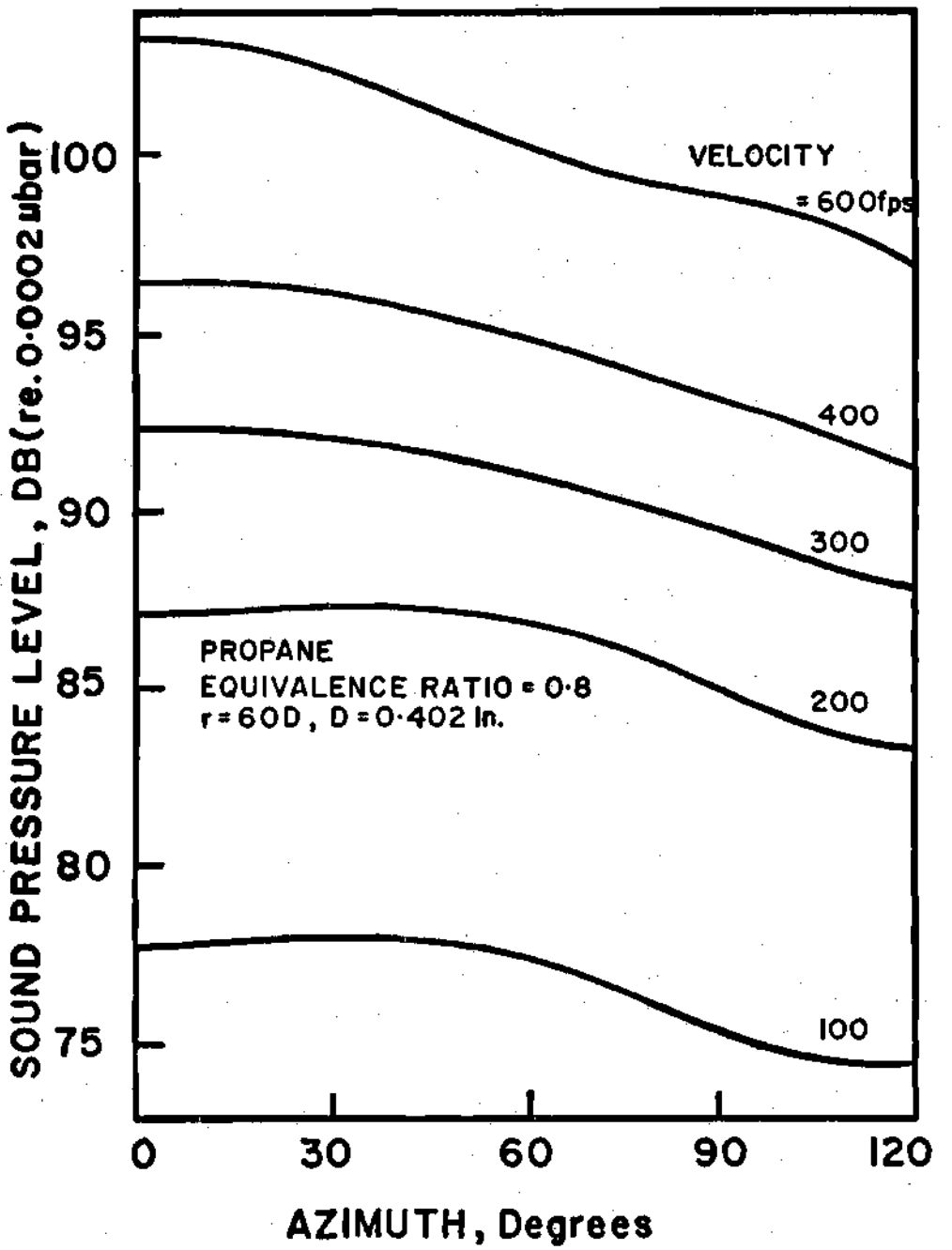

Figure 10. Directionality as a Function of Flow Velocity.

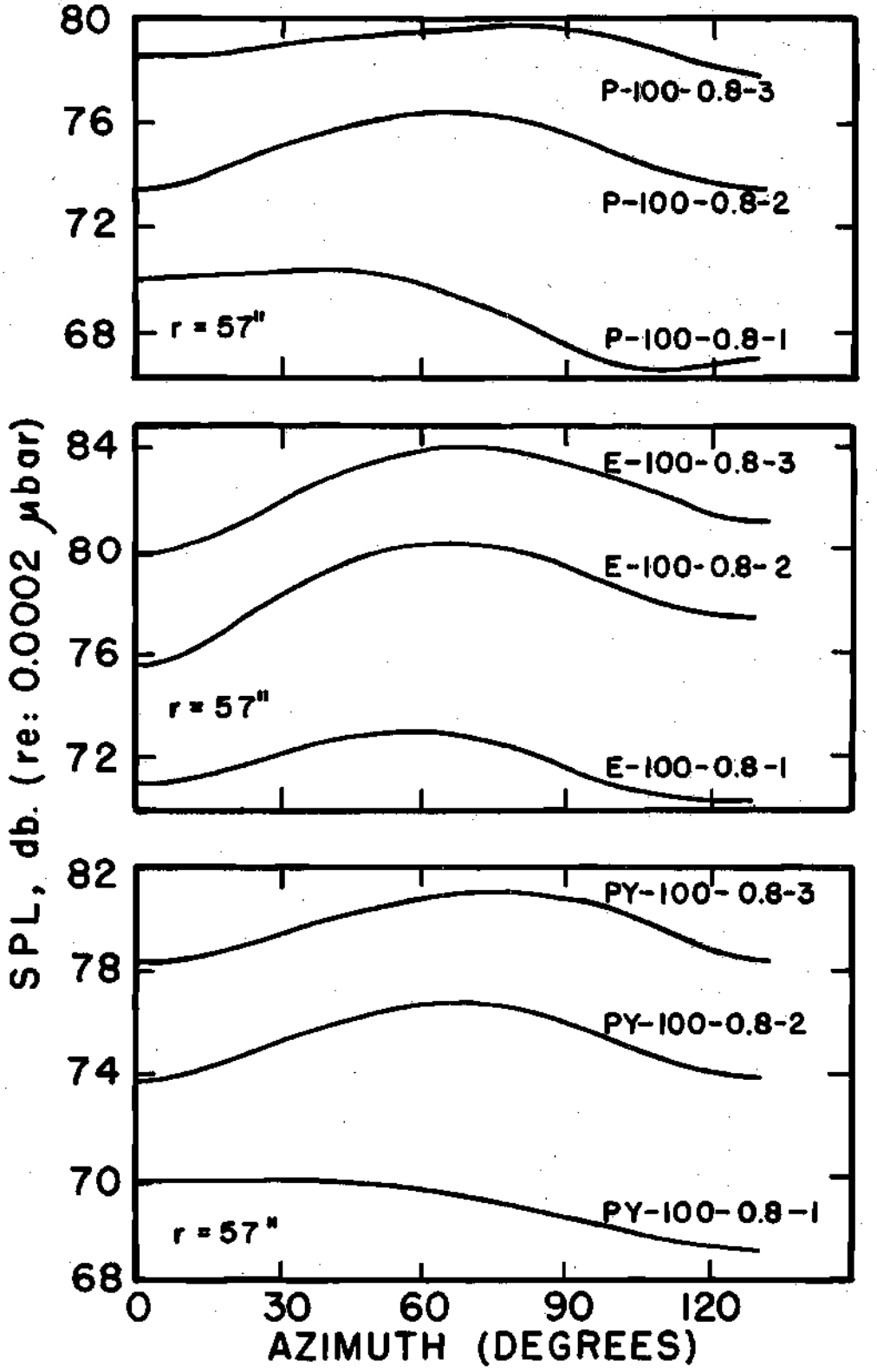

Figure 11. Directionality as a Function of Burner Diameter.

fuels, ethylene-air flames exhibit a stronger directionality than either the propane-air or propylene-air flames.

Directionality curves as a function of equivalence ratio are plotted in Figure 12. The range of ϕ included is between 0.6 and 1.0; that is, from fuel-lean to stoichiometric. The effect of equivalence ratio on directionality can be seen to be very minor. Again, ethylene cases show maximum directionality.

Scaling Laws on Acoustic Power Radiated

Velocity Scaling. Velocity of the reactants is one of the primary parameters that influence noise radiation from regions undergoing turbulent combustion. Here, the behavior of acoustic power as a function of velocity is presented in Figures 13 and 14. In Figure 13 the acoustic power radiated is plotted as a function of mean velocity of reactants at the burner exit for all the three fuels, propane, propylene and ethylene. The equivalence ratio is 0.8 and the burner diameter is 0.402". Over a 12:1 velocity range, a $U^{2.9}$ law is seen to be appropriate for acoustic power radiated. The ethylene flames appear noisier, which will be seen to be a laminar flame speed effect in the succeeding paragraphs. Also, ethylene data points appear to prefer an exponent on mean flow velocity slightly lower than 2.9. Figure 14 shows the results obtained for 0.652" and 0.96" burners. There is a good agreement with the scaling law obtained for a 0.402" burner, although in this case, a $U^{2.6}$ law fits the data better. This result is in agreement with the results of Reference 17 which predicted a velocity scaling exponent to be greater than 2. Also, this velocity exponent is much lower than the velocity scaling for subsonic jet noise[19,20].

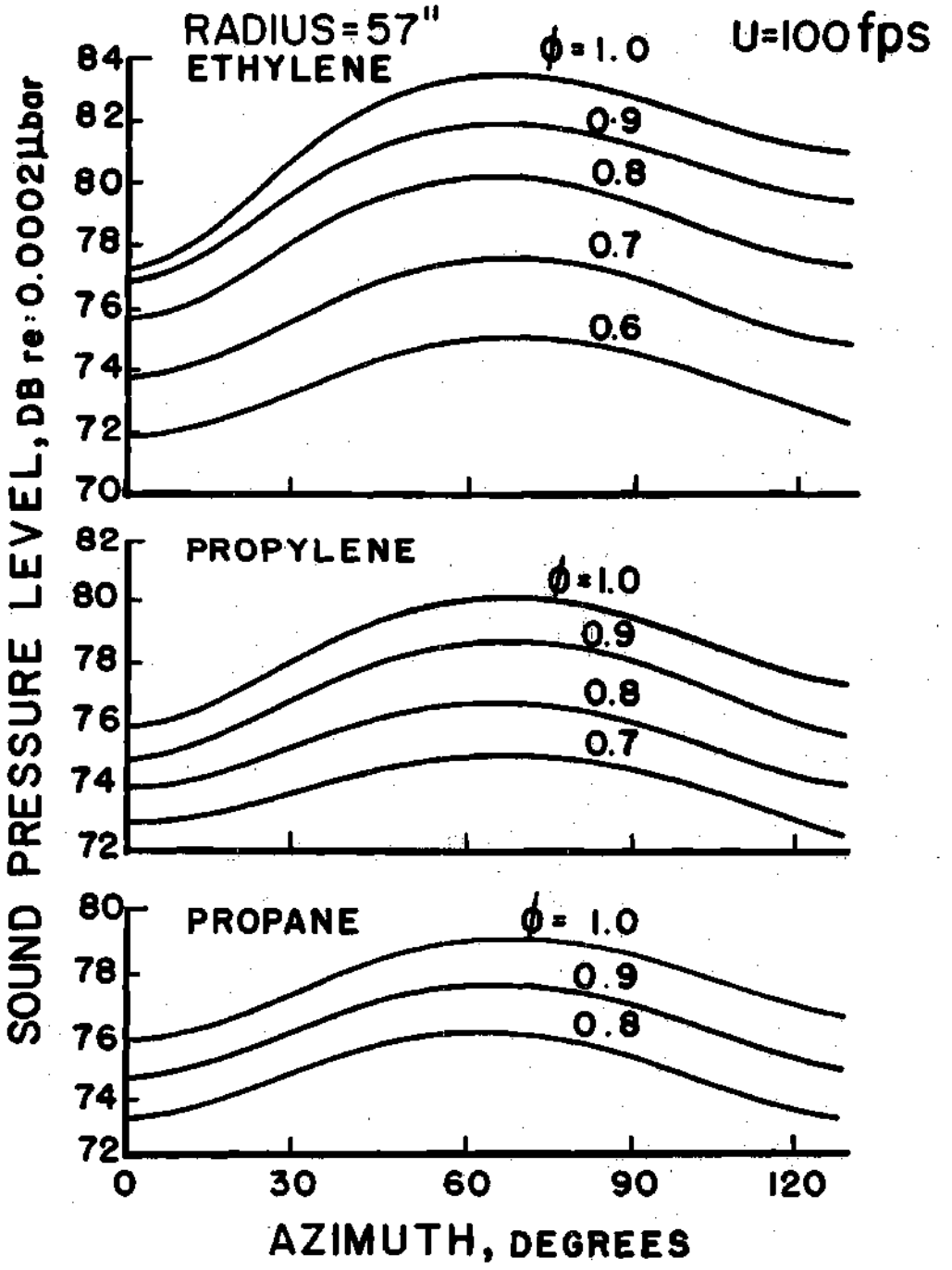

Figure 12. Effect of Equivalence Ratio on Directionality for a Burner of Diameter 0.652".

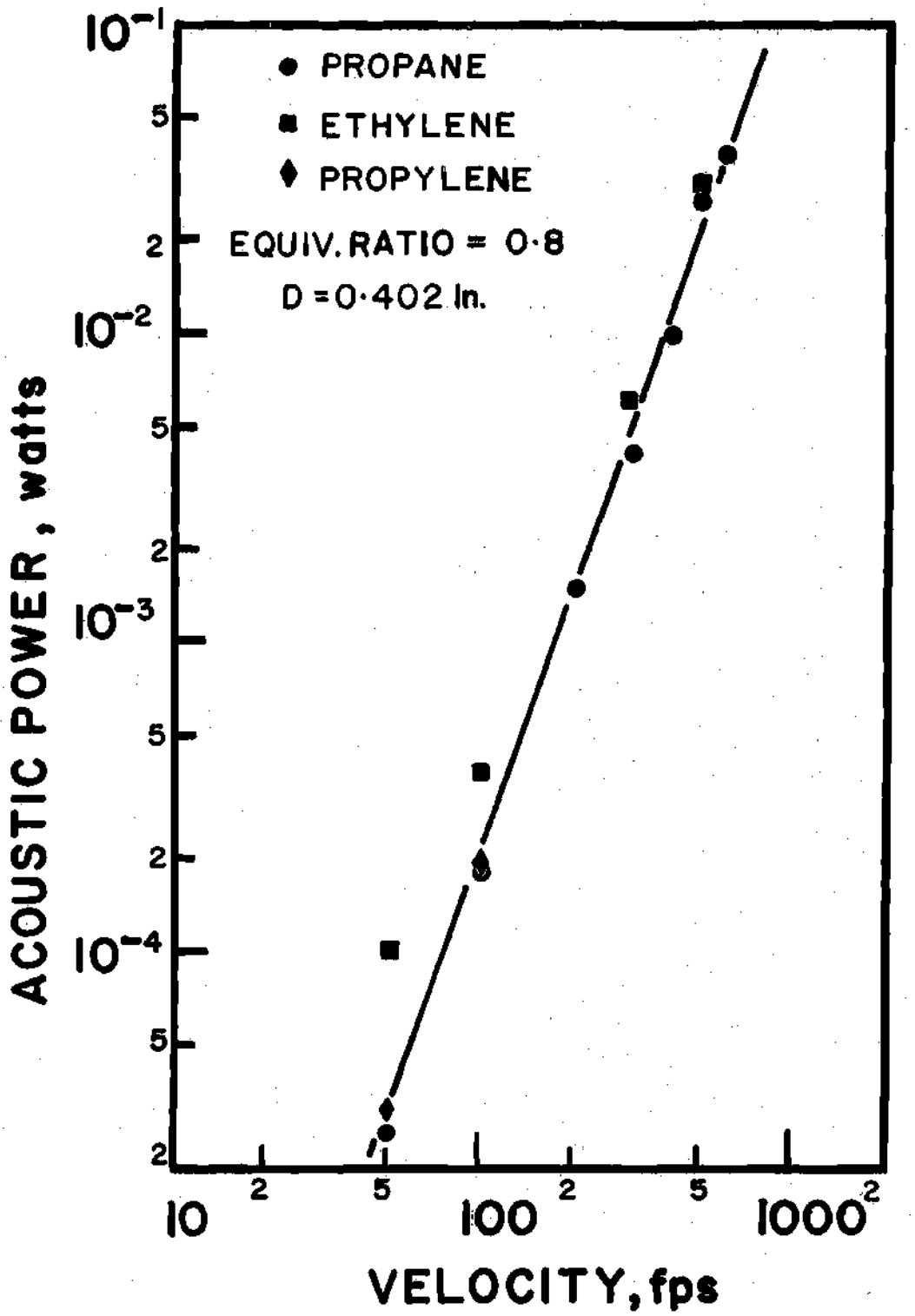

Figure 13. Acoustic Power as a Function of Velocity for a Burner of Diameter 0.402".

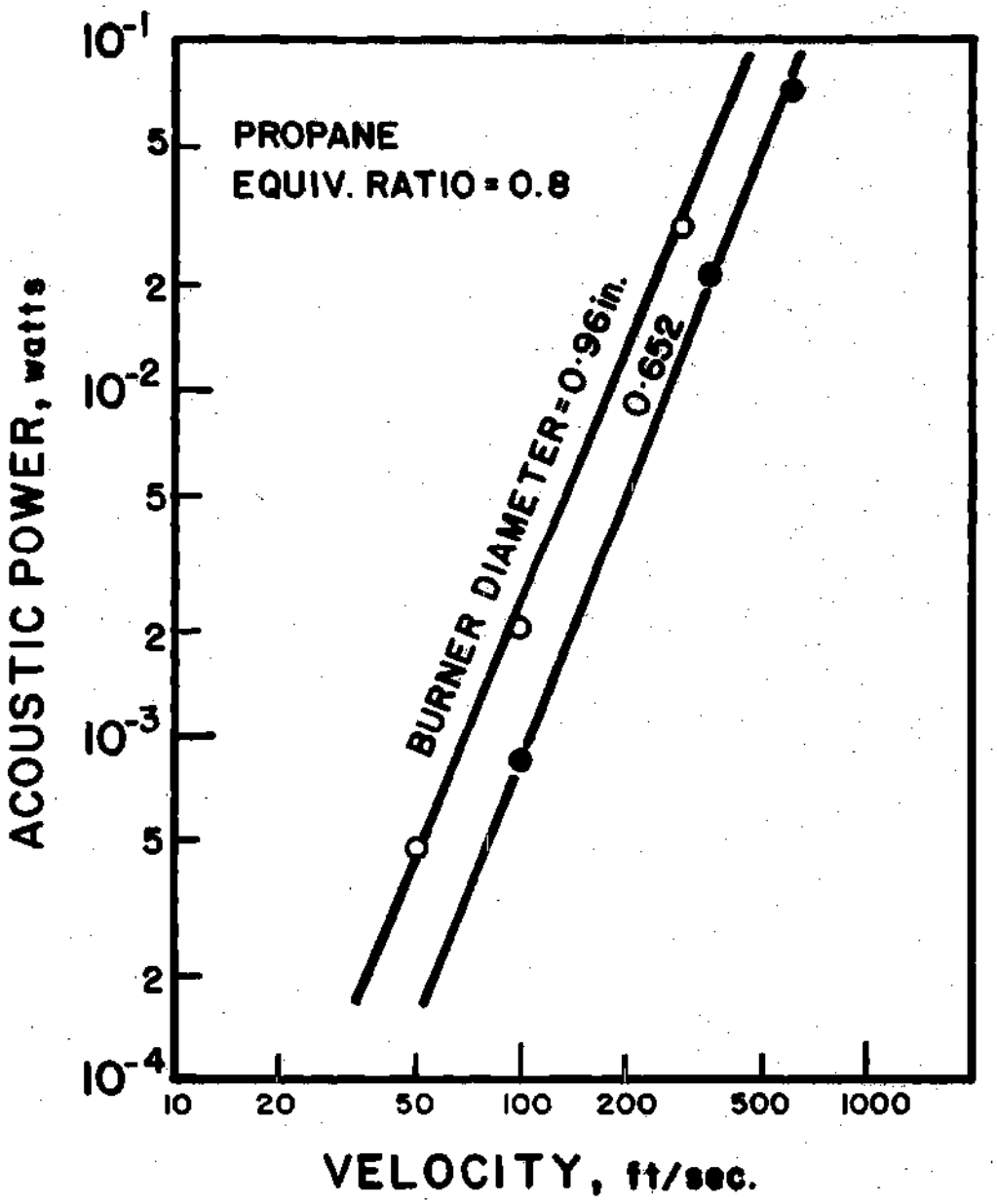

Figure 14. Acoustic Power as a Function of Velocity for Burners of Diameters 0.96" and 0.652".

Diameter Scaling. The diameter of the burner is yet another parameter of interest in noise radiation from flames. A positive exponent of U obtained in the preceding paragraph would suggest lowering of flow velocity to decrease noise output. This would imply that burner size would have to be increased to maintain the same mass flow. The effect of diameter, therefore, becomes quite important. Primarily, the knowledge of the diameter effect is required in order to predict the noise output from larger burners.

Figure 15 shows the results of the experiments conducted to determine the diameter effect. An acoustic power scaling of $D^{3.0}$ is obtained in the case of all the three fuels. The effect of decreasing flow velocity can now be considered. For a burner of circular cross section the mass flow is given by

$$\dot{m} \propto \rho_o U D^2 \qquad (7)$$

Thus, reducing the velocity by a factor of 4, say, would mean increasing diameter by a factor of 2 to maintain constant $\dot{m}$. Since the noise exponents on U and D are almost equal to each other, there seems to be a definite advantage in choosing the lowest value of the flow velocity possible within the other design restrictions.

Laminar Flame Speed Scaling. Laminar flame speed, S_L, is a measure of the reactivity of the fuel. It represents the velocity of propagation of a laminar flame through a reactive mixture. For turbulent flames, a turbulent flame speed, S_t, could be defined. There is sufficient

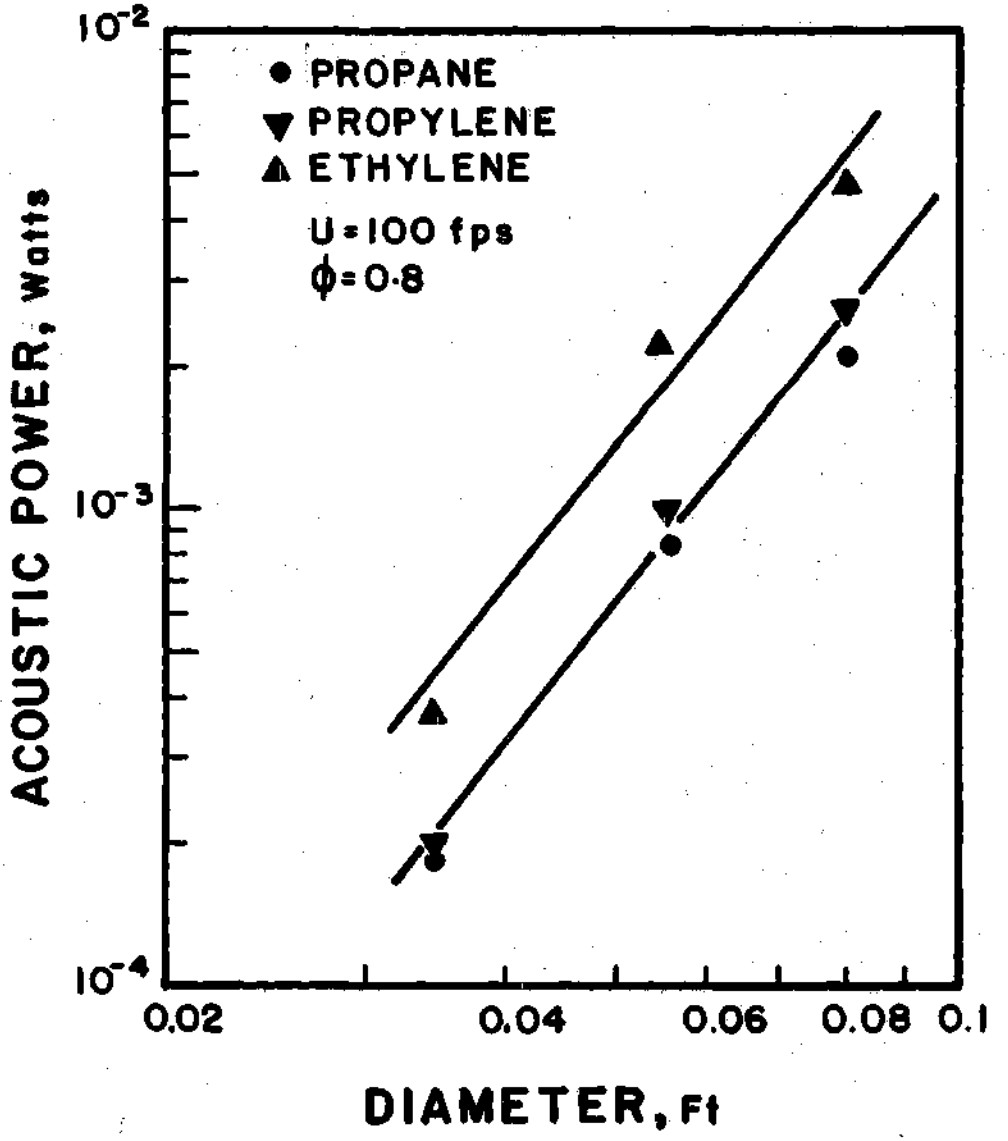

Figure 15. Acoustic Power as a Function of Burner Diameter for Fuel-Lean Flames.

evidence[24] to show that turbulent flame speed is proportional to laminar flame speed; S_t is always higher due to faster transport processes in a turbulent flame. Further, S_t is dependent on flow conditions as well. Thus, if flow conditions like mean flow velocity, turbulence intensity and scale are being considered independently, laminar flame speed would appear to be the correct parameter to choose. In this analysis, therefore, laminar flame speed has been chosen to represent the chemistry effects due to changes in fuel and mixture ratio. The values used in this analysis for S_L are calculated from the equation

$$\frac{S_L}{S_{L_{max}}} = 2.6 \log_{10} \phi + 0.94 \qquad (8)$$

$$(\phi \leq 1.0)$$

from Reference 25. The values of $S_{L_{max}}$ were also chosen from Reference 25. Table 3 shows the values of $S_{L_{max}}$ used.

Table 3. Values of Laminar Flame Speed from Reference 25 for Combustion with Air at Atmospheric Pressure and Room Temperature

Fuel	$\frac{S_{L_{Max}}}{S_{L_{Max,\ Propane}}}$	$S_{L_{Max}}$ Ft/Sec
Propane	1.00	1.41
Ethylene	1.75	2.46
Propylene	1.12	1.58

Figure 16 shows the variation of acoustic power with laminar flame speed. The independent variation of S_L is obtained by changing fuels with all other parameters held constant. But, there is a certain variation in fuel mass fraction F even when ϕ is constant because

$$F = \frac{\phi\left(\frac{F}{1 - F}\right)_{Stoic}}{1 + \phi\left(\frac{F}{1 - F}\right)_{Stoic}} \tag{9}$$

and $\left(\frac{F}{1 - F}\right)_{Stoic}$ for propane, propylene and ethylene are 0.064, 0.0625 and 0.0677 respectively. However, this variation in F is small in comparison with the S_L variation and it will be shown later that the exponent on F is smaller, also. Figure 16 should, therefore, yield estimates of the scaling on S_L. Acoustic power appears to scale to an exponent of 1.4 - 1.6 with S_L for fuel lean to stoichiometric mixtures. This confirms the belief that noise reduction can be achieved by reducing the reactivity of the fuel. The extent of reduction possible, however, cannot be appreciable due to a rather low value of the exponent.

Combined Scaling Law. Although the study of a phenomenon dependent on many parameters can be made by varying them one at a time and this results in ease and clarity of analysis, it is not without disadvantages. The most serious disadvantage is that a large number of experiments would have to be performed, this number increasing rapidly with the number of independent parameters. Also, such an analysis using one variable at a time does not utilize all the information that can be obtained from the

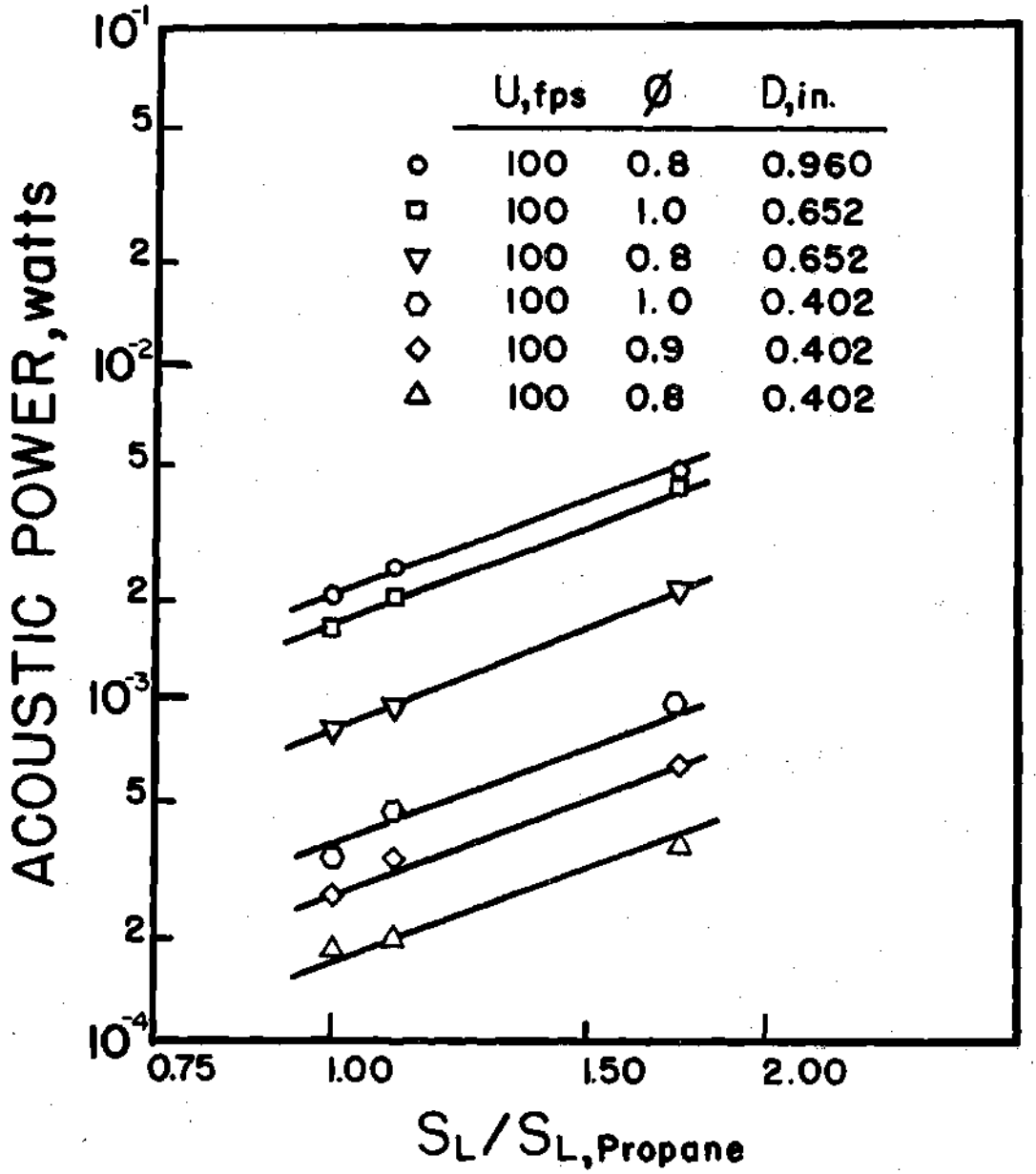

Figure 16. Acoustic Power as a Function of Laminar Flame Speed.

test results. Furthermore, in a real situation, the various parameters vary simultaneously rather than one at a time. Thus it would be meaningful to try to deduce a combined scaling law utilizing all the experimental results generated for the particular quantity.

An effective means of examining the experimental data is by regression analysis in which a theoretically derived law is fitted to the experimental data. In this case, the possible law would be of the type

$$y = K \prod_{i=1}^{N} x_i^{c_i} \tag{10}$$

where K and the c_i's are constants and the x_i's are parameters affecting a quantity y. By taking logarithms on both sides of Equation (10), it is possible to curve fit as a linear problem by the method of least squares.

For the case of acoustic power P scaling, Strahle has suggested that the parameters are U, D, S_L and F. Using 57 different tests the following expression was obtained for the acoustic power radiated from open turbulent premixed flames:

$$P = 4.89 \times 10^{-5}\ U^{2.68}\ D^{2.84}\ S_L^{1.35}\ F^{0.41} \text{ watts} \tag{11}$$

where

$$50 \leq U(\text{fps}) \leq 600$$

$$0.0335 \leq D(\text{ft}) \leq 0.08$$

$$0.6 \leq \phi \leq 1.0$$

and U and S_L are in fps; D is in ft

An analysis of errors due to the regression fit showed a mean error of 5.7% with 124% and -55% as the maximum and minimum errors respectively. The standard deviation was 37%. These errors appear at first sight to be rather large. However, they can be considered very reasonable because of the following reasons:

a) A very wide range of acoustic powers (from 10^{-1} to 10^{-5} watts) are included in Equation (11).

b) The instrumentation accuracies are of the order of a db (if power P_1 is 1 db larger than P_2, then P_1/P_2 will be as large as 1.25), and

c) The flow measurement accuracy was no better than 3% of full flow rates. The flow inaccuracies can affect U and mixture ratio. The error in mixture ratio will introduce errors in both F and S_L.

In order to graphically observe the significance of the regression fit, the calculated values of acoustic power ($P_{regression}$) were cross plotted against the measured values ($P_{measurement}$) in Figure 17. Without doubt it can be said that Equation (11) fits the experimental data very well. Thus, it can be stated that acoustic power can, in fact, be represented by a power type law with respect to the parameters U, S_L, D and F. Further, laminar flame speed S_L appears to be quite adequate to represent the chemistry effect due to various fuels.

It is interesting to note that some of the Smith and Kilham[3] data plotted on Figure 17 show that the measurements of Smith and Kilham can be reproduced satisfactorily by Equation (11). Reference 3 deduced a $(US_LD)^2$ law for acoustic power. Equation (11) can explain the results of Reference 3 and has been obtained over a much wider range of acoustic

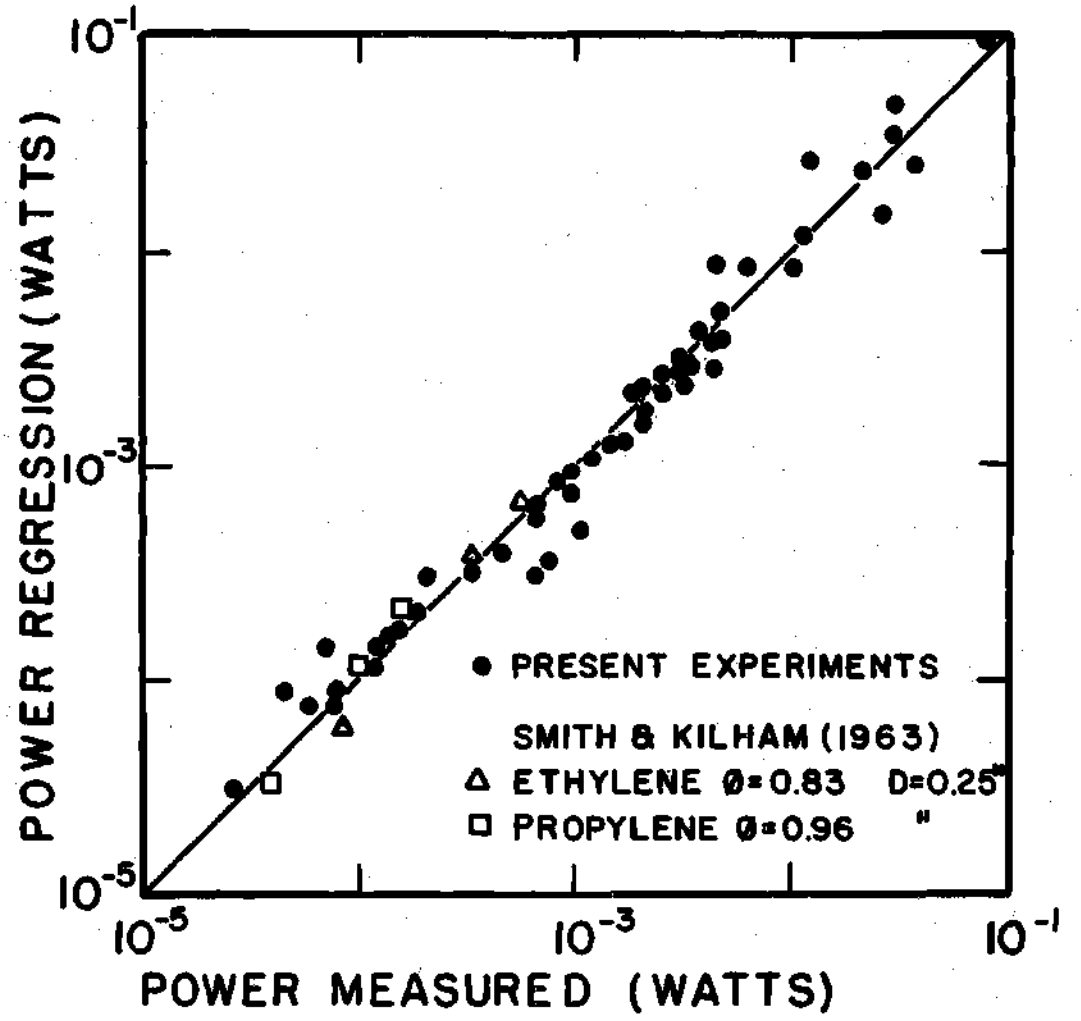

Figure 17. Significance of the Regression Fit for Acoustic Power.

powers, thus establishing a clear preference over the $(US_L D)^2$ law. Surprising as it may seem, Equation (11) is the first empirical relation published from which acoustic power can be calculated directly for noise from hydrocarbon-air turbulent flames. Equation (11) should prove quite useful to anyone interested in determining noise output from combustion zones.

Thermo-Acoustic Efficiency

Thermo-acoustic efficiency is a measure of the portion of total thermal input to the flame converted into noise radiation. Thermo-acoustic efficiency η_{ta} is defined as

$$\eta_{ta} = \frac{\text{Acoustic Power Radiated}}{\text{Thermal Input}} \tag{12}$$

If $\dot{m}$ is the mass flow rate of reactants, and H is the heating value per unit mass of fuel, then

$$\text{Thermal input} = \dot{m}FH$$

where as before F is the fuel mass fraction,

$$\dot{m} = \rho_o \frac{\pi}{4} D^2 U$$

and ρ_o is the density of mixture of reactants. Thus,

$$\eta_{ta} = \frac{P'}{\frac{\pi}{4} \rho_o U D^2 F H} \qquad (13)$$

Therefore, the scaling laws for η_{ta} can be obtained from scaling laws for acoustic power radiated. For the premixed open turbulent flames of this study, $\eta_{ta} \propto U^{1.7} D^{0.8} F^{-0.6} S_L^{1.4}$ would represent the behavior of η_{ta}. Some representative values of thermo-acoustic efficiency are presented in Table 4. The results for a burner of diameter 0.402" and equivalence ratio of 0.8 are shown over the entire velocity range. The maximum η_{ta} is of the order of 10^{-6}. This indicates that for high velocity flames combustion noise could in fact be quite substantial.

Table 4. Thermo-Acoustic Efficiency

Test	Power Watts	$\eta_{ta} = \frac{\text{Power Radiated}}{\text{Thermal Input}}$
P- 50-0.8-1	0.264×10^{-4}	8.36×10^{-9}
P-100-0.8-1	0.183×10^{-3}	2.89×10^{-8}
P-200-0.8-1	0.154×10^{-2}	1.22×10^{-7}
P-300-0.8-1	0.423×10^{-2}	2.23×10^{-7}
P-400-0.8-1	0.104×10^{-1}	4.10×10^{-7}
P-500-0.8-1	0.271×10^{-1}	8.57×10^{-7}
P-600-0.8-1	0.382×10^{-1}	1.01×10^{-6}

Spectral Content of Combustion Noise

The acoustic emission from regions of turbulent combustion has

been recognized in the literature as a broad-band noise with a single peak in the 250 Hz - 1500 Hz range. Discrete frequency components appear when the combustion is confined by enclosures[22,26]. This is not of interest to the present study of open turbulent flames. The frequency spectra will clearly indicate the type of acoustic material that will be needed for noise reduction treatments. Furthermore, the peak frequency will establish the characteristic time in the flame and comparison with the theories in References 17 and 18 will assist in determining the most plausible mechanism of noise generation.

Procedure. The frequency spectra of noise were obtained from the tape recording of sound pressure signals. A Hewlett Packard Fourier analyzer was used. The analyzer was programmed to produce power spectra by the following process. First the analog signal is digitized. Then, the Fourier transform is taken. This is multiplied by its own complex conjugate. The process is repeated a fixed number of times to obtain a stable average. The number of samples required depends on the particular signal being analyzed. Also, the number of digital bits of information used in each sample decides the maximum frequency and the frequency resolution.

A low-pass filter was inserted between the Fourier analyzer and the tape-recorder (Figure 5) to eliminate all frequency components above a preselected maximum. If this is not done the high frequency components will fold over and appear as spurious low frequency components due to the inherent quality of all A to D converters called aliasing. After a preliminary study, the maximum frequency was selected at 8 kHz for the noise spectra. Since the filter frequency response is not flat

beyond 0.8 $f_{cut\text{-}off}$ only spectra up to 5 kHz are presented in this report. The initial spectra were obtained with the number of samples used in averaging between 15 and 200. The 15 sample averaging was found to be adequate to obtain all the information required while the 200 sample averaging resulted in smoother spectra with less scatter. Thus a majority of the combustion noise spectra were obtained with 15 to 50 sample averaging.

The frequency spectra depend on U, D, S_L and F. Also, if combustion noise radiation directionality is frequency dependent, then the spectra depend on the microphone location as well. The spectra shown in the figures that follow are smooth lines drawn through the spectra plotted on the x-y plotter. Figure 18 shows both the actual x-y plot and the smooth line drawn through the mid-points for a typical case. The smooth line is found to be quite satisfactory for representing the spectrum.

Results. The frequency dependence of directionality is studied in Figures 19(a) and (b). Very similar spectra were obtained in all the tests conducted. The azimuth and radius are referenced to the burner exit in these figures. Thus, amplitude comparisons cannot be made directly without correcting the results for the acoustic center. The information regarding directionality can, of course, be obtained from Figures 19(a and b) without any corrections. If the directionality patterns were independent of frequency the spectra at various azimuthal locations would be parallel to each other. An examination of the spectra reveals that directionality of noise generated is almost independent of frequency except for the locations near the axis of the flame which

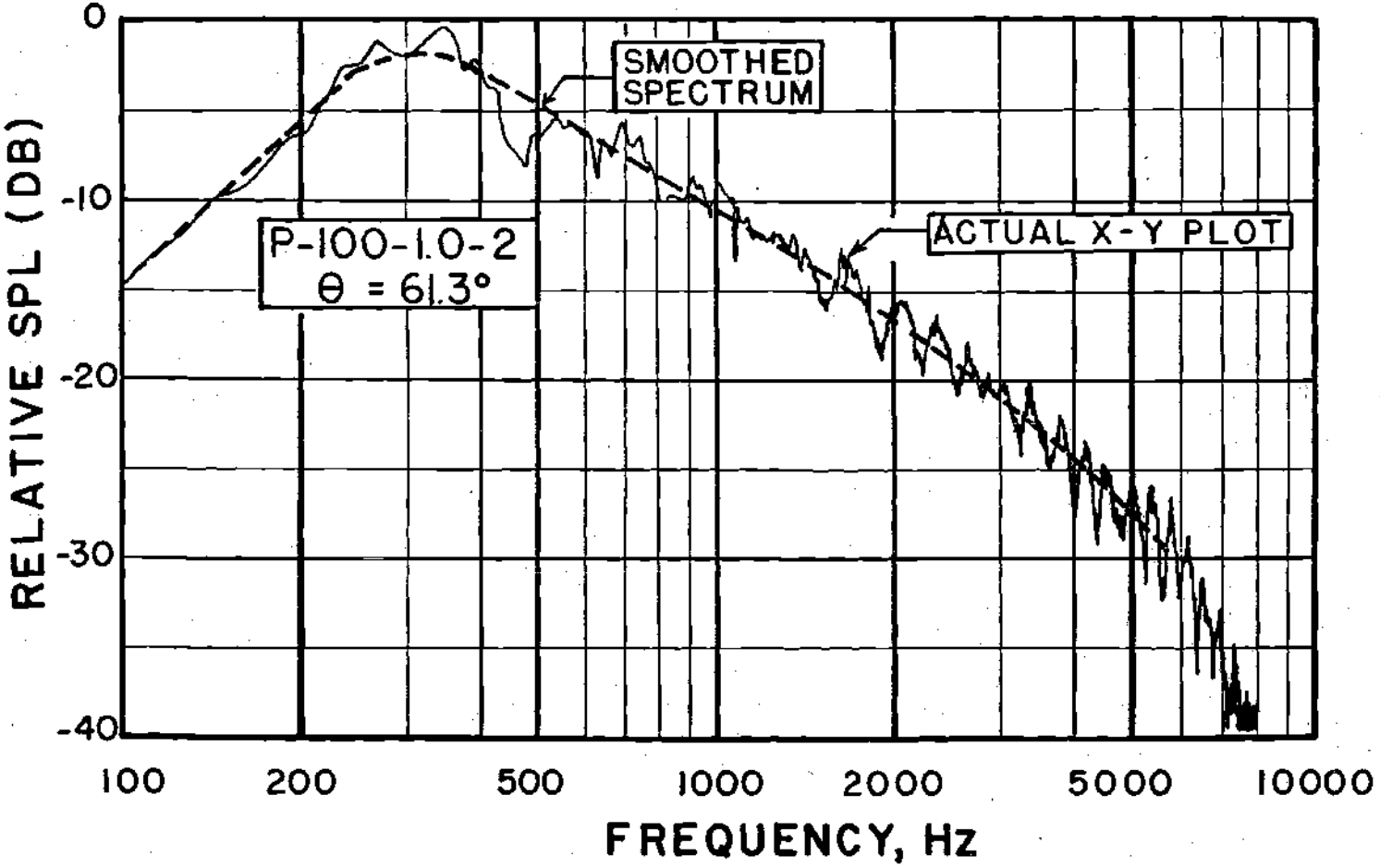

Figure 18. Actual X-Y Plot and Smoothed Spectrum.

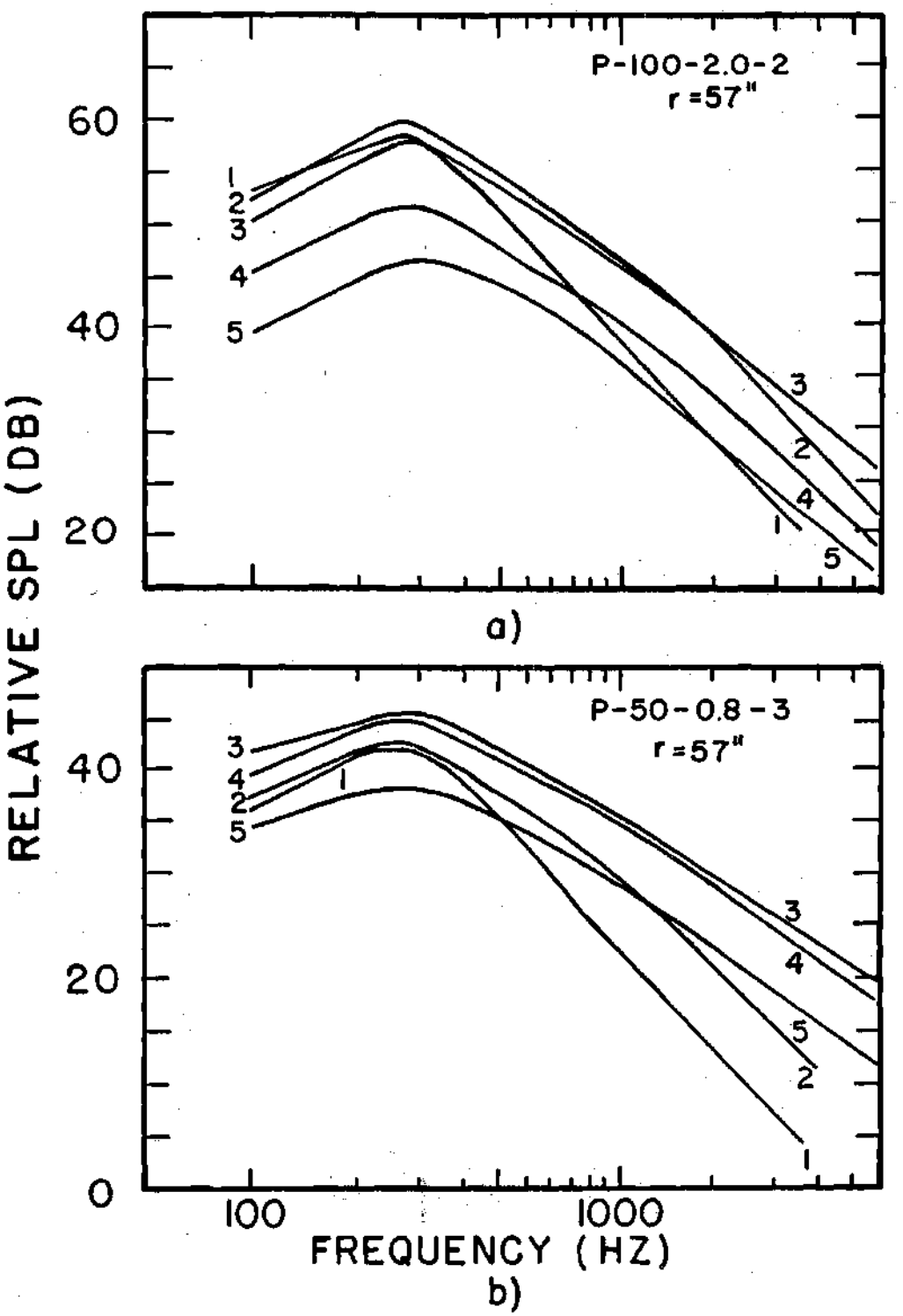

Figure 19. Frequency Dependence of Directionality. The Numbers 1 to 5 Indicate Microphone Locations between 15° and 120°.

exhibit a strong reduction in the high frequency components. Reference 9 observed a much stronger dependence for pure diffusion flames of CH_4 and H_2 burning in air.

Figure 20 presents the effects of flow velocity and laminar flame speed on the frequency spectra. There is clearly a tendency for the peak frequency (frequency corresponding to maximum amplitude on the spectrum) to increase with flow velocity. However, the rate of increase is small. For propane over a 12:1 velocity range the peak changes from 350-270 Hz while for ethylene over a 10:1 velocity range the peak frequency varies between 650 and 350 Hz. The increase in peak frequency is a little more marked for ethylene-air mixtures in comparison with propane-air mixtures. In any case, the peak frequency is a very weak function of flow velocity and it appears doubtful if using Strouhal number ($f\ D/U$) as a non-dimensional parameter as suggested in References 3 and 5 would serve any useful purpose. Use of Strouhal number has been found appropriate for jet noise in Reference 20, where the peak frequency is found to scale inversely with D and directly with U. The experiments for fuel rich flames also showed a similar velocity behavior. Further, Figure 20 shows that the peak frequency for ethylene is higher than that for propane. Since ethylene has higher S_L values this is clearly an effect due to S_L. It appears, therefore, that the characteristic time in the flame is considerably influenced by the chemical time.

Combustion noise can be seen to peak at lower frequencies with an increase in burner diameter in Figures 21(a), (b) and (c). This diameter effect, however, is quite small when compared with a $1/D$ dependence for jet noise. Again, Strouhal number appears to be inappropriate for

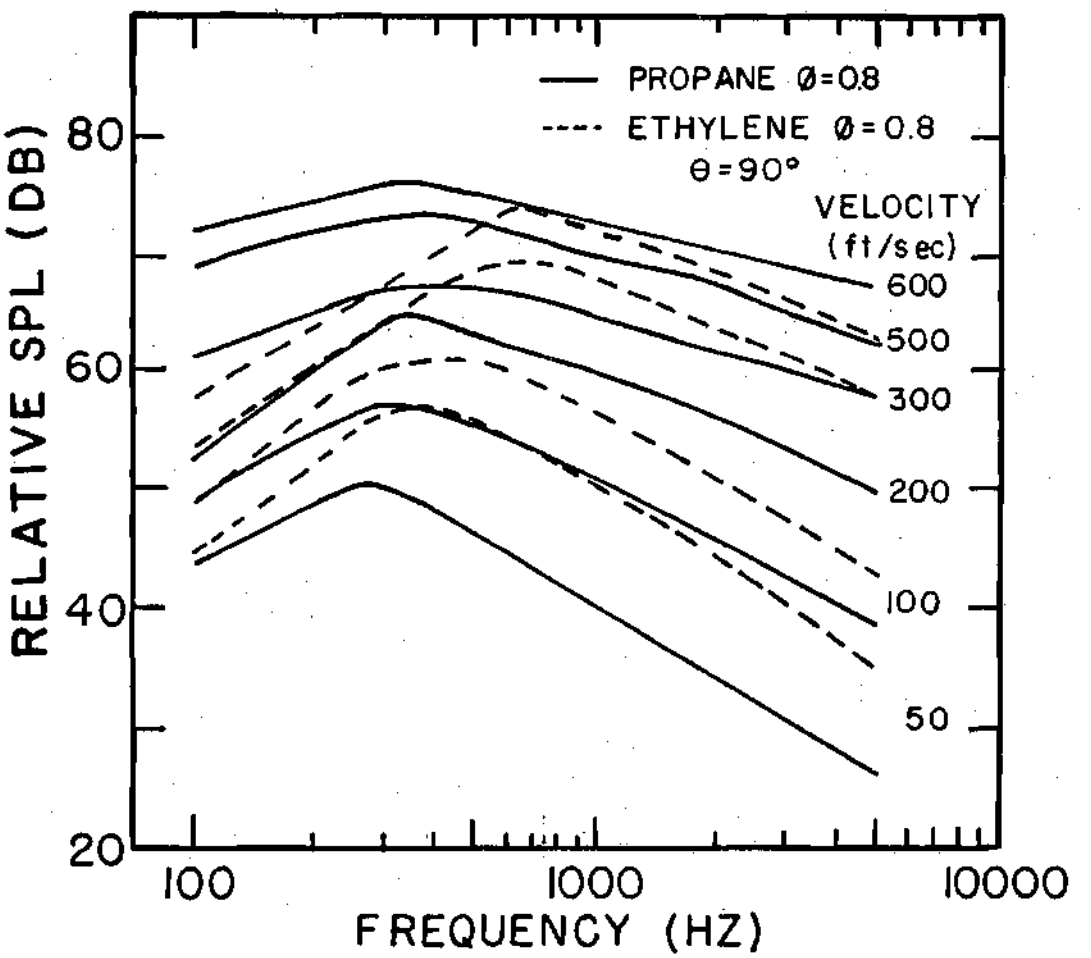

Figure 20. Effects of Velocity and Laminar Flame Speed on the Frequency Spectra.

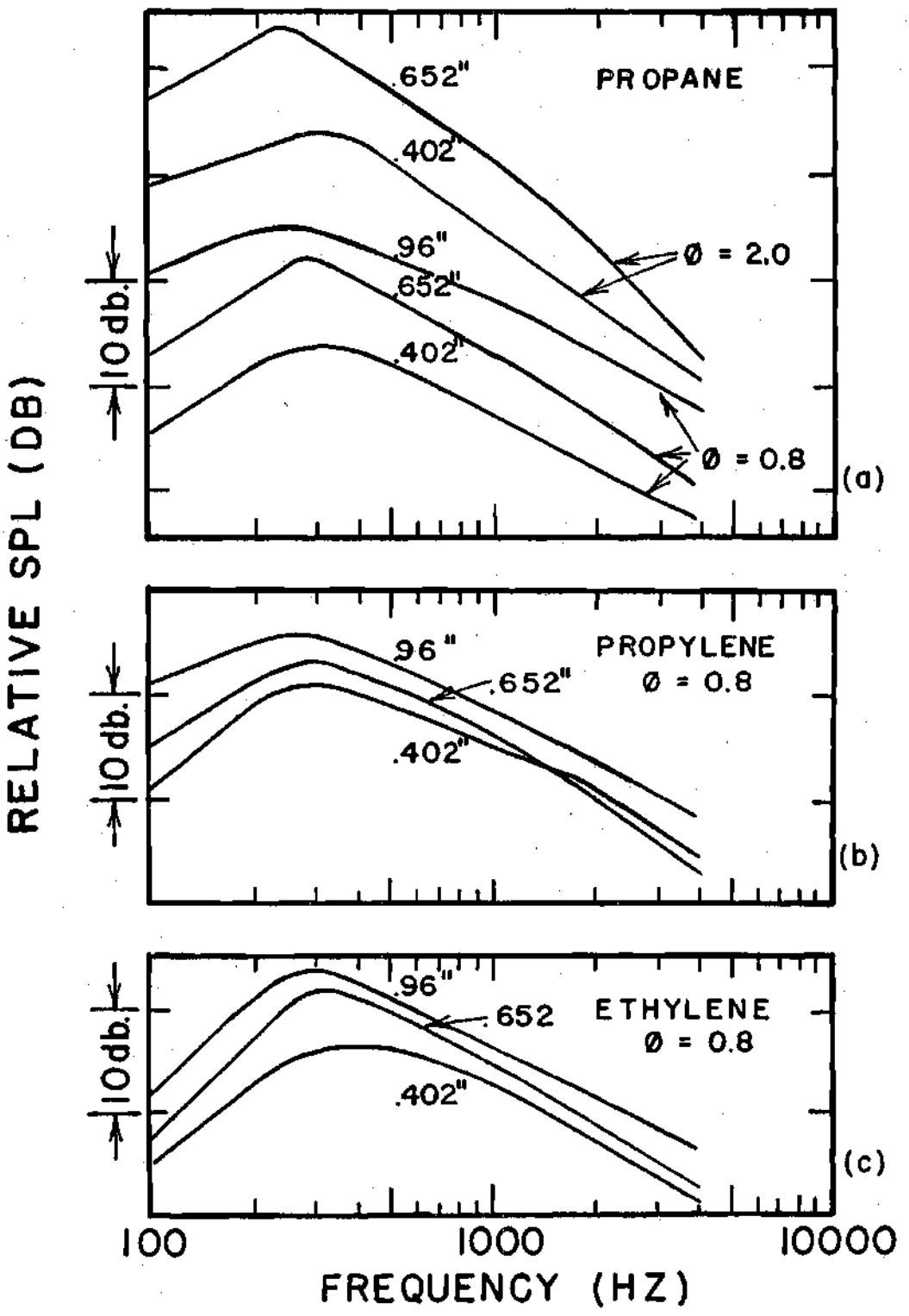

Figure 21. Effect of Burner Diameter on the Frequency Spectra.

combustion noise.

Figure 22 shows the effect of equivalence ratio on frequency spectra. While propane and propylene flames show negligible effects the ethylene flames show some effect due to equivalence ratio.

Peak Frequency. A power type law (Equation (10)) was fitted by regression analysis to the peak frequencies measured. The procedure followed was identical to the one used for obtaining acoustic power law (Equation (11)). If f_c is the peak frequency then the regression analysis gives

$$f_c = 11.83\ U^{0.19}\ D^{-0.082}\ S_L^{0.53}\ F^{-0.69}\ \text{Hz} \qquad (14)$$

where U and S_L are in fps; D is in ft

and

$$0.6 \leq \phi \leq 1.0$$
$$50 \leq U(\text{fps}) \leq 600$$
$$0.0335 \leq D(\text{ft}) \leq 0.08$$

The number of tests was 56, the mean error was 0.85% and the standard deviation was 13.4%. Equation (14) shows that S_L and F have the most effect on peak frequency and U and D effects are negligible. An inverse S_L and F scaling would explain the negligible ϕ dependence of propane and propylene flames shown on Figure 22. The behavior of f_c of ethylene flames with ϕ is somewhat anomalous.

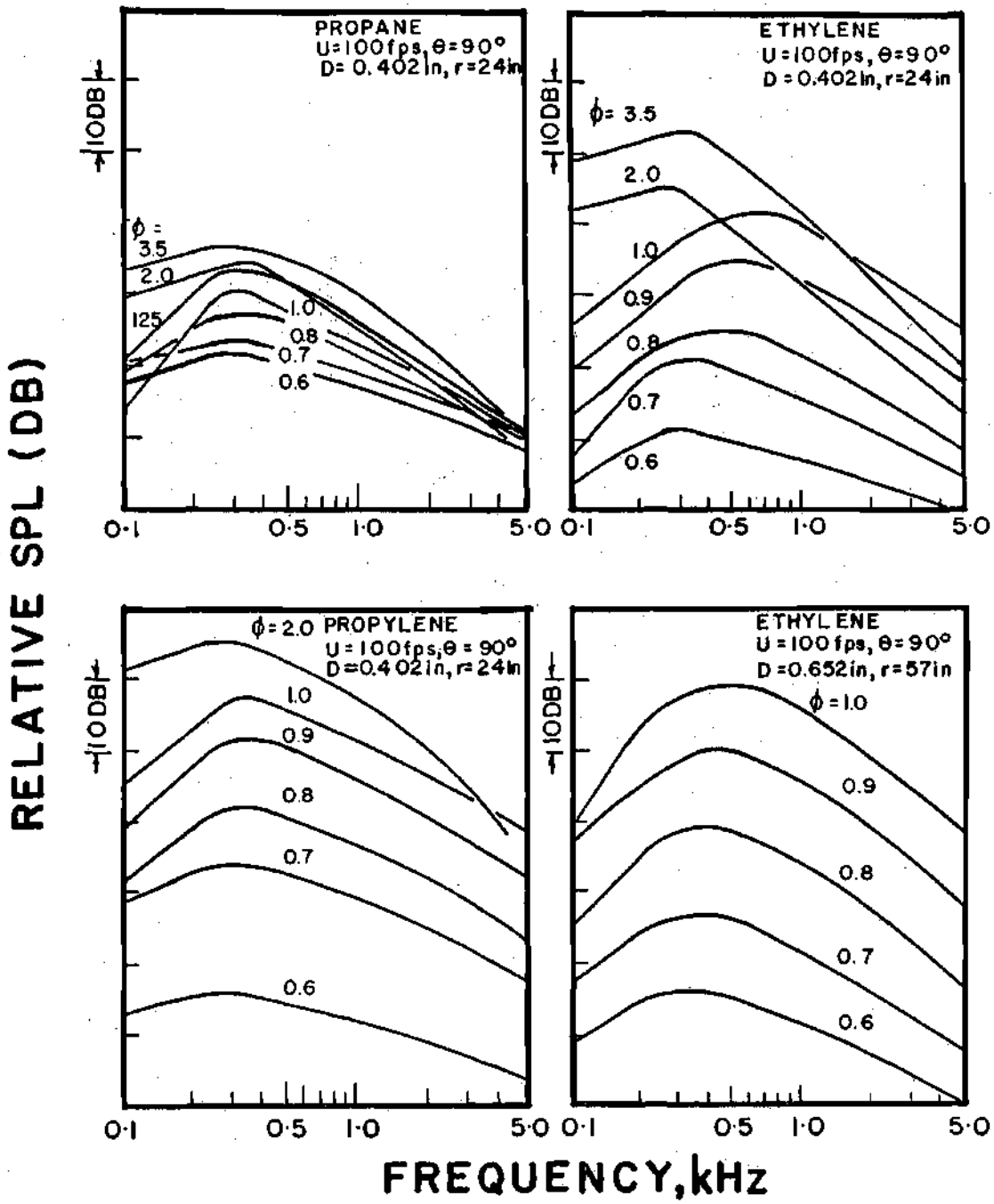

Figure 22. Effect of Equivalence Ratio on Frequency Spectra.

Experimental Results for Fuel Rich Flames

Until now the fuel-lean cases have been discussed. Their directionality, scaling laws for spectral content, acoustic power and thermo-acoustic efficiency have been studied in detail. However, combustion processes, in practice, do not always take place in the fuel-lean condition. Pure diffusion and fuel-rich flames are quite common. Therefore, exploratory research on the behavior of fuel-rich flames was undertaken. Fuel-rich flames have some characteristics of both premixed and diffusion flames. After initial reaction with the oxidizer available in the mixture, the unburned reactants, due to excess fuel, react with the oxygen in the surrounding air to complete the combustion process.

At a certain flow velocity for a given burner, the physical size of the flame increases at a rapid rate with equivalence ratio for $\phi >$ 1.0 (see Figure 31(a) Chapter III). The flame width is no longer of the order of magnitude of the burner diameter; instead, the flame grows to an oblong balloon-like shape several burner diameters wide. Since the burner axis in these experiments is horizontal, there is a noticeable tendency for an upward deflection of the flame-tip due to buoyancy effects when $\phi \gtrsim 2.0$. The foregoing description of the flame has been presented in order to emphasize that in the case of fuel-rich flames the acoustic measurements would experience the following difficulties:

1. The noise generating region has a size comparable to the radius of the microphone position. The maximum radius at which microphones can be mounted is decided by the size of the anechoic chamber. Thus, some deviations from the far field conditions may arise in the

sound pressure readings.

2. The noise radiation has been assumed to be axially symmetric for calculating the acoustic power. If the flame is deflected upwards due to the buoyancy effects, the assumption of axial symmetry will be only approximately satisfied.

Despite the above difficulties, some useful results can be obtained. The spectral content at microphone locations away from the axis should be quite representative of the true spectra. Due to the integration process involved in the calculation of acoustic power, errors should be reduced to a certain extent and the results obtained should be within reasonable limits of error.

The acoustic emissions from fuel-rich flames were seen to possess qualitative similarities with the corresponding fuel-lean flame results. The directionality patterns for both the cases are similar. Figure 19 shows that the frequency dependence of directionality is independent of whether or not the flame is fuel-rich. The general result that for hydrocarbon-air flames combustion noise peaks in the 250-700 Hz range appears to hold good for fuel-rich flames as well.

Figure 23 shows the acoustic power as a function of mean flow velocity for fuel-rich propane-air flames on a 0.402" burner. A $P \propto U^3$ law is apparent. Thus the similarity in acoustic emission between fuel-lean and fuel-rich flames appears to extend to the velocity scaling of acoustic power also.

The diameter scaling for acoustic power is seen to be $P \propto D^2$ in Figure 24. The exponent on D is lower than that for fuel-lean flames.

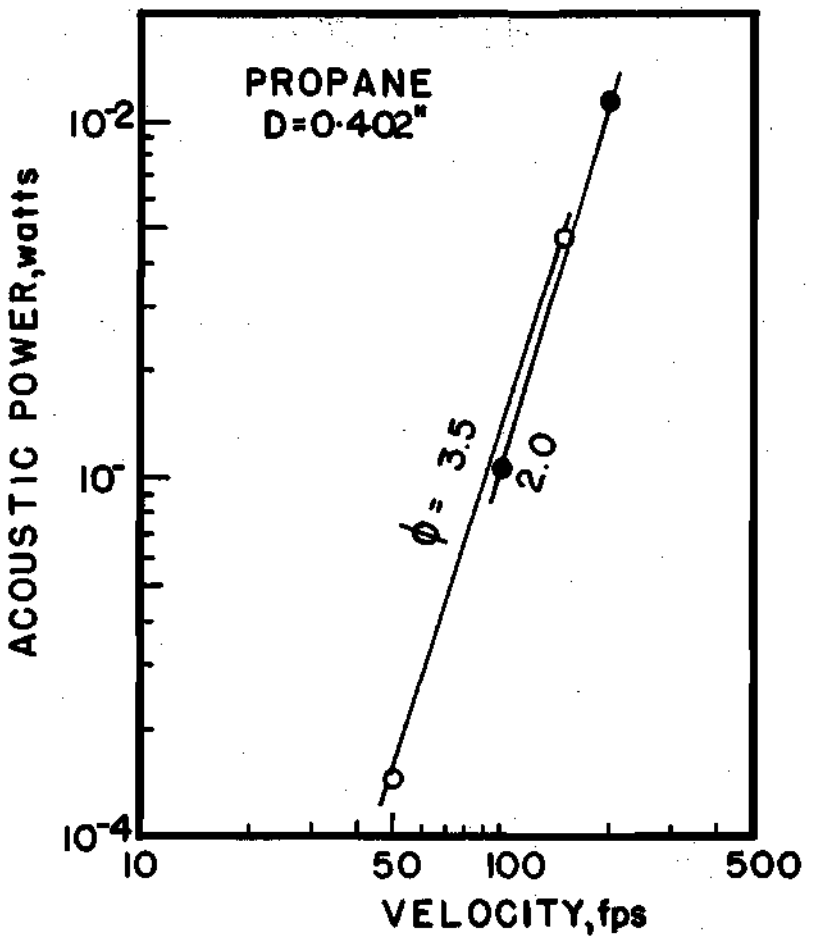

Figure 23. Acoustic Power as a Function of Flow Velocity for Fuel-Rich Propane Flames on a 0.402" Diameter Burner.

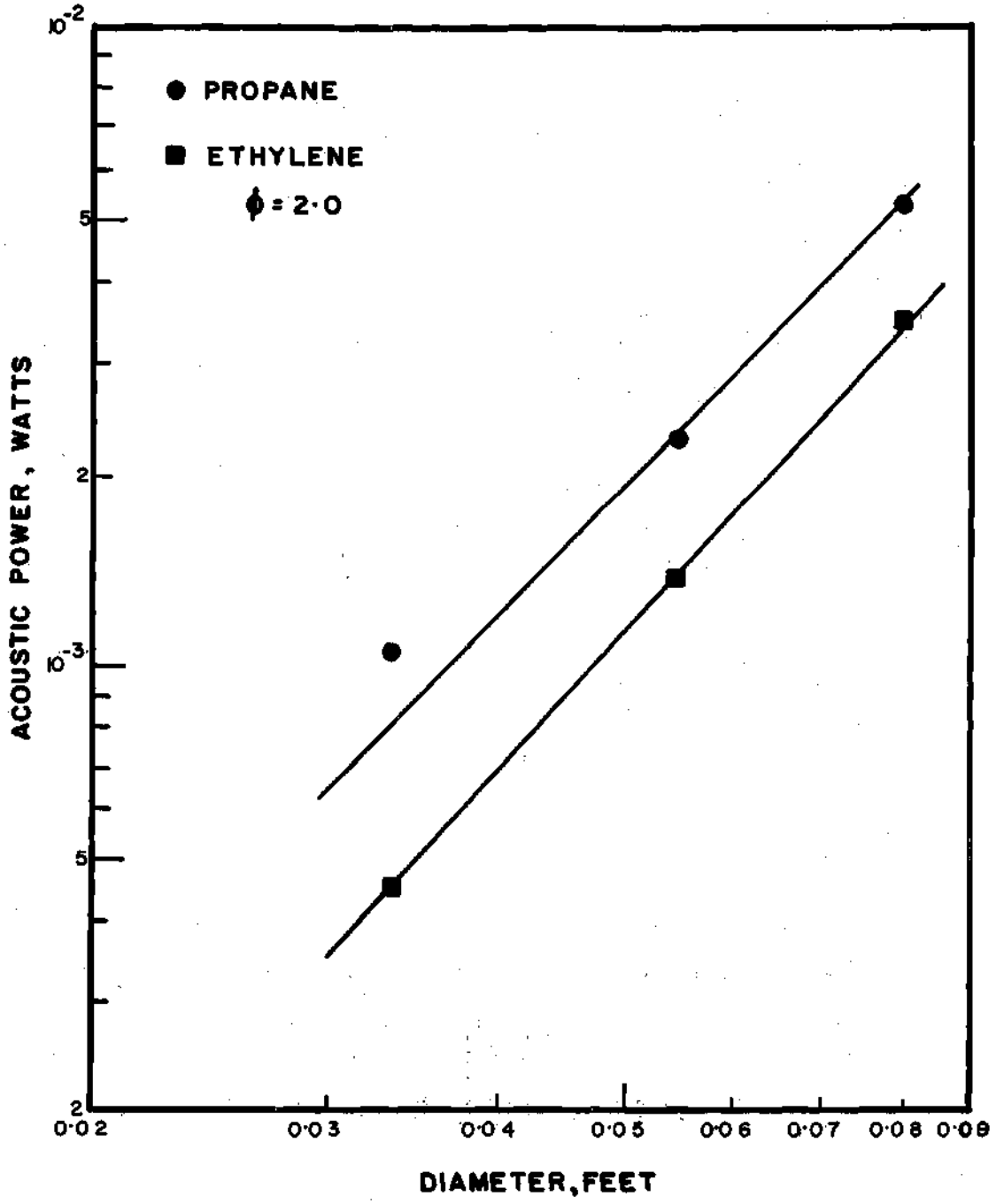

Figure 24. Acoustic Power as a Function of Diameter -- Fuel-Rich Flames.

The D^2 scaling would make the thermo-acoustic efficiency of fuel-rich flames independent of D. In Figure 24, it is seen that the ethylene-air results generate less noise than propane-air flames for a given set of experimental conditions. This is just the opposite of the fuel-lean flame results where ethylene-air flames were shown to be more efficient noise generators. In an effort to explain this effect,the acoustic power values were plotted as a function of equivalence ratio in Figure 25.

Figure 25(a) presents the result for propane-air flames. Acoustic power is seen to increase monotonically with ϕ. The rate of increase of acoustic power with ϕ is almost constant for $\phi \leq 1.0$. For $\phi > 1.0$ the acoustic power increases at a lower rate; the rate of increase becoming lower as ϕ is increased. Figure 25(b) shows essentially the same trend for propylene-air flames. Figure 25(c) presents the results for ethylene-air flames. The behavior is anomalous. All the three burners show a decrease in noise output between ϕ values of 1 and 2. The reason for this behavior is unknown at the present time.

In view of the anomalous results obtained for fuel-rich ethylene-air flames, a combined scaling law similar to Equation (11) could not be obtained for fuel-rich flames. In addition there are ambiguities involved in assigning the value of laminar flame speed for fuel-rich flames which cannot be considered as either premixed or diffusion flames; as has been discussed earlier in this section.

A Pure Diffusion Flame Result

In comparing the combustion noise and jet noise it was observed

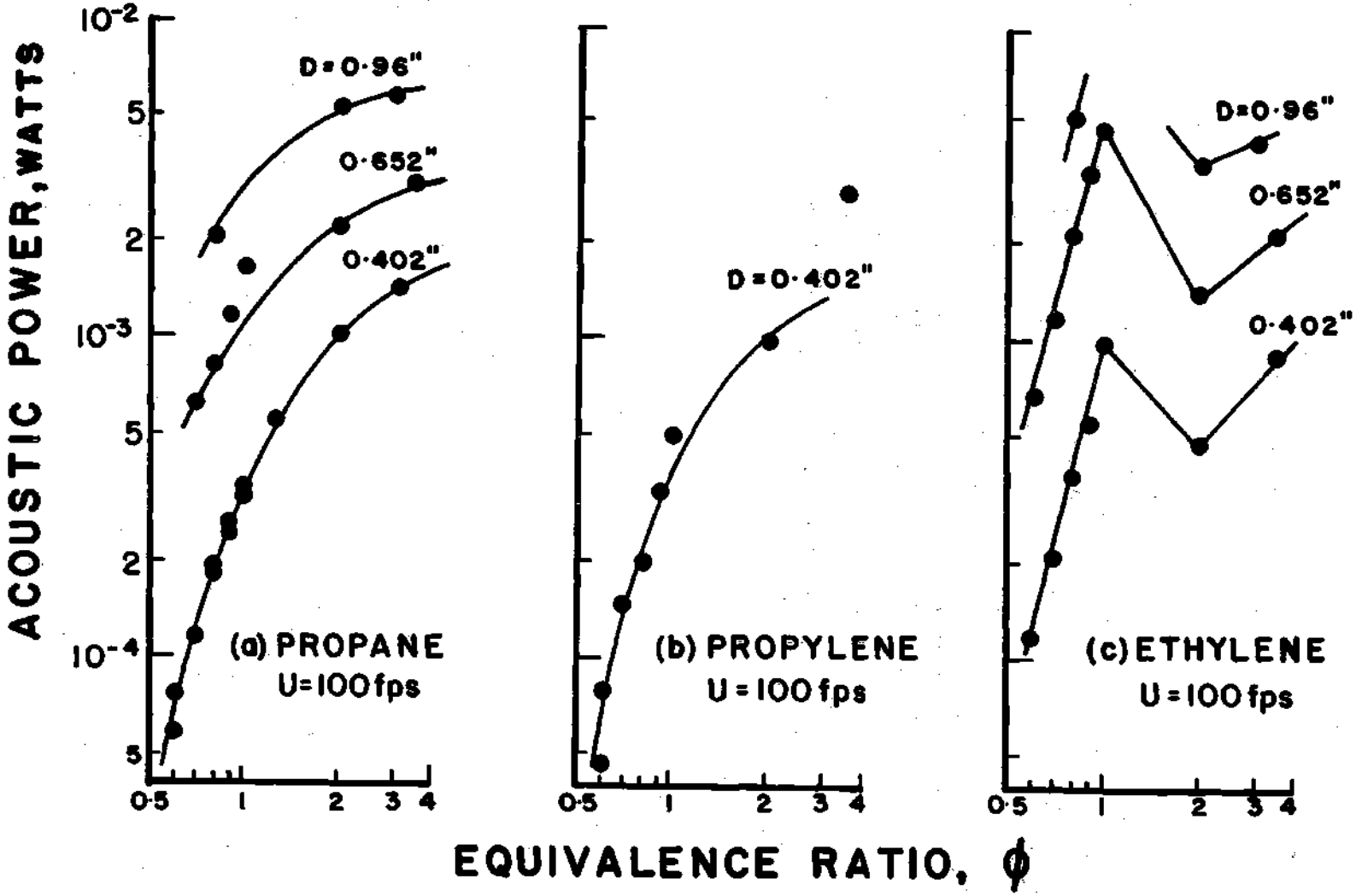

Figure 25. Acoustic Power as a Function of Equivalence Ratio.

that the diffusion flame of hydrogen used for flame stabilization was very quiet when burning alone and that it would produce noise appreciably louder than the jet noise when the main air jet was flowing. This result is shown by the air + pilot line falling above the air-only line in Figure 7.

Figure 26 shows a probable mechanism of noise generation of this flame. The annular diffusion flame interacts with the turbulent mixing layer producing a turbulent flame which generates noise.

In one particular experiment the hydrogen flow was changed from 2 to 5% by volume of the jet flow. The resulting sound pressure levels are shown on Figure 27. Assuming spherical symmetry the result shown on Figure 27 implies that acoustic power for pure diffusion flames follows a $\dot{m}_f^{2.8}$ law, where $\dot{m}_f$ is the mass flow rate of fuel. The mean flow velocity of the main air jet was 100 ft/sec. The velocity of hydrogen at maximum flow would be about 11.5 fps.

Discussion of Results

Fuel-Lean Flames

A discussion of the experimental results of this study in the light of the theories of Strahle[16,17,18] and other experimental results that are available, will be presented in the succeeding paragraphs.

The directionality of combustion noise is seen to be rather weak. In this study the maximum difference, between the maximum sound pressure level and the minimum sound pressure level (observed at $\theta = 0$) over a constant radius path around the flame in a plane containing the flame axis, was about 4 db. The general lack of strong directionality would

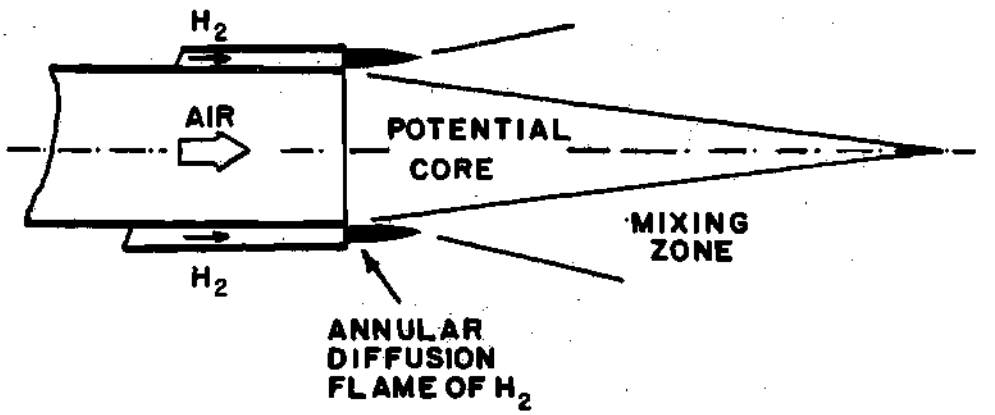

Figure 26. Diffusion Flame of Hydrogen.

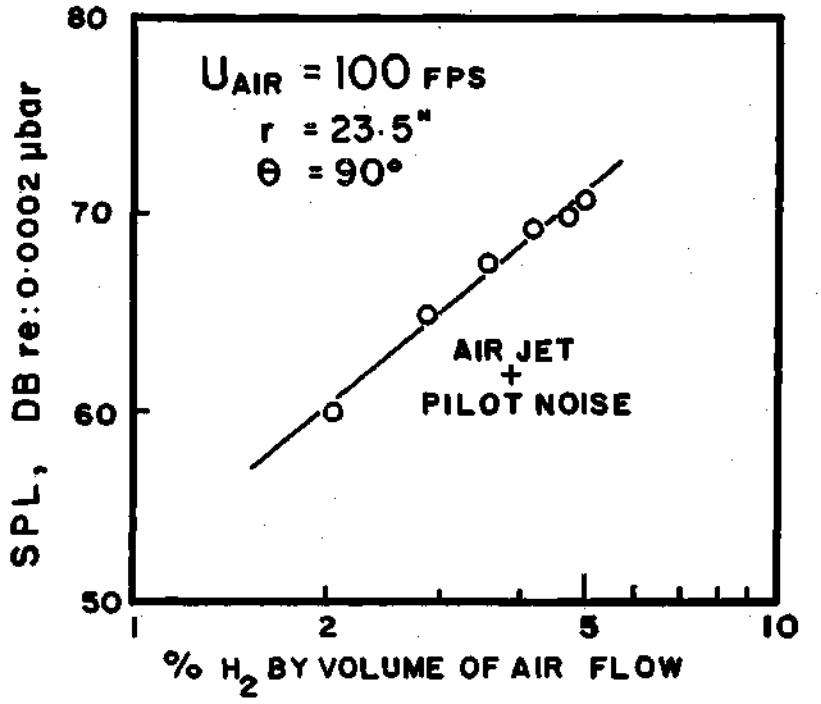

Figure 27. A Scaling Law for Pure Diffusion Flame.

support the monopole theory of noise generation. Further, there is some similarity between the experimental results for directionality and the directionality patterns deduced in Reference 18 considering refraction at temperature discontinuities. Thus, the directional patterns can qualitatively be explained by the refraction theory. The general tendency for the location of peak sound pressure to shift towards the flame axis with an increase in velocity is a result of the convection effect. The spectra of the sound pressures as measured by the five microphones at various azimuthal positions have shown that directionality is frequency dependent to the extent that the high frequency components drop off rather rapidly towards the burner axis. The results of Reference 18 considering refraction effects showed a similar effect with increasing frequencies. Thus, the high frequency fall-off near the axis could be at least qualitatively explained by the refraction effect. The directionality patterns of Reference 3 have general similarity with those presented here. Price *et al*[9] saw a more marked effect of frequency on directionality for a pure diffusion flame of H_2-CH_4 burning in air. Except for some results with the 0.402" burner all other results show a maximum noise radiation around 50° - 80° to flow direction and with reference to the acoustic center. An off-axis maximum is very important for noise reduction efforts using acoustic liners.

The spectra of combustion noise show a predominantly low frequency nature. They show a broad-band noise with a single peak and a gradual amplitude fall-off on either side of the peak. The rate of fall-off on the high velocity cases was observed to be rather slow. This could be due to the fact that the difference between jet noise and combustion

noise decreases with flow velocity as shown in Figure 7. Thus, the higher velocity flames show a slight increase in higher frequency components. The noise spectrum, however, is decided by the predominant combustion noise. The peak frequency does not seem to be strongly influenced by any parameter. F and S_L appear to have the most effect. For all practical purposes one could summarize the experimental findings by stating that combustion noise peaks in the 250-700 Hz frequency range for hydrocarbon-air flames. The values of peak frequencies obtained here are in excellent agreement with the values obtained by References 3, 11 and 15 for premixed flames. Even diffusion flames of Reference 12 seem to support the above statement. Hurle et al[8] report a peak frequency of 1200 Hz for a stoichiometric ethylene-air flame on a 0.175" diameter burner. This value is slightly higher than what would be obtained from the peak frequency relation deduced in this work (Equation (14)). However, the spectra of Kotake and Hatta[5], which show for stoichiometric natural gas-air flames a flat low frequency spectra, look improbable in view of the extensive analysis of the present study which always showed a recognizable low frequency fall-off. Also, it appears quite improper to try to use Strouhal number to non-dimensionalize combustion noise peak frequencies as suggested by References 3 and 5.

The results shown in Equation (14) emphasize that chemical time is an important characteristic time in the flame. Referring to Strahle's[17] theories, all the three models of turbulent combustion can explain the values of peak frequencies reported.

The scaling laws for acoustic power and thermo-acoustic efficiency

generated in this work are considered to be a needed addition to the noise data on open turbulent flames. The scaling laws have been obtained over a much wider range of values of the parameters compared to those of the only other similar work[3]. Also, Smith and Kilham[3] deduced the scaling laws on only U by actual sound pressure measurement around the flame while obtaining those on S_L and D by a single microphone sound pressure measurement. Further, the important parameter F was not considered in their work. In addition, the experimentally measured acoustic powers of Reference 3 could be reproduced by the experimental regression equation, Equation (11) of this study as shown on Figure 17. Thus, it is felt that the scaling laws for acoustic power presented in Equation (11) are more representative of noise radiation than the $(US_LD)^2$ scaling of Reference 3.

The scaling laws for acoustic power deduced by Strahle[17] show that for premixed fuel-lean flames,

$$P = K\, U^{a_1}\, S_L^{a_2}\, F^{a_3}\, D^{a_4}\, \ell_t^{a_5}\, \vartheta^{a_6}$$

where $a_1 = 2 - 3.5$, $a_2 = 2 - 5$, $a_3 = -1.8$, $a_4 = 2$, $a_5 = 1.5 - 3$ and $a_6 = 0 - 2.5$, depending upon the model of turbulent combustion considered. To arrive at the above expression for P from Reference 17 the quantity $(\Delta\rho/\rho_o F)^2$ in the theory was replaced by $F^{-1.8}$. This relation between $(\Delta\rho/\rho_o)$ and F was obtained, for premixed fuel-lean hydrocarbon-air flames, based on the data of Steffensen et al[27].

Comparing the scaling laws stated above with those obtained in Equation (11), it can be seen that the exponent on U is within the values of a_1 specified by the theory. Whereas in the theory ℓ_t and D are considered independently the experimental results consider a single parameter D. However, in Chapter III, it will be shown that $\ell_t \propto D$. Using this result the theory would allow an exponent between 3.5 and 5 for D as compared with the experimental value of 2.8. For S_L, the theoretical expectation allows an exponent between 2 and 5 and experimentally an exponent of 1.4 is observed. It has been noticed that in the scaling law of the theory a term F^2 has been left out. If the theoretical law is corrected for this error an $F^{0.2}$ law would result against the experimental $F^{0.4}$ law. Thus, the theoretical estimates of Reference 17 do not fall completely in line with the experimentally generated scaling laws. The basic differences may be attributed to incorrect order of magnitude estimates made in the theory which used the extremely limited knowledge available at that time. It is believed that the results presented in this chapter and in Chapters III and IV provide a body of experimental data which should prove useful in generating improved theoretical laws. Further work in these directions should prove to be an interesting research problem.

Fuel-Rich Flames

Fuel-rich flames, in general, behave very similar to fuel-lean flames as far as spectral content, directionality and acoustic power scaling on U are concerned. The exponent on D in acoustic power scaling is slightly lower than in the fuel-lean case. The Kotake and Hatta[5] data for fuel-rich flames were obtained from single microphone sound

pressure readings. Furthermore, a convergent nozzle was used. The turbulence structure at the exit of a convergent nozzle would be different from the pipe flow turbulence used in the present work. The acoustic environment for the noise measurements of Reference 5 is not known. Thus the Kotake and Hatta scaling for acoustic power appears to be erroneous for open turbulent flames. Knott's[14] experiments on similar flames were conducted at a much higher velocity, and, hence, are not compared. Giammar and Putnam[13] conducted experiments on fuel-rich flames on commercial burners. These burners had a 50% convergent nozzle at the exit. Reference 13 obtained a result that the thermo-acoustic efficiency scales as the square of the Mach number. This would imply a $P \propto U^3$ law which is in agreement with the present findings.

Comparison with Strahle's theory for pure diffusion flames in Reference 18 can be made only on a very qualitative basis. According to this theory $P \propto U^2 D^2 \ell_t^2$, considering only the parameters of interest to the present work. For fuel-rich flames ℓ_t behavior is unknown. The experimental scaling law $P \propto U^3 D^2$ would be in accord with the theory only with certain restrictions on ℓ_t. Thus, the information available from fuel-rich experiments appears to be insufficient to draw any conclusions regarding the scaling laws of Reference 18.

CHAPTER III

DIRECT FLAME PHOTOGRAPHY

The decomposition of combustion noise scaling rules can be in part achieved by a direct flame photographic technique. Considering Equation (4),

$$P \propto \int_V dV\,(\underset{\sim}{r}_o) \int_{V_d} C(\underset{\sim}{r}_o, \underset{\sim}{d})\, dV\,(\underset{\sim}{d}) \tag{15}$$

where C is an autocorrelation of the reaction rate and V_d is a correlation volume. The second integral is over V, the reacting volume, which is of interest to this study. It is furthermore shown that the order of magnitude of Equation (15) may be expected to be given by

$$P \propto V\, V_d\, \bar{C} \tag{16}$$

where $\bar{C}$ is an order of magnitude estimate of C. The reacting volume is, therefore, a fundamental quantity in establishing the scaling laws for combustion noise. The scaling laws on reaction volume directly affect the scaling rules for combustion noise. An investigation of the parametric behavior of the flame volume could, therefore, be a useful step in understanding the origin of combustion noise. A theoretical evaluation in Reference 17 deduced an analytical expression for the order of

magnitude of the reacting volume based on physical reasoning. Three different models of turbulent combustion were considered. The analytical expression developed was

$$V = K\, U^a\, D^b\, S_L^c\, F^d\, \ell_t^e\, \vartheta^f \qquad (17)$$

where V is the flame volume, U is the mean flow velocity, D the burner diameter, S_L the laminar flame speed, F the fuel mass fraction, ℓ_t the turbulence length scale and ϑ the relative intensity of turbulence. K, a, b, c, d, e and f are constants. Depending upon the model of turbulence chosen the exponents would take the values as shown in Table 5.

Table 5. Scaling Laws on Reacting Volume from Strahle's Theory

	Exponents on					
	U	D	S_L	F	ℓ_t	ϑ
Model of Turbulent Combustion	a	b	c	d	e	f
Wrinkled Flame (WF)	1	2	-1	0	1	0
Slow Distributed Reaction (SDR)	$\frac{1}{2}$	2	-2	0	$\frac{1}{2}$	$\frac{1}{2}$
Fast Distributed Reaction (FDR)	1	2	-1	0	1	0

Thus having established the importance of analyzing the flame volume in the development of the theory of combustion noise a need of an experimental study of the subject became evident. If the scaling laws could be experimentally determined for the turbulent flame volume and

compared with the theoretical predictions of Reference 17 a substantial improvement in the understanding of scaling laws for combustion generated noise would result. Also, an investigation of this kind would answer, at least partially, questions on the turbulence structure in the reaction zone.

An experimental program was therefore developed to decompose the scaling rules for the flame volume. Spectroscopic studies[28] of hydrocarbon flames have shown that the luminosity of the flame brush is due to the emission of active radicals like CH, C_2 and OH in the reaction zone. Since these active radicals are present only in the active reaction zone, the volume of the combustion region can be obtained by direct photography viewing the flame through an optical filter centered on the radiation of a particular radical. The volumes could be measured by tracing out the density curves on a microdensitometer.

The technique of direct photography is fast, direct and simple compared to methods where thermocouples are used to estimate the extent of the reaction zone. In fact, the direct photography method is free from the errors due to the presence of the probe in the flame and the positional inaccuracy of the probe caused by vibrations and deflections due to aerodynamic forces[29]. An evaluation of the accuracy of the photographic method will be done at a later stage in this chapter.

Dimensional Analysis

Dimensional analysis is based on the fundamental requirement of dimensional homogeneity in a physical equation. If it is possible to recognize all the parameters that affect a physical quantity dimensional

analysis can provide an insight into the parametric behavior. The functional form, however, cannot be determined by the dimensional analysis. Following the arguments of Reference 17 it is reasonable that the parameters that can affect the reacting volume V are: flow velocity, U, burner diameter, D, laminar flame speed, S_L, turbulence velocity in the axial direction, u', turbulence length scale, ℓ_t, and finally the fuel mass fraction, F, which is already nondimensional. Thus over a limited range of the independent variables it is fair to assume

$$V = K\, U^{\ell}\, D^{m}\, S_L^{n}\, u'^{p}\, \ell_t^{q}\, F \tag{18}$$

Here, since the fundamental dimensions involved are only length and time and there are six unknowns to determine, there will be four nondimensional groups. By dimensional reasoning the following V dependence is obtained

$$\frac{V}{D^3} = \text{fn}\left\{\left(\frac{u'}{U}\right),\ \left(\frac{U}{S_L}\right),\ \left(\frac{\ell_t}{D}\right),\ F\right\} \tag{19}$$

Any further explanation based on Equation (19) will be deferred until after the experimental results are presented.

Experimental Procedure

The burners and flow systems used have already been explained in Chapter II. The flame is photographed using a Graflex Speed Graphic Camera with 4" x 5" black-and-white panchromatic film. An optical

filter centered on the CH radiation (4315Å) is used in this work since CH is one of the predominant components in the emission spectra of these flames. More importantly, however, it is found from Reference 30 that the spectral intensity of CH emission is much more pronounced than any other in fuel-lean flames of propane-air. Thus, CH emission is more appropriate for determining the reaction volume since a majority of the experiments were planned using this fuel.

The filter used in this investigation has a half peak transmittance bandwidth of about 500 Å and a peak in the vicinity of 4300 Å. The flames are photographed inside an anechoic chamber since these experiments are done parallel with the acoustic measurements. As far as optical studies are concerned the anechoic chamber serves to prevent extraneous drafts around the flame and also eliminates stray light when photographs are being taken. A microdensitometer is used to measure the image of the flame recorded on the photographic negative. A microdensitometer works as follows: Light from an electric lamp passes through a set of lenses and slits to give a narrow ($\approx$ 0.5 mm diameter was used for the present study) beam of light. This beam of light passes through the photographic negative. The intensity of the transmitted light is inversely proportional to the density (darkness) of the image. A photomultiplier tube is used to measure the intensity of the transmitted light. The output of the photomultiplier tube is connected to the y-input of a plotter. In order to get the spatial distribution of the density, the photographic negative is moved across the beam of light along a straight line. This motion is mechanically linked to the

x-axis of the plotter. Thus, the output of the microdensitometer will be plots of density against distance. A number of such plots will describe the density distribution over the entire area photographed.

Measurement of the Flame Volume

A turbulent premixed flame stabilized at the end of a burner tube has a luminous zone contained between fairly well-defined inner and outer cones. Although the inner and the outer cones of the flame are qualitatively simple to visualize, a quantitative study requires that certain criteria be adopted for the flame volume computation. In this study, it was decided to fix the outer boundary of the flame by defining it as the surface which has an intensity 0.1 I_{max}, where I_{max} is the maximum intensity recorded on the photograph. The definition of the inner cone presents additional difficulty since it is viewed through a part of the flame brush by the camera lens. A reasonable estimate is obtained, however, by considering the inner cone to be defined by the peaks in the densitometer trace. Figure 28 clearly explains the procedure adopted. In order to obtain the volume of the flame the densitometer traces were taken at various short distances along the length of the flame. From the traces the inner and outer radii were measured as shown in Figure 28. The volumes of the outer and inner cones between the adjacent sections were computed as truncated cones. The difference between their volumes gives the reaction volume between the two measurement sections. The total flame volume is then obtained as a simple sum of all such elemental volumes.

At this stage, it should be realized that an analysis of this

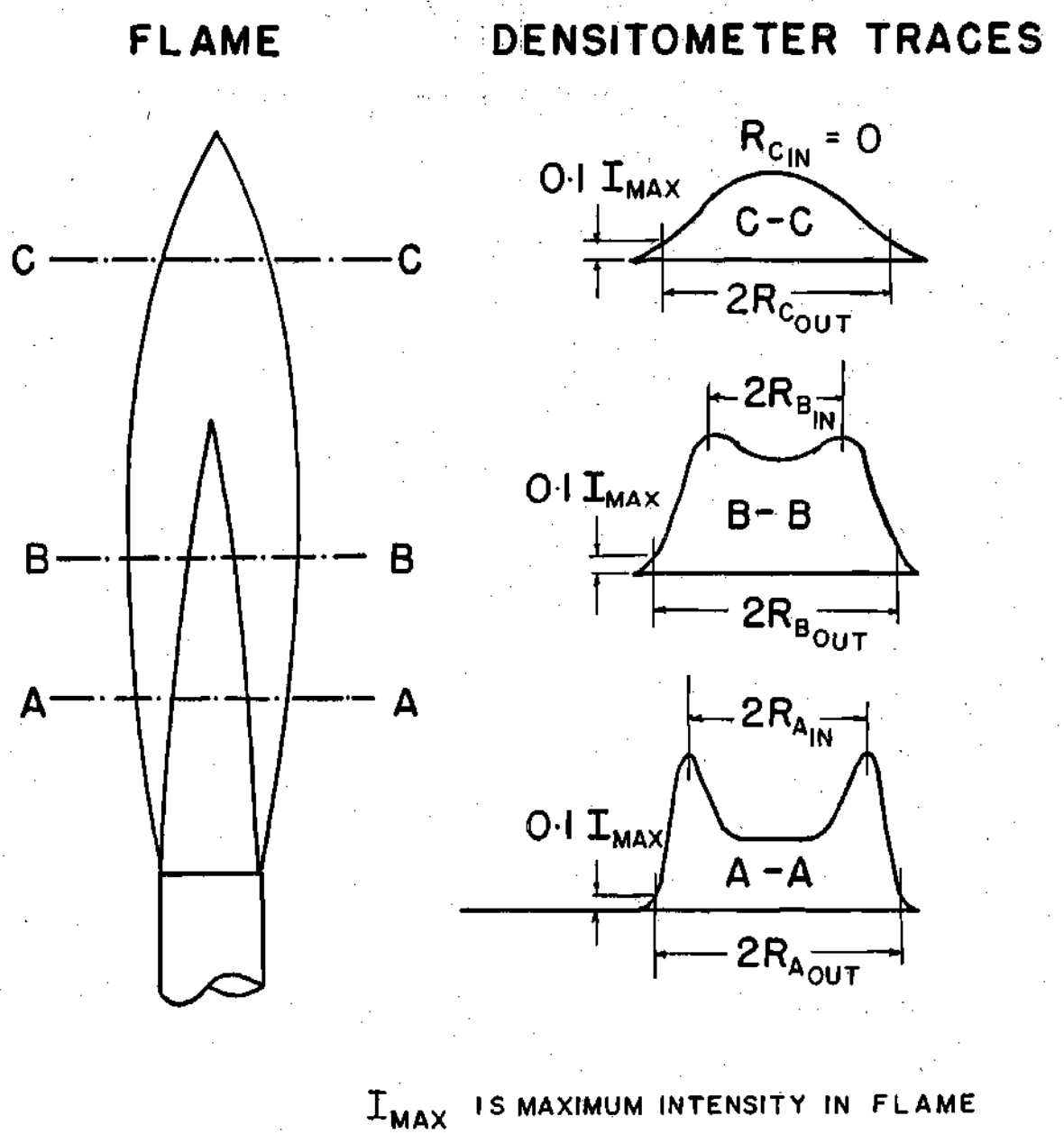

Figure 28. Flame Volume Measurement - Location of Inner and Outer Cones.

kind does not yield the true volume of the reaction zone in a strict sense; but such an analysis is capable of furnishing acceptable scaling laws when the criteria set forth are consistently adhered to in all the tests.

Experimental Results

Acoustic Center Location

The determination of the location of the acoustic center was one of the important contributions to the acoustic measurements. Earlier it has been stated that the volume of the flame was computed as a simple arithmetical sum of the elemental volumes between various longitudinal sections. These elemental volumes were divided by the corresponding elemental length of the flame to obtain the volume per unit length which is plotted as a function of the flame length. Figure 29 shows two such plots. The acoustic center corresponds to the location of the maximum volume per unit length in the flame. The results of present experiments showed that the fraction of flame length at which the maximum volume per unit length occurred could be expressed as a function of equivalence ratio ϕ alone. This result simplified the task of determining the acoustic center to one of measuring the length of the flame. The relationship between ϕ and fraction of flame length measured from burner port at which the acoustic center is located is shown in Figure 30. Figures 31(a), (b) and (c) present some data on the length of the flame which could be used in the determination of acoustic center. It is interesting to note that the flame length increases as only $U^{\frac{1}{2}}$ (Figure 31(a)) and as $D^{\sim 0.64}$ (Figure 31(b)). Further, the flame length achieves

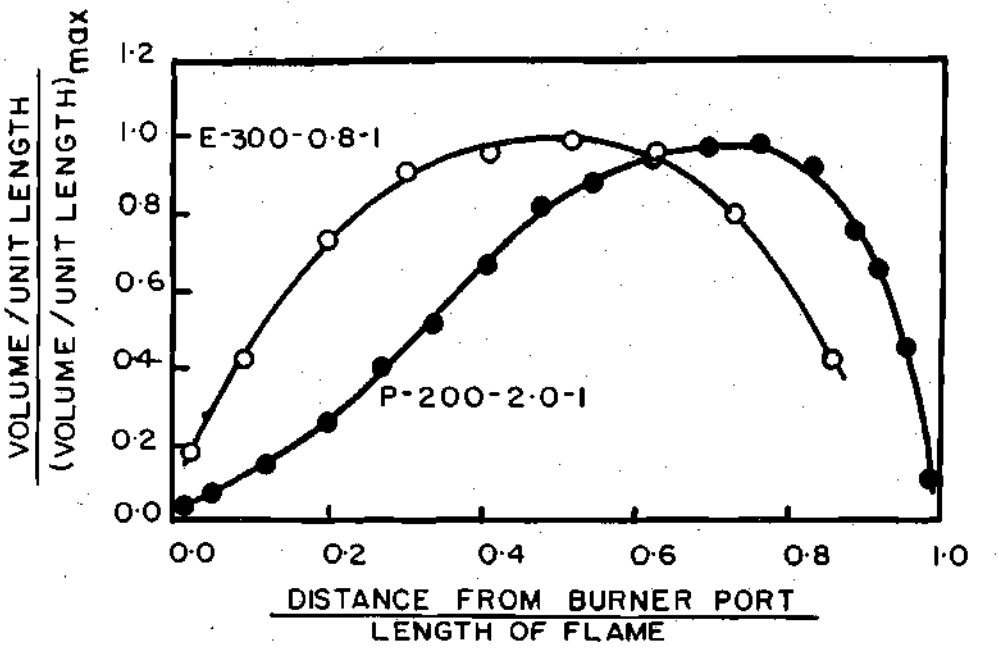

Figure 29. Flame Volume Distribution.

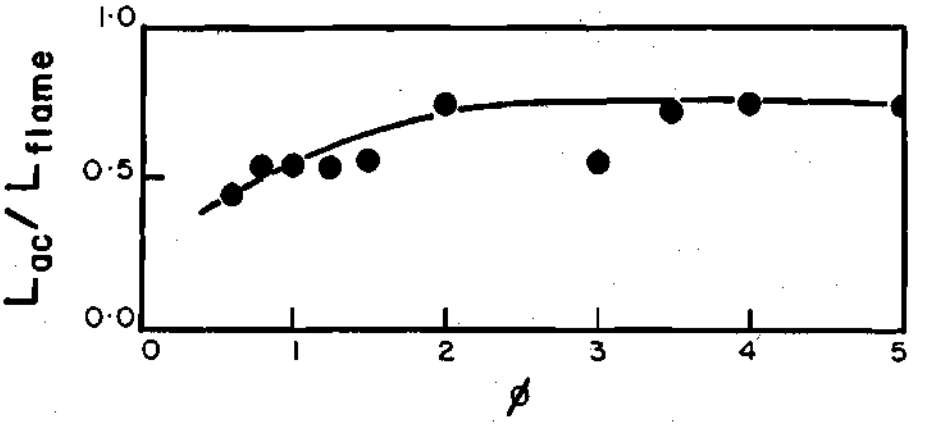

Figure 30. Distance L_{ac} from Burner Port at which Acoustic Center is Located as a Function of Equivalence Ratio.

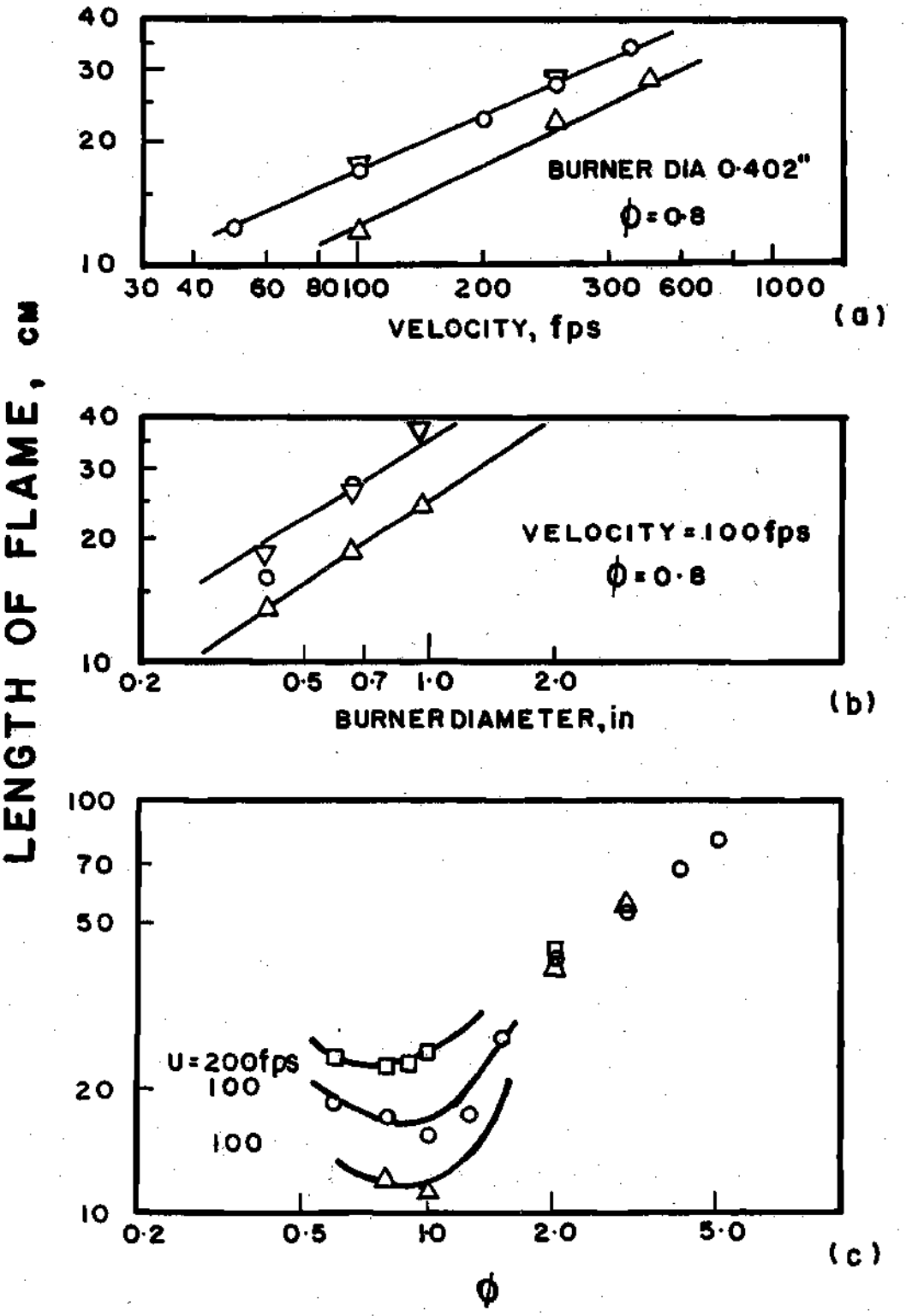

Figure 31. Length of Flame as a Function of a) Velocity, b) Burner Diameter, and c) Equivalence Ratio. ○ -- Propane △ -- Ethylene ▽and □ -- Propylene.

a minimum near stoichiometric mixtures as seen on Figure 31(c). This is simply a reflection of the fact that maximum laminar flame speed (and hence the turbulent flame speed) is obtained for conditions near stoichiometry.

Flame Volume Scaling Laws

The behavior of the flame volume with burner diameter is shown in Figure 32. It can be seen that the flame volume increases as the cube of the burner diameter. A look at Table 5 shows that both WF and FDR models of Strahle's theory can explain this result if the turbulence length scale ℓ_t is proportional to D. In cold jet flows it is known that the turbulence length scale is proportional to the jet diameter[31]. The result $V \propto D^3$ therefore presents a strong possibility that the turbulence length scale in the reaction zone is also proportional to the burner diameter. In Figure 32 the effect of S_L has not been eliminated from the data points.

Figure 33 presents the flame volume as a function of the mean flow velocity of the reactants in the burner tube. Based on the result of Figure 32 a $(\text{Diameter})^3$ correction has been applied to the flame volume so as to take away the diameter effect from the data points. The flame volume is seen to scale linearly with flow velocity, which is in accord with the theories of Reference 17. Again on this plot the effects of S_L and F have not been considered. The tendency of the ethylene data points to remain below those for propane is an indication of the inverse scaling of V with S_L. Following the procedure adopted to get scaling laws for acoustic power and peak frequency by regression analysis the

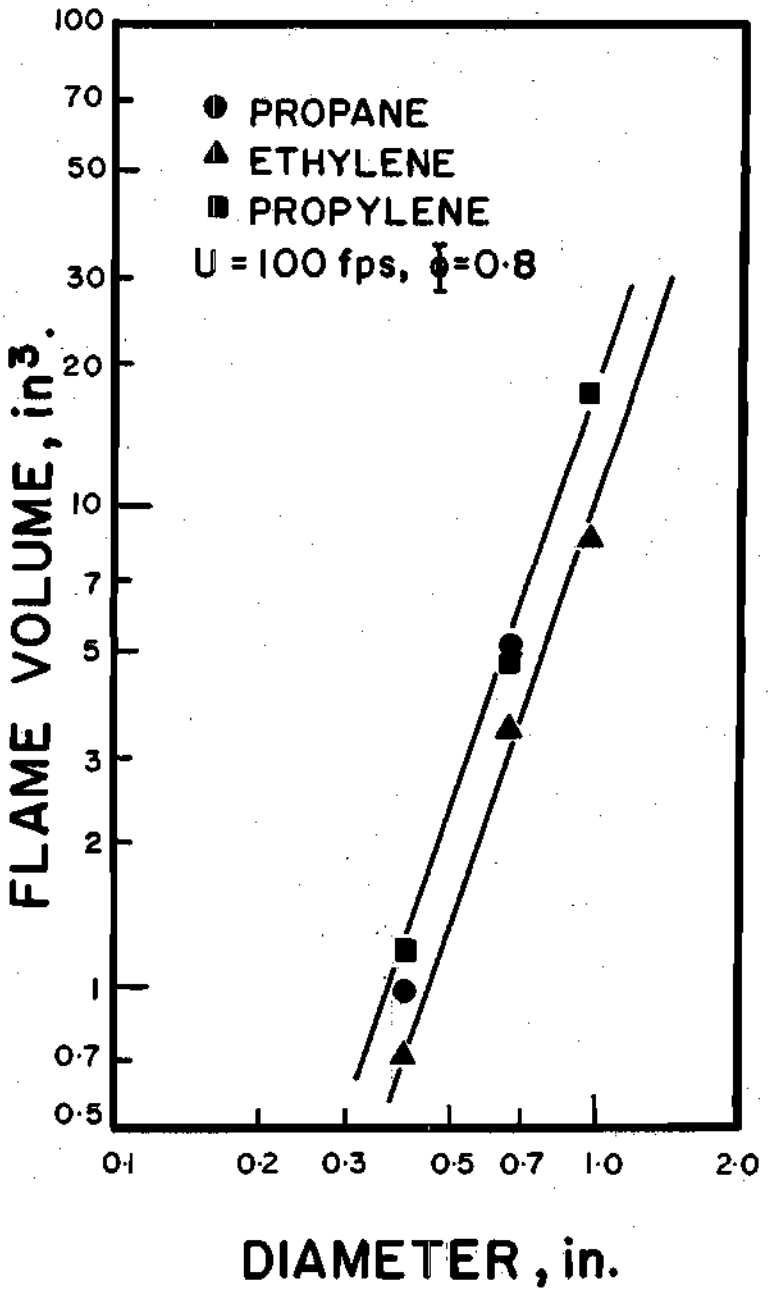

Figure 32. Flame Volume as a Function of Burner Diameter.

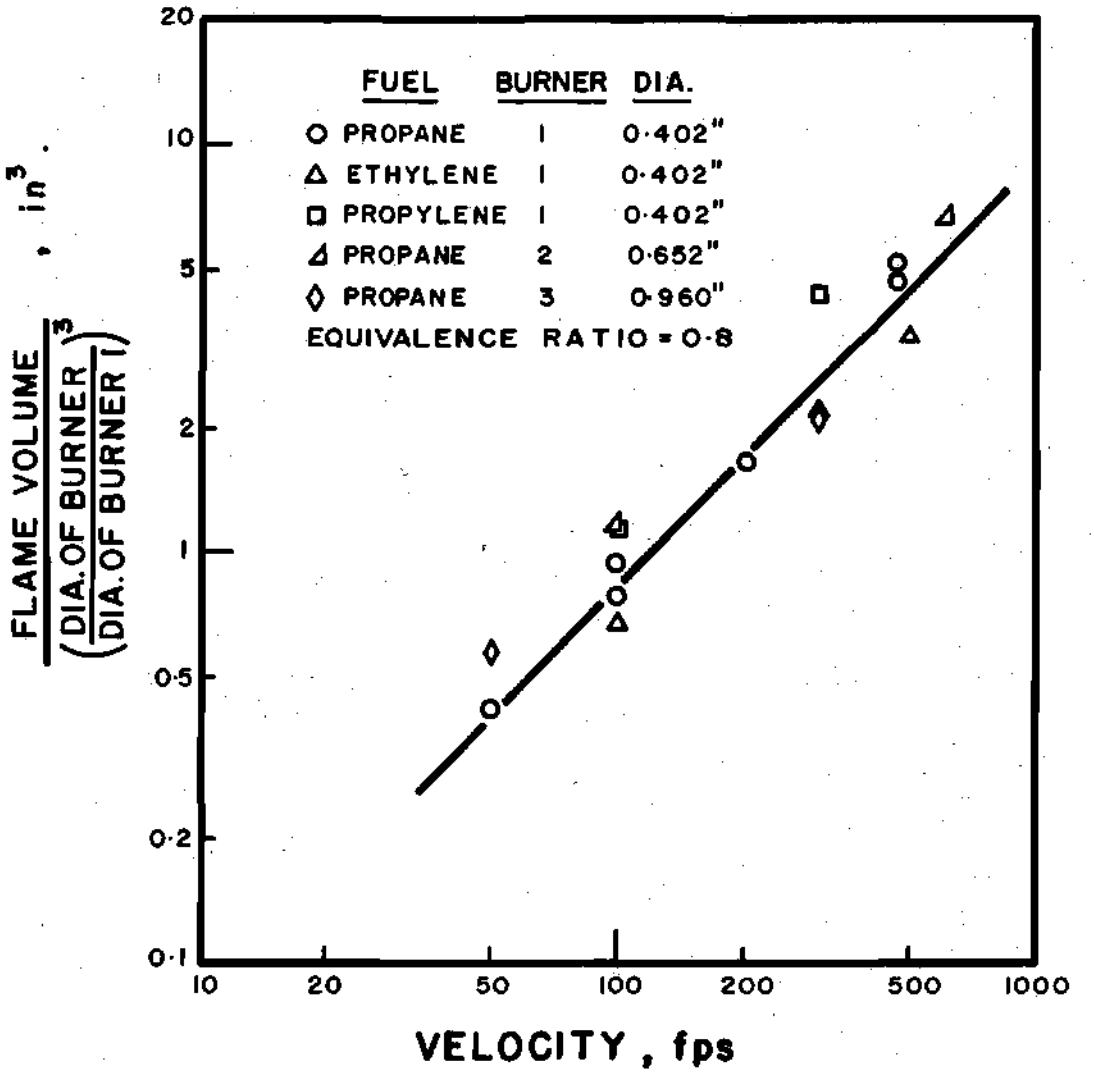

Figure 33. Flame Volume as a Function of Mean Flow Velocity of Reactants.

volume scaling laws were also deduced.

Using 39 different tests on the three burners and the three fuels at various equivalence ratios between 0.6 and 1.0 and velocities from 50 fps to 600 fps the following relation is obtained:

$$V = 3.4 \times 10^{3} \, U^{0.87} \, D^{3.2} \, S_L^{-0.85} \, F^{2.8} \qquad (20)$$

where V is in ft^3, U is in ft/sec, D is in ft and S_L is in ft/sec. The analysis of the errors due to the fit obtained in Equation (18) gave a mean error of 3.2% with a standard deviation of 29%. The maximum error was 82%. The rather high standard deviation of the error distribution was not unexpected. Any linear inaccuracy in linear dimensions on the photograph shows up cubed in volume computations. The important aspect of this analysis, however, is not the accuracy of measuring the reaction volume but rather obtaining the scaling laws. It has been noticed that the exponents on U, D, S_L and F obtained from the regression fit are quite stable in as much as the exponents varied very little when the number of tests used for the fit was varied from 14 to 39, the tests being picked at random. Thus, it is reasonable to assume that good statistical stability is attained for the results of the correlation of interest.

The scaling laws obtained from Equation (20) fall in line with those deduced from Figures 32 and 33. The scaling on S_L is in favorable agreement with the estimates of Reference 17.

However, Reference 17 does not allow for any dependence on F

while experimentally there is quite a strong cubic dependence. It is as if each linear dimension were being increased in proportion to the temperature difference across the flame, since the temperature difference is roughly proportional to F (Reference 27). There is no apparent reason for this dependence. Although a dependence upon F to the first power might be reasoned through a temperature (density) effect upon ℓ_t, the cubic law is puzzling. Since only relative photographic intensity and not absolute intensity is being measured, this cannot be a radiation intensity effect.

Referring back to Equation (19) from the dimensional analysis a comparison of the experimental data with the nondimensional equation can be made. An experimental D^3 dependence can only be explained if $\ell_t = D$. This independently confirms the earlier deduction that the turbulent length scale should be proportional to the burner diameter. Further, the exponents on U and S_L obtained in Equation (20) are 0.87 and -0.85, respectively. This shows that the U and the S_L effects mutually balance in Equation (19). Thus, a dimensional homogeneity can only be achieved when u'/U is a constant. This result implies that the turbulence intensity in the flame is relatively independent of the other scaling parameters. Since it is known for fully developed pipe flow that u'/U is a constant[31], this analysis tends to support the statement that the turbulent intensity is not affected by the flame. The conclusion to be reached on the turbulence structure in the reaction zone is therefore that there is no major modification to the turbulence structure due to the flame.

Comparison With Acoustic Power Scaling Laws

It is now possible to compare the flame volume scaling law of $V \propto U^{0.87} D^{3.2} S_L^{-0.85} F^{2.8}$ with the acoustic power scaling law of Equation (11). As was expected in the theory, the flame volume does partially explain the scaling laws on acoustic power. Both flame volume and the acoustic power scale to about D^3 with burner diameter. This shows that almost all the diameter effect perhaps comes from the scaling of reacting volume. The reacting volume accounts only partially for the velocity scaling. This is in accord with the expectations of Reference 17. The scaling law on S_L in flame volume tends to lower the S_L exponent for acoustic power radiated. As has been discussed earlier the F scaling remains unexplained at this time.

Summarizing the comparison with Strahle's theory[17], it can be observed that the expression deduced for far field acoustic radiation in the form of Equation (3) appears to be satisfactory, considering the experimental results of References 8 and 9. Further, estimates of reaction volume are quite satisfactory except for the F scaling. Thus, the order of magnitude estimates of autocorrelation function of the time derivative of the reaction rate and the correlation volume can be suspected to be incorrect.

Concluding Remarks

A comparison of the predictions of the combustion noise theory of Strahle with the experimental results has shown that the theoretical estimates are reasonable. Summarizing the findings, the following conclusions can be drawn:

1. The direct photography technique has been shown to be a useful tool in decomposing the scaling rules of combustion noise.

2. The turbulence length scale in the reaction zone has been shown to be proportional to the burner diameter.

3. The preference for WF and FDR models has been established. Since both these theoretical models yield the same scaling laws for the flame volume, it is not possible to judge the superiority of either of the two models by this method.

4. An evaluation of the experimental findings with the results of dimensional analysis has demonstrated that the turbulence structure is determined primarily by the pipe flow process and not by the flame.

CHAPTER IV

OPTICAL EMISSION STUDIES

There is both experimental[8,9] and theoretical[17] evidence to show that noise generation by flames could be deduced from optical emission studies. Hurle et al[8] and Price et al[9] obtained a good correlation between the instantaneous pressure and time derivative of the emission intensity traces for various flames over a limited band-width of the signals. The limitation of band-width was primarily necessitated by the large amount of noise in the optical circuitry. Since the band-width considered did include the predominant frequencies of combustion noise, the correlation could be considered significant. In an attempt to theoretically explain the results of Hurle et al[8] and Price et al[9], Strahle[17] obtained an expression for the far field acoustic density. Considering Equation (3),

$$\rho \propto \int_V \omega_t \left(\underset{\sim}{r}_o, t - \frac{r}{a_o}\right) dV \left(\underset{\sim}{r}_o\right)$$

where ω_t is the time derivative of the reaction rate referred to a retarded time corresponding to the distance r between the source and the far field location at which densith is measured. This results supports the findings of References 8 and 9 and states that the far field acoustic density can be expressed as a volume integral of the time derivative of

the time-retarded global reaction rate.

The implications of these results are that at least some of the scaling laws on acoustic power can be deduced by the optical technique without the use of any sound measuring equipment. Also, a good correlation between the sound pressure and dI/dt, where I is the emission intensity and t is the time, would establish that the noise emitters are solely restricted to the region of combustion thereby leading to a better understanding of the origin of combustion noise.

The experimental study described in this chapter is conducted with the aim of determining if the correlation between the acoustic and optical emissions does exist over a wide range of mixture ratios and flow velocities. Instead of restricting the study to a comparison of instantaneous time traces, correlation techniques and spectral analysis are used. Using optical emission r.m.s. readings, a velocity scaling law for the acoustic power is deduced.

Procedure

The experimental set-up used in these experiments was the same as the one used for acoustic measurements. The anechoic chamber provided a satisfactory dark chamber for optical measurements to be performed. The image of the flame was focused on the cathode of a photomultiplier tube using a f/4.5, 50 mm enlarger lens fixed to the front of the photomultiplier tube housing. The photomultiplier tube was placed at such a distance to capture the optical emission from the entire flame brush. In the experiments conducted the distance between the burner and the front of the lens was kept at 53.5 inches. At this

distance it was possible to cover an area of about 25 inches in diameter at the plane of the burner. This area was more than adequate to accommodate the largest flame which was tested, namely, the 600 ft/sec flame on the 0.402 inch burner. The light collected by the lens was filtered through a narrow band optical filter centered on C_2 radiation (5165 Å). The peak transmission of the filter was at 5155 Å with a half-peak transmittance band-width of about 50 Å. The selection of the filter was based on the recommendations of References 8 and 9. It is known from spectroscopic studies that radicals like CH, C_2 and OH exist only in the zone of reaction. The mean intensity of emission of any one of these active radicals should be proportional to the global reaction rate in the flame while the time derivative of the emission intensity should be proportional to the time derivative of the global reaction rate. Thus, by focusing the entire flame onto the photomultiplier tube an effective volume integration is performed over the reacting volume.

Figure 34 shows the instrumentation used in this study. The output of the photomultiplier tube was suitably amplified and passed into a differentiating curcuit. The particular differentiating circuit was known to produce $-de(t)/dt$ when a voltage $e(t)$ was introduced at the input. Thus, in the analysis of the experimental results the negative sign introduced by the differentiating circuit was suitably known. The differentiated signal was then passed through a band-pass filter and recorded on one of the channels of a multi-channel magnetic tape recorder using the necessary amplification.

Two microphones stationed at 90° to the flow direction with

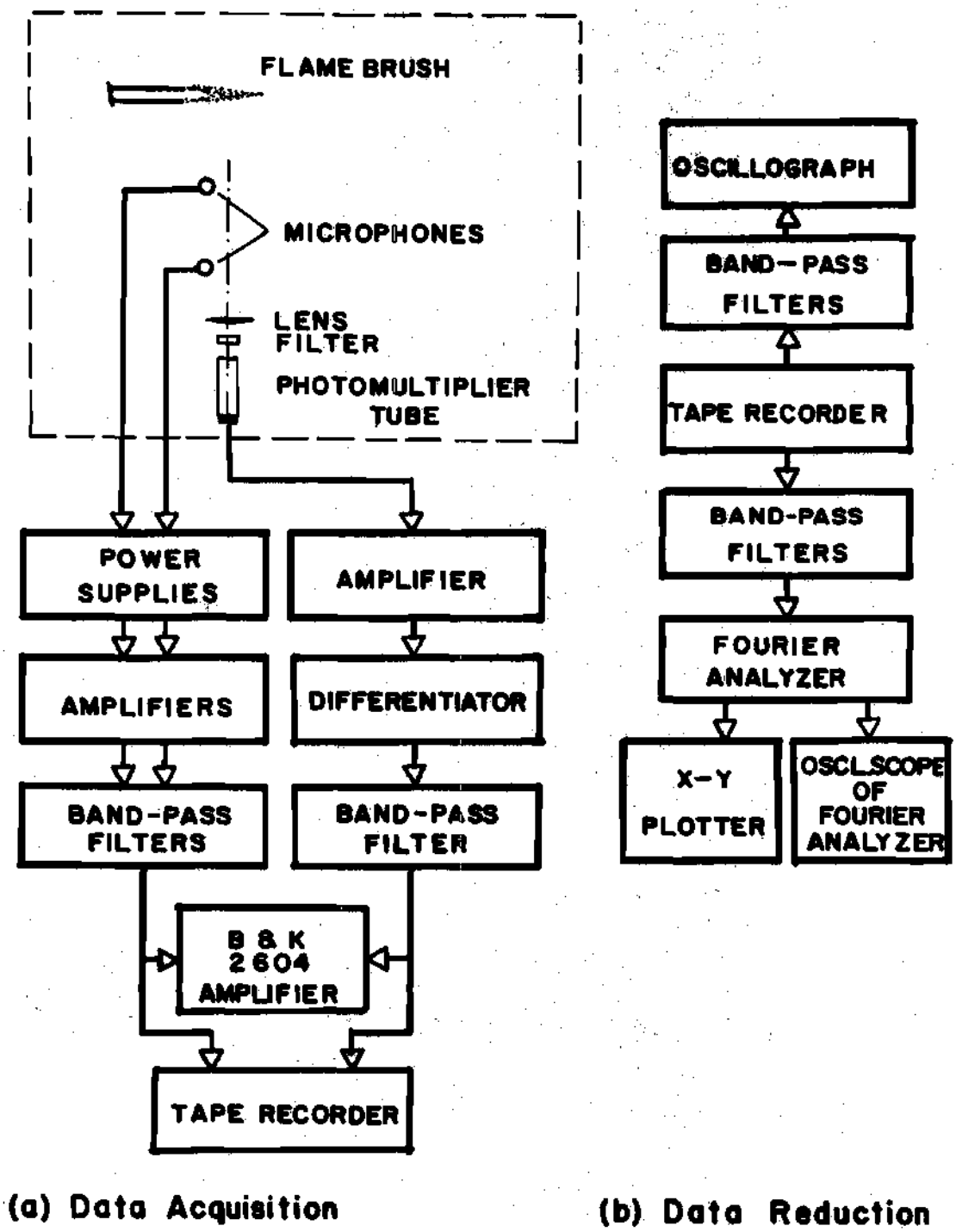

Figure 34. Instrumentation Schematic for Optical Emission Study.

reference to the burner exit were used for sound pressure measurement. The microphones were placed at 14" and 24" from the burner port. The output of the microphones was passed through band-pass filters identical to the one used on the optical circuit. The band-width settings were also identical. The sound pressure waveforms were recorded simultaneously with dI(t)/dt on two other channels of the tape recorder. In some instances, the filtering of the waveforms was done during reproduction from the tape recorder. The tape recorder was run at 30 ips tape speed during the recording phase. At this tape speed the tape recorder has a flat response up to 10 kHz. In order to expand the time scale of instantaneous traces on the oscillograph the tape was played back at 1-7/8 ips producing a speed reduction of 16. The reproduced signals were plotted on a paper chart using a CEC type 5-124 A oscillograph. A paper speed of 64 inches/sec was used for this purpose. The spectra of both dI/dt and p were obtained on the HP Fourier analyzer. The procedure has been explained in detail in Chapter II. The cross-correlation between the signals was also obtained on the HP Fourier analyzer. In order to obtain stable correlations a 100 sample averaging technique was used.

Comparison of Instantaneous Waveforms

Figure 35 shows a comparison between the instantaneous time traces of p(t) and dI(t)/dt for two cases, namely, P-600-0.8-1 and P-100-1.25-1. The waveforms shown are oscillograph recordings redrawn incorporating a time shift τ^*. $\tau^* = \frac{r}{a_o}$ is the amount of time by which the p(t) waveform is moved in the -t direction to account for the time

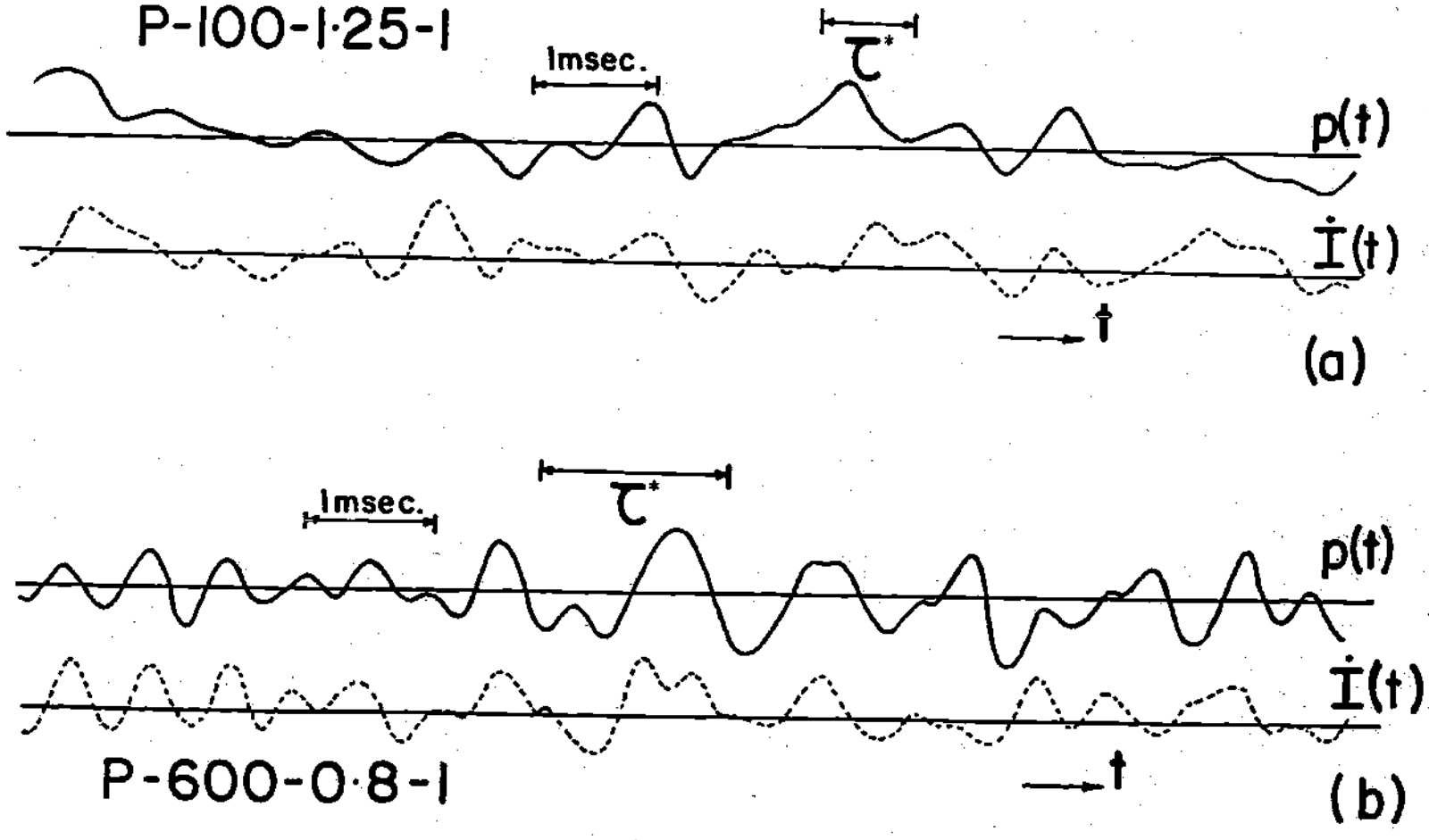

Figure 35. Comparison Between p(t) and $\dot{I}(t)$ Waveforms. p(t) Waveforms are Shifted to Left by Time τ^*. Band-Width: 60-2000 Hz. a) For P-100-1.25-1. b) For P-600-0.8-1.

taken by sound to travel the distance between the source (the flame) and the receiver (the microphone). The optical radiation from the flame reached the photomultiplier almost instantaneously in comparison with τ^*. The tape recorder used is known to introduce phase differences between signals recorded on different channels. The maximum phase difference is about 20° for a signal of frequency 1000 Hz. Also, the phase difference is directly proportional to the frequency. Due to this phase difference it is possible that an error of the order of 5% (of τ^*) is introduced in the time shift τ^* on Figure 35. Thus, the error in τ^* is within acceptable limits. Some similarities exist between the corresponding $p(t)$ and $dI(t)/dt$ waveforms in Figure 35. Thus, it has been demonstrated that the results of References 8 and 9 can be extended to include a 600 fps flame also. The most important conclusion of this correlation between optical and acoustic emissions is that sources of combustion noise are primarily located in the visible flame brush. This can be considered to support the theory of Reference 17 which recognized the value of evaluating the flame volume in studying combustion noise scaling laws. Thus, the value of flame volume measurements of Chapter III is reaffirmed.

Although, comparing the instantaneous $p(t)$ and $\dot{I}(t)$, where $\dot{I}(t)$ is used to denote $dI(t)/dt$, would establish a one-to-one correspondence directly, certain experimental difficulties are involved. These difficulties arise mainly due to spurious electronic noise in the instrumentation. The $p(t)$ is relatively free from spurious noise. However, the differentiator in the optical circuitry tends to magnify the relative importance of noise making the signal/noise ratio in $\dot{I}(t)$ rather

low. Thus, a reasonable comparison between the acoustic and optical waveforms could not be obtained for cases like P-100-0.8-1. Additional details about the spurious noise in the $\dot{I}(t)$ will be presented at a later stage in this chapter.

The foregoing discussion clearly demonstrates that more definite evidence than what has been presented in Figure 35 is required before a one-to-one correspondence between optical and acoustical emissions from turbulent flames can be accepted. Therefore, resort was made to further experimentation aimed at obtaining cross-correlation and spectral distributions.

Cross-Correlation

The cross-correlation function[23] gives a measure of the similarity between two waveforms used in the calculation. If the same signal is used in the place of both waveforms an auto-correlation function would result. The autocorrelation function is an extension of the concept of the root-mean-square value of a wave. The autocorrelation function is always symmetric about the point of zero delay; it has a maximum value equal to the mean square value of the wave at the point of zero delay.

The cross-correlation function, on the other hand, does not always maximize at zero delay. In fact, the point at which the maximum occurs is one of the most significant results arising from the cross-correlation function analysis of two signals. This delay time at which the maximum occurs forms an important basis in isolating the source of a disturbance.

Correlation techniques have been used extensively in aero-acoustic

problems, for example, Bhatt[32] and Goff[33]. Recently, Abdelhamid[22] employed this technique to establish correlation between the noise from high-speed jets and combustor pressure disturbances. Mathematically, the cross-correlation function G between two waveforms x(t) and y(t) can be expressed as

$$G(\tau) = \lim_{T \to \infty} \left\{ \int_{-\frac{T}{2}}^{\frac{T}{2}} x(t)\ y(t - \tau)\ dt \right\} \tag{21}$$

For the case at hand

$$\begin{aligned} x(t) &\equiv p(t) \\ y(t) &\equiv \dot{I}(t) \end{aligned} \tag{22}$$

Recall that the sound wave takes a time τ^* to reach the microphone. Thus, for a one-to-one correspondence between p(t) and $\dot{I}(t)$, we should have

$$x(t) = Ky(t - \tau^*) \tag{23}$$

where K is some constant. The cross-correlation function, therefore, becomes

$$G(\tau) = \lim_{T \to \infty} \left\{ \int_{-\frac{T}{2}}^{\frac{T}{2}} K_y(t - \tau^*)\, y(t - \tau)\, dt \right\} \qquad (24)$$

and would maximize at $\tau = \tau^*$. Thus, the experimental cross-correlation function should maximize at $\tau = \tau^*$ for establishing a one-to-one correspondence between the optical and acoustic emissions.

The correlation functions of Figures 36, 37 and 38, presented here, are drawn from photographs of the digital display on the screen of the oscilloscope used as a part of the Fourier analyzer system. Figure 36 shows the autocorrelations for both p(t) and $\dot{I}(t)$ waveforms. These waveforms maximize at $\tau = 0$. In Figure 36 as well as in Figures 37 and 38 trace lengths of $\tau/4$ have been cleared at both ends of the time axis, in order to eliminate wrap-around errors[34]. Figure 37(a) shows an autocorrelation function for the p(t) of the P-600-0.8-1 case. Figure 37(b) is a display of the cross-correlation function between p(t) as measured by the microphones at 14" and 24" from the flame. Notice that the cross-correlation maximizes at $\tau \approx 0.8$ msec which corresponds to the time taken by sound waves to travel the distance between the two microphones. Cross-correlation functions between $\dot{I}(t)$ and p(t) waveforms over various experimental conditions are presented in Figure 38. Figure 38(a) shows the cases for which p(t)'s from the microphone at 14" have been used. The cross-correlations maxmize for $\tau \approx 1.0$ msec in these cases. Figure 38(b) is for p(t)'s from microphone at 24". The time delay at which maxima occur is ≈ 1.8 msec. In Figure 38 the experiments include a flow

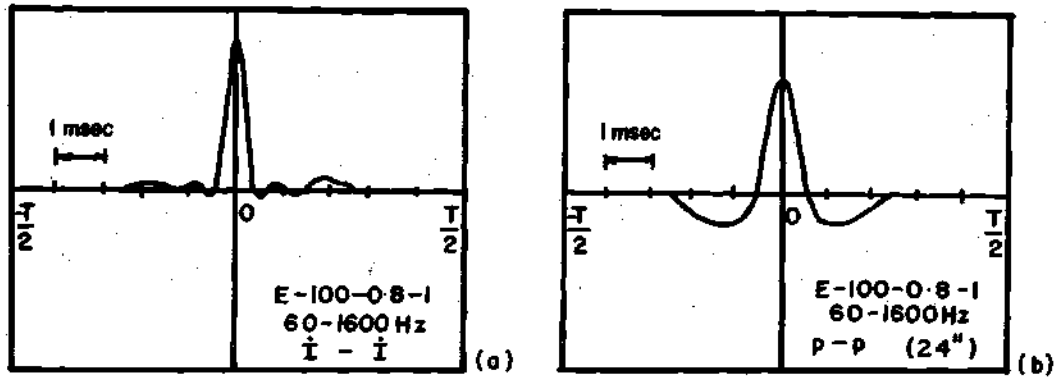

Figure 36. Autocorrelation Functions a) for $\dot{I}(t)$ b) for p(t). Vertical Scale is Arbitrary.

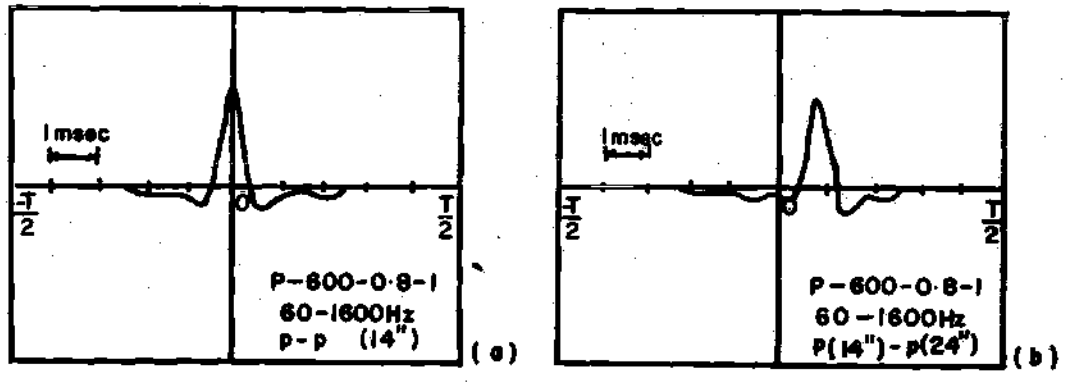

Figure 37. Cross-Correlation Function Between a) p(t) Waveform with Itself and b) p(t) at 14" with p(t) at 24". Vertical Scale is Arbitrary.

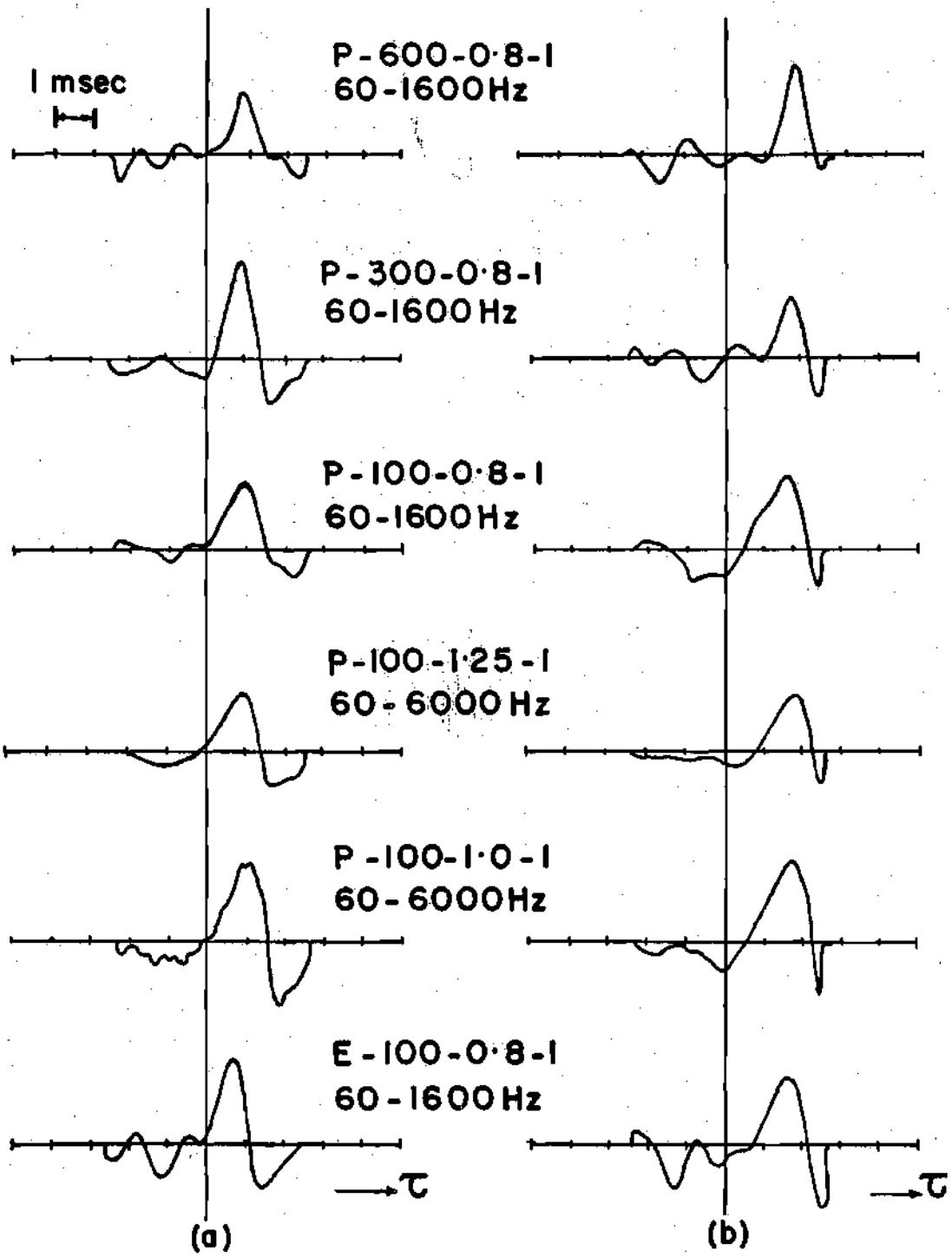

Figure 38. Cross-Correlation Between p(t) and $\dot{I}(t)$ Waveforms. a) p(t) from Microphone at 14". b) p(t) from Microphone at 24".

velocity range of 100-600 fps. The fuels propane and ethylene are used and both fuel-lean and fuel-rich mixtures are used. Thus, over a wide range of parameters a good cross-correlation between p(t) and $\dot{I}(t)$ exists.

Frequency Spectra of Optical Emission

After having established that a good cross-correlation exists between the acoustic and optical emissions, the spectra of $\dot{I}(t)$ and p(t) were compared. These spectra should show identical frequency distributions if a one-to-one correspondence exists.

First, the P-100-1.25-1 case is considered. The comparison between the instantaneous p(t) and $\dot{I}(t)$ traces was shown to be quite reasonable in Figure 35(a) for this case. Figure 39 shows that the spectra of $\dot{I}$ and p are in excellent agreement up to 1000 Hz. The correspondence between the spectra grows progressively worse due to electronic noise at higher frequencies. Since in Figure 35(a) the waveforms were restricted to 2000 Hz, it was possible to observe a reasonable similarity.

Figure 40 shows the spectra for the case P-100-0.8-1. It has been stated earlier that an instantaneous waveform comparison was found to be extremely difficult for this case. The spectrum for optical emission is almost flat over the entire frequency range showing that the $\dot{I}(t)$ signal is dominated by spurious noise. The reason for the difference in behavior between the two cases shown in Figures 39 and 40 can be explained to some extent by their mean intensities. It will be shown later, in Figure 42, that electronic noise dominates for flames with low mean intensity. The P-100-1.25-1 flame, being much brighter

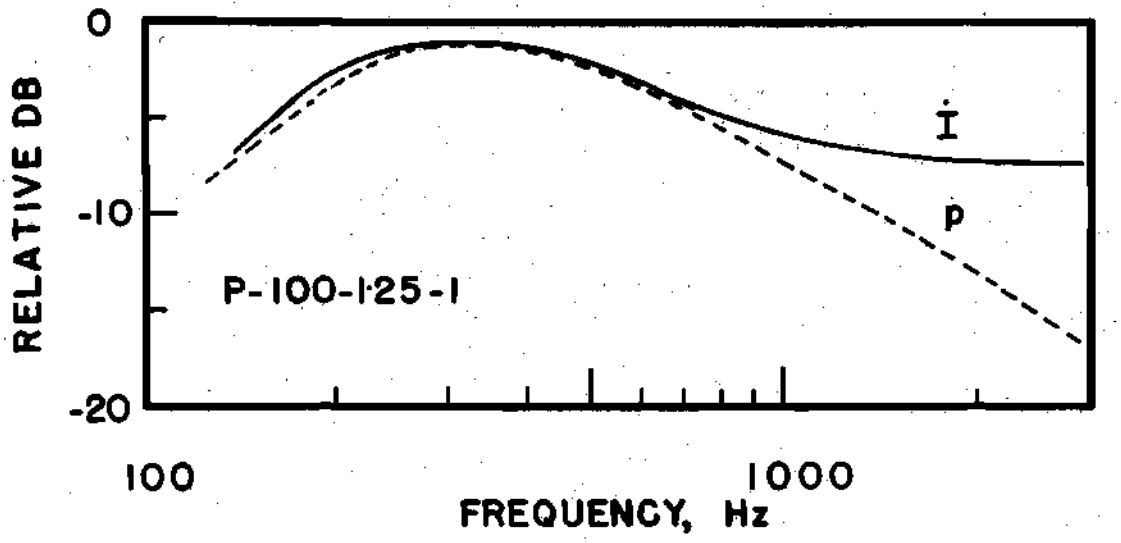

Figure 39. Frequency Spectra of $\dot{I}$ and p for the P-100-1.25-1 Case.

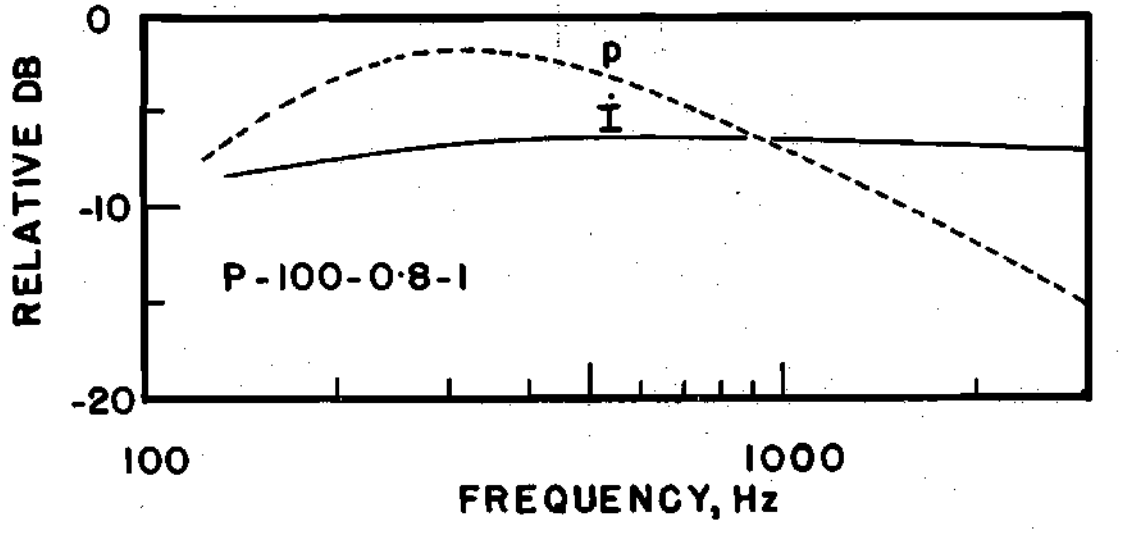

Figure 40. Frequency Spectra of $\dot{I}$ and p for the P-100-0.8-1 Case.

than the P-100-0.8-1 flame, has a better signal to noise ratio and, therefore, shows a reasonable spectral comparison.

Similar spectral comparisons were made at various other experimental conditions. In general, it was observed that above about 1000-2000 Hz frequency electronic noise dominates $\dot{I}(t)$. Thus, any study using optical emissions from flames should exclude frequency components above 1000-2000 Hz unless better electronics are available. Since, in Chapter II, it has been established that for hydrocarbon-air flames the combustion noise peaks in the 250-700 Hz range, this should not be a major restriction. Nevertheless, electronic noise appears to be a major problem to guard against in optical emission studies.

Velocity Scaling of Acoustic Power from Optical Emission Measurements

The investigation discussed in this section arises as a natural consequency of the results presented so far in this chapter. If, in fact, there is a one-to-one correspondence between $p(t)$ and $\dot{I}(t)$, then it should be possible to obtain at least the scaling laws on U and D for the acoustic power by optical experiments. The scaling laws with respect to S_L and F would require the use of more than one fuel. Since the line intensities in the optical spectra for various fuels differ, there are bound to be additional corrections required for mean intensities. The following paragraphs describe experiments on a 0.402" diameter burner using propane as fuel designed to recover the U scaling on the acoustic power.

Experimental Details

The photo-multiplier tube output was amplified and differentiated.

The differentiated signal was passed through a band-pass filter set to allow frequencies between 180-1000 Hz. This restriction on frequency was decided by the results of the spectral analysis. The filtered $\dot{I}$ was measured by the volt meter of a B & K 2604 microphone amplifier. The r.m.s. value of $\dot{I}$ was read out as db (re. 1 $V_{r.m.s.}$). A 20-10,000 Hz linear meter response was used. The meter was set to the slow position. The gains on the amplifiers, the band-widths, voltage supply to photo-multiplier tube, etc. were left undisturbed over the entire set of experiments so that changes in the $\dot{I}_{r.m.s.}$ measured would be representative of the changes at the flame. The $\dot{I}_{r.m.s.}$ measured were therefore representative of both the true signal and the electronic noise. Since it had been determined that electronic noise is appreciable it was necessary to correct the measured $\dot{I}_{r.m.s.}$ for electronic noise.

Electronic noise in $\dot{I}$ is known to be a function of the mean intensity I received by the photo-multiplier tube. Figure 41 shows the variation of mean intensity of the particular flame under consideration with flow velocity. These mean intensity values were measured by a d.c. volt meter at the input to the differentiator without disturbing any of the instrument settings. Using a standard lamp supplied with ripple-free d.c. current a light source with negligible light flickering was obtained. The $\dot{I}_{r.m.s.}$ measured for this case should be indicative of the electronic noise. Figure 42 shows the $(\dot{I}_{r.m.s.})_{elec.\ noise}$ as a function of mean intensity I. Using Figures 41 and 42 together the values of electronic noise at various flow velocities for the particular

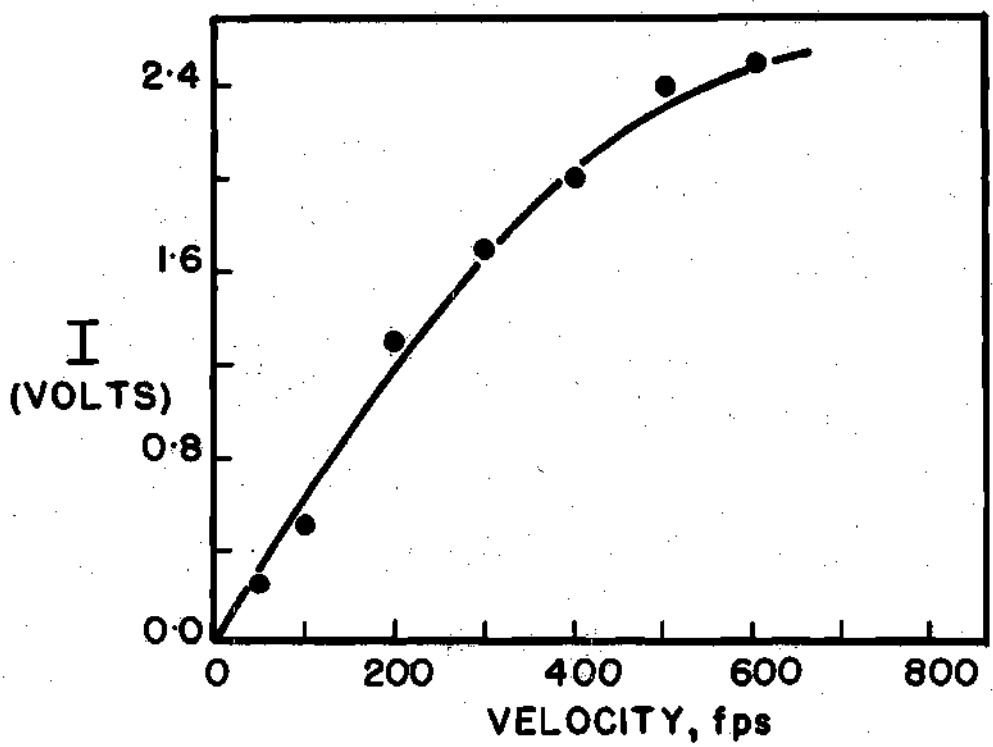

Figure 41. Mean Intensity as a Function of Flow Velocity.

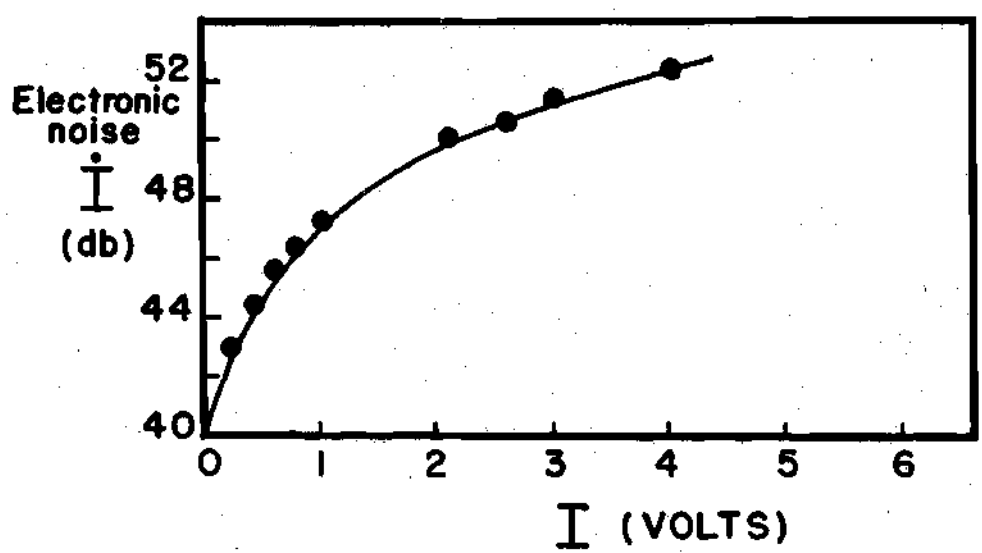

Figure 42. Electronic Noise İ as a Function of Mean Intensity.

flame could be determined. Now,

$$\left(\dot{I}_{r.m.s.}\right)_{\substack{true \\ in\ db}} = \left(\dot{I}_{r.m.s.}\right)_{\substack{measured \\ in\ db}} - \text{db correction}$$

The values of db correction were obtained from standard background noise correction graphs[23].

Figure 43 shows $(\dot{I}_{r.m.s.})_{true}$ as a function of flow velocity U. Also, values of $(\dot{I}_{r.m.s.})_{total}$ have been shown on Figure 43 to indicate that corrections applied are quite heavy. $(\dot{I})^2_{r.m.s.}$ appears to scale as $U^{2.7}$. This implies a $P \propto U^{2.7}$ scaling which is in excellent agreement with the $U^{2.7}$ law of Equation (11). However, it should be cautioned against considering the optical method to be accurate based on the $\dot{I}^2_{r.m.s.} \propto U^{2.7}$ result. Below 200 fps, the signal to noise ratio was so low as to make it impossible to get $(\dot{I}_{r.m.s.})_{true}$. Also, recall that a rather restricted frequency range of 180-1000 Hz has been used for these experiments.

Discussion

The experiments described in this chapter have shown that despite the experimental difficulties due to electronic noise in the differentiated photo-multiplier output, it is possible to observe one-to-one correspondence between the acoustic pressure and the time derivative of emission intensity from turbulent flames. This work supports the experimental findings of References 8 and 9 and the theoretical prediction of Strahle (see Equation (3)). Whereas References 8 and 9

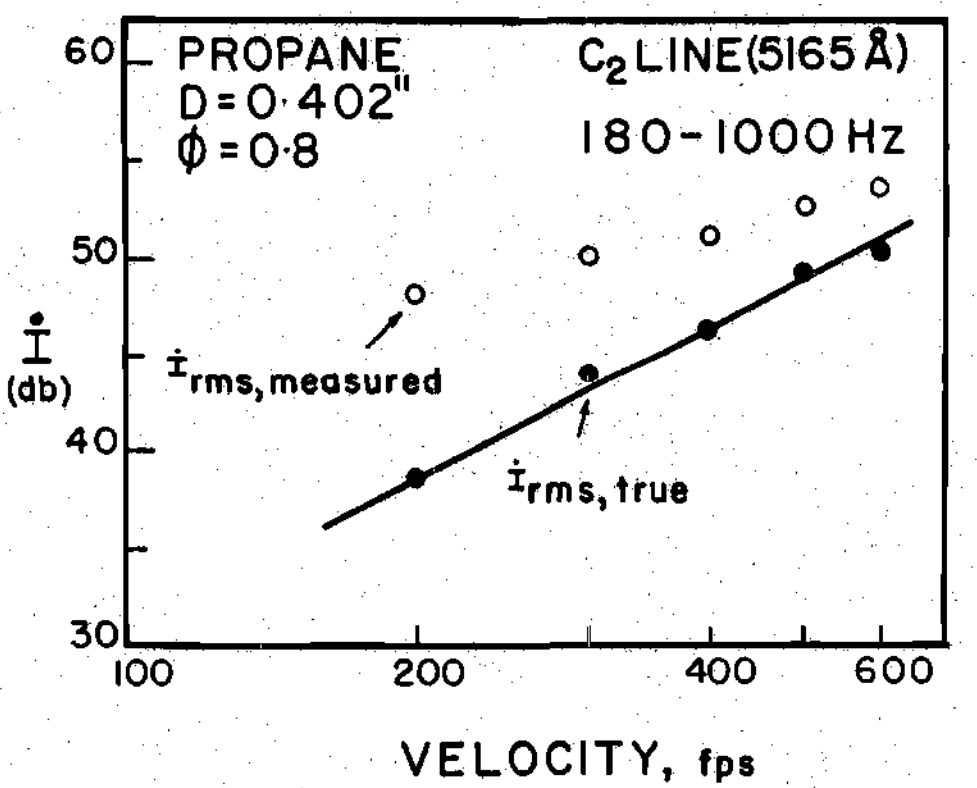

Figure 43. Acoustic Power Scaling Law with Velocity by Optical Technique.

compared $p(t)$ and $\dot{I}(t)$ directly, the experiments reported here have established the correspondence on a much sounder basis using correlation techniques in addition to direct comparisons. Also, necessary emphasis has been given on spectral analysis. Further, the velocity scaling for acoustic power has been obtained by the optical method under a frequency limited band-width of 180-1000 Hz. The scaling obtained compared favorably with the result of acoustic experiments when necessary corrections were applied for electronic noise. A practical implication of this is that noise output from regions of combustion can perhaps be deduced directly from the flame optical emissions without having to use an anechoic chamber. However, poor signal/noise ratio would remain a major drawback of this method. The most important outcome of the optical emission study is the result that combustion noise sources are primarily located within the visible flame brush.

CHAPTER V

CONCLUSIONS AND RECOMMENDATIONS

Conclusions

An experimental study of the radiation of noise by open turbulent flames has been made. Gaseous propane, propylene and ethylene fuels have been used with air as the oxidizer. The burner sizes have been 0.4" to 0.96" in diameter. The flow velocities have been varied between 50 and 600 fps. The study has shown that combustion noise dominates over jet noise over the entire range of experimental results obtained and that it differs from jet noise in terms of scaling laws, directionality and spectral content. Summarizing the results of this investigation it can be concluded that:

1. Combustion noise predominates over jet noise even for flow velocities as high as 600 fps.

2. The noise from open turbulent flames is weakly directional. The directionality behavior can be qualitatively explained by refraction and convection effects of Strahle's theory.

3. Combustion noise is a low frequency broad band radiation with a single peak. The peak frequency for fuel-lean ($\phi \leq 1.0$) flames has been obtained in the form $f_c \propto U^{0.18} S_L^{0.53} D^{-0.08} F^{-0.69}$. However, for all practical purposes it may be sufficient to consider combustion noise to peak in the 250-700 Hz range for hydrocarbon fuels burning with air as the oxidizer.

4. Acoustic power for fuel-lean flames has been found to follow the law $P \propto U^{2.7} D^{2.8} S_L^{1.4} F^{0.4}$. An empirical expression from which acoustic power can be directly calculated has been generated by regression analysis of the experimental data. For fuel-rich flames a $P \propto U^3 D^2$ dependence has been obtained. Ethylene-air flames have shown an anomalous behavior with equivalence ratio on the fuel-rich side.

5. Thermo-acoustic efficiency for fuel-lean flames has been shown to follow a $\eta_{ta} \propto U^{1.7} D^{0.8} S_L^{1.4} F^{-0.6}$ law. For a 600 ft/sec flame a η_{ta} as high as 10^{-6} has been obtained showing that noise output from high velocity flames could be appreciable. Thermo-acoustic efficiency of fuel-rich flames has been shown to be independent of burner diameter.

6. Scaling laws on flame volume obtained by a direct flame photographic method have been shown to be useful in decomposing combustion noise scaling rules. The flame volume has been determined to scale as $V \propto U D^3 S_L^{-1} F^3$. This study has shown that the turbulence structure in the flame is mainly decided by the pipe flow process and not by the flame.

7. Optical emission studies using direct time trace comparisons of acoustic and optical emissions and the use of a correlation technique and spectral analysis have shown that the sound pressure and the time derivative of the emission intensity are correlated. Acoustic power scaling with respect to flow velocity has been recovered by the optical study. It has been shown that sources of combustion noise are primarily located in the visible flame brush.

8. Comparison of the experimental results of premixed flames

with Strahle's theory has shown that the theoretical solution to the noise problem is reasonably good. The order of magnitude estimates for flame volume are satisfactory. Optical studies have confirmed the theoretical result that the far field acoustic density (pressure) can be obtained as a global integration over the reacting volume of the Eulerian time derivative of the time-retarded reaction rate irrespective of whether the flame is premixed or of a diffusion type. However, in the scaling laws for premixed flames, the order of magnitude estimates for the autocorrelation function of the time derivative of the reaction rate and the correlation volume appear to be incorrect, leading to poor overall scaling laws. Scaling laws on diffusion flames from Strahle's theory need further experimentation before any comparison can be attempted.

Recommendations for Future Research

During the course of the present study many new areas of research became apparent. Some topics for future research are listed below:

1. Noise studies on larger burners, of sizes and configurations similar to those employed in aircraft turbo-propulsion systems and industrial furnaces, are required. This will extend the results of combustion noise experiments into the size range of practical burner systems.

2. A detailed study of the interaction between the turbulence structure (both scale and intensity) and the noise generated is suggested. This could, perhaps, be done using turbulence generating grids upstream of the burner port. The present experiments which were con-

ducted using fully developed pipe flow turbulence do not give specific indications regarding the effects of the turbulence structure on the noise produced. Also, the diameter scaling obtained in the present study contains the turbulence scale effect as well. Thus, experiments are required to isolate diameter effects from turbulence scale effects.

3. Additional experiments on fuel-rich and pure diffusion flames are needed. An effort to explain the anomalous behavior of fuel-rich ethylene-air flames (with equivalence ratio) is required.

4. A study of the effects of duct enclosures on combustion noise is suggested. Combustor cans and industrial burners are some practical examples. A duct will augment the noise from the flame at frequencies corresponding to the resonant frequencies of the duct. Further, there could be a coupling between the combustion process and the acoustic field in the duct which could affect the source behavior. An equally important area of research appears to be noise experiments on flames stabilized on "bluff-body flame-holders." This method of flame retention is quite extensively used in industry.

APPENDIX

APPENDIX A

FLOW CALIBRATION

This appendix lists the flow calibration equations for the various flow meters used in this study. Figure A-1 below shows the basic flow diagram adjacent to the flow meters.

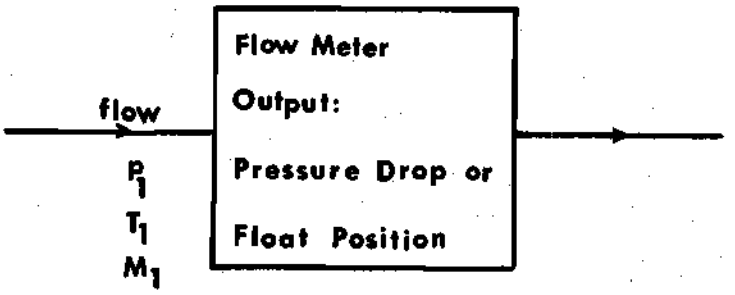

Figure A-1. Flow Meter Schematic.

p_1, T_1, and M_1 are the pressure, temperature, and molecular weight of the gas at the inlet to the meter. The orifice meter would indicate the flow rate by a pressure drop Δp and the rotameters would indicate the flow rate by the float position.

Air Flow Meters

Two rotameters have been used to measure the air flow. Rotameter

#1 was calibrated by the manufacturer between 0.2 and 2.0 PPM @ 34.7 psia and 75°F for air. Thus, if p_1 is in psia and T_1 is in °R and subscript o denotes operating and i denotes indicated

$$(PPM)_o = (PPM)_i \sqrt{\frac{p_1}{34.7}} \cdot \frac{535}{T}$$

or

$$(SCFM)_o = 52.38\ (PPM)_i \sqrt{\frac{p_1}{T_1}}$$

Rotameter #2 was calibrated by the manufacturer from 3.0 to 12.0 PPM @ 234.2 psia and 530°R for air. Thus

$$(PPM)_{o,air} = (PPM)_i \sqrt{\frac{p_1}{234.2} \cdot \frac{530}{T_1}}$$

or

$$(SCFM)_{o,air} = 20.068\ (PPM)_i \sqrt{\frac{p_1}{T_1}}$$

Again p_1 is in psia and T_1 is in °R.

Fuel Orifice Meters

For the measurement of fuel flow rate a $\frac{1}{2}$" orifice meter with concentric circular orifice and flange taps was used. The pipe diameter was 0.546". Two orifice plates were used. Orifice Plate #1 had a 0.048" diameter orifice. Using a calibrated rotameter and air as the working fluid, the following expression was obtained

$$(SCFM)_{operating} = 0.968 \sqrt{\frac{\Delta p \cdot p_1}{T_1 M_1}}$$

where Δp is in $"H_2O$

p_1 is in psia

T_1 is in $^\circ R$

M_1 is the molecular weight of the gas being metered

Orifice Plate #2 had a 0.259" diameter orifice. Calibration gave

$$(SCFM)_{operating} = 30.1 \sqrt{\frac{\Delta p \cdot p_1}{T_1 M_1}}$$

where again Δp is in $"H_2O$, p_1 is in psia and T_1 is in $^\circ R$. M_1 is the molecular weight of the gas being metered.

Hydrogen Orifice Meter

A $\frac{1}{2}$" orifice meter with square edge concentric circular orifice and flange taps was used. The pipe diameter was 0.546" and the orifice

diameter was 0.045". The meter was calibrated using calibrated rotameters and helium as the working fluid. The following expression was obtained for the flow rates measured by this meter

$$(SCFM)_{operating,H_2} = 0.6405 \sqrt{\frac{\Delta p \cdot p_1}{T_1}}$$

where p_1 is in psia

T_1 is in $^{\circ}R$

Δp is in inches H_2O.

BIBLIOGRAPHY

1. Tucker, M., "Interaction of a Free Flame Front with a Turbulence Field," NACA Report No. 1277 (1956).

2. Bragg, S. L., "Combustion noise," Journal of the Institute of Fuel, 36, p. 12 (1963).

3. Smith, T. B. J., and Kilham, J. K., "Noise generated by open turbulent flames," Journal of the Acoustical Society of America, 35, p. 715 (1963).

4. Smith, T. B. J., "Combustion Noise," Ph.D. Thesis, University of Leeds (1961).

5. Kotake, S., and Hatta, K., "On the noise of diffusion flames," Bulletin of JSME, 8 (30), p. 211 (1965).

6. Bollinger, L. E., Fishbruke, E. S., and Edse, R., "Contribution of Combustion Noise to Overall Rocket Exhaust Jet Noise," NACA CR-463 (May 1966).

7. Thomas, A., and Williams, G. T., "Flame noise: Sound emission from spark-ignited bubbles of combustible gas," Proceedings of the Royal Society of London A294, p. 449 (1966).

8. Hurle, I. R., Price, R. B., Sugden, T. M., and Thomas, A., "Sound emission from open turbulent premixed flames," Proceedings of the Royal Society of London A303, p. 409 (1968).

9. Price, R. B., Hurle, I. R., and Sugden, T. M., "Optical studies of the generation of noise in turbulent flames," Twelfth Symposium (International) on Combustion, Pittsburg, the Combustion Institute, p. 1093 (1968).

10. Smithson, R. N., and Foster, P. J., "Combustion noise from a Meker burner," Combustion and Flame, 9, p. 426 (1965).

11. Powell, A., "Noise measurement of a turbulent gasoline vapor flame," Journal of the Acoustical Society of America, 35, p. 405 (1963).

12. Giammar, R. D., and Putnam, A. A., "Combustion roar of turbulent diffusion flames," Journal of Engineering for Power, p. 157 (April 1970).

13. Giammar, R. D., and Putnam, A. A., "Combustion roar of premix burners, singly and in pairs," Combustion and Flame, 18, p. 435 (1972).

14. Knott, P. R., "Noise generated by turbulent non-premixed flames," AIAA Paper no. 71-732 (1971).

15. Seebold, J. G., "Combustion noise and its control in process plant furnaces," ASME Paper no. 71-Pet-6 (1971).

16. Strahle, W. C., "On combustion generated noise," Journal of Fluid Mechanics, 49, p. 399 (1971).

17. Strahle, W. C., "Some results in combustion generated noise," Journal of Sound and Vibration, 23, p. 113 (1972).

18. Strahle, W. C., "Refraction, convection and diffusion flame effects in combustion generated noise," Fourteenth Symposium (International) on Combustion (to be published).

19. Lighthill, M. J., "On sound generated aerodynamically, I. General theory," Proceedings of the Royal Society of London, A211, p. 564 (1952).

20. Lighthill, M. J., "On sound generated aerodynamically, II. Turbulence as a source of sound," Proceedings of the Royal Society of London, A222, p. 1 (1954).

21. Kushida, R., and Rupe, J., "Effect on supersonic jet noise of nozzle plenum pressure fluctuations," AIAA Journal, 10, p. 946 (1972).

22. Abdelhamid, A. N., Harrje, D. T., Plett, E. G., and Summerfield, M., "Noise characteristics of combustion augmented high speed jets," AIAA Paper No. 73-189 (1973).

23. Peterson, A. P. G. and Gross, Jr., E. E., "Handbook of Noise Measurement," Seventh Ed. General Radio, Massachusetts (1972).

24. Williams, F. A., Combustion Theory, Addison-Wesley (1965).

25. "Basic Considerations in the Combustion of Hydrocarbon Fuels with Air," NACA Report No. 1300 (1957).

26. Putnam, A. A., Combustion-Driven Oscillations in Industry, American Elsevier, New York (1971).

27. Steffensen, R. J., Agnew, J. T., and Olson, R. A., "Tables for Adiabatic Flame Temperature and Equilibrium Composition of Six-Hydrocarbon Fuels (With Air and Oxygen)," Engineering Experiment Series No. 122, Purdue University (1966).

28. Gaydon, A. G., and Wolfhard, H. G., Flames: Their Structure, Radiation and Temperature, 3rd Ed., Rev., Chapman and Hall, London (1970).

29. Fristrom, R. M., and Westenberg, A. A., Flame Structure, McGraw-Hill, New York (1965).

30. John, R. R., and Summerfield, M., "Effect of turbulence of radiation intensity from propane-air flames," Jet Propulsion, 27, p. 169 (1957).

31. Schlicting, H., Boundary-Layer Theory, 6th Ed., McGraw-Hill, New York (1968).

32. Bhat, W. V., "Use of correlation technique for estimating in-flight noise radiation by wing-mounted jet engines on a fuselage," Journal of Sound and Vibration, 17 (3), p. 349 (1971).

33. Goff, K. W., "Application of correlation techniques to some acoustic measurements," Journal of the Acoustical Society of America, 27 (2), p. 236 (1955).

34. Hewlett Packard Fourier Analyzer System 5450A/5452A Systems Operating Manual, Hewlett Packard (1970).

VITA

Belur Narayana Shivashankara was born in Bangalore, India on October 23, 1946. He received his Bachelor of Engineering degree in Mechanical Engineering from the Bangalore University in 1967. He attended the Indian Institute of Science in Bangalore, India where he graduated with a Master's degree in Aeronautical Engineering in 1969. During 1969-70 he worked in an engineering position at the Space Science and Technology Centre, Trivandrum, India. He entered the Georgia Institute of Technology in 1970 as a graduate student.